THE LIGAND PREFERENCES OF INNATE IMMUNE RECEPTORS RIG-I AND LGP2

By

CHEN WANG

A dissertation submitted to the

School of Graduate Studies

Rutgers, The State University of New Jersey

In partial fulfillment of the requirements

For the degree of

Doctor of Philosophy

Graduate Program in Microbiology and Molecular Genetics

Written under the direction of

Joseph Marcotrigiano

And approved by

_____

_____

_____

_____

New Brunswick, New Jersey

May, 2018

ABSTRACT OF THE DISSERTATION

THE LIGAND PREFERENCES OF INNATE IMMUNE RECEPTORS RIG-I AND LGP2

By CHEN WANG

Dissertation Director:
Joseph Marcotrigiano, Ph.D.

The innate immunity serves as the first line against pathogen defense. Many receptors and factors play important roles in the innate immune response. A receptor family, retinoic-acid-inducible gene I (RIG-I)-like receptors (RLRs) consist of three members, RIG-I, MDA5 and LGP2. RIG-I specifically distinguishes viral RNAs in a diverse cellular RNA environment. When activated by these RNAs, RIG-I triggers downstream pathways and induces innate immune responses such as interferon production to establish an anti-viral state in host cells.

Based on previous studies, the 5' triphosphorylated (5'ppp) blunt-ended RNA bearing a double-strand (ds) panhandle structure at the 5' end is the ligand for RIG-I. This 5' triphosphorylation is often seen in viral RNAs. Cellular RNAs, such as messenger RNAs, are usually "capped" at the 5' end with a 7-methyl guanidine (m7G) via a triphosphate bridge (cap-0). Since the triphosphate is "protected" by the m7G, it was believed that the structural basis of RNA discrimination by RIG-I was the presence of m7G. However, our biochemical, biophysical and cell signaling studies show that RIG-I can recognize dsRNA with cap-0 to a similar extent as 5'ppp dsRNA. Structural data of RIG-I in complex with Cap-0 RNA reveals the ability of RIG-I to accommodate the m7G moiety. In contrast, dsRNA with m7G and an additional 2'-O-methyl group on the 5' end nucleotide ribose (cap-1) does not stimulate RIG-I and abrogates RIG-I

signaling through a mechanism involving residue His830. This histidine is critical for RNA discrimination by RIG-I.

Unlike RIG-I, the role of the innate immune receptor LGP2 is not well understood. Lacking domains for signaling, LGP2 is believed to be a regulator of RIG-I and MDA5. Characteristics of nucleic acid binding by LGP2 are not understood, and its relationship with RIG-I needs further studies. Our biochemical studies of LGP2 show higher ATP turnover rate in the presence of 5'OH dsRNA than viral RNA mimics, and the binding affinity of LGP2 with 5'OH dsRNA is relatively tight. 5'OH dsRNA has been shown to activate RIG-I, indicating an overlap in ligands between LGP2 and RIG-I. Competition assays show 5'OH dsRNA preferentially interacts with LGP2, suggesting a mechanism in which LGP2 sequesters non-PAMP ligand of RIG-I to diminish misactivations.

Overall, the studies provide further understanding of the early steps in the anti-viral process from the activation stage, which could aid in vaccine development and the design of compound agonist to complement approaches for developing RLR based therapeutics.

ACKNOWLEDGMENTS

I am deeply honored and extremely lucky to have Dr. Joseph Marcotrigiano as my mentor, who is smart, knowledgeable, determined and highly passionate in science. With no background in crystallography when I joined the lab, I learned so much from Joe and routinely asked him questions about crystallography, who is always patient and explains to me in great details. I am grateful I have the opportunity to work on RIG-I project, in which I learned so much and worked with so many talented scientists.

Dr. Smita Patel has been an unofficial co-advisor for my graduate research, who is wise, thoughtful and serious about science. I am always impressed and inspired by the way she looks into a problem, the questions she brings up and the advice she gave me whenever I was confused.

I would like to thank my committee member Dr. Eddy Arnold and Dr. Derek Sant'Angelo, who have been supportive and given me inspiring advice on my research with their expertise. Thank you for encouraging and challenging me.

Dr. Fuguo Jiang has been an extraordinary model to me in scientific research. His devotion and passion about science greatly influence me. We worked together for one month during which the training was intense but thorough, clear and detailed. I took over RIG-I project from Fuguo after he left for his post doctorate training. He continued giving me advice on the project as well as my career. A lot of gratitude I failed to express in words, leaving two simple words: Thank you.

I always feel lucky that I have such wonderful lab members, without any of you, I would not be me today. Dr. Jillian Whidby trained me during my rotation in the lab, who is patient and supportive. Dr. Abdul Khan is so hard-working that I am motivated by his diligence. Dr. Matthew Miller is extremely experienced and one of the nicest person I have ever known. Thank you for

teaching me so much in crystallography, from crystal mounting to structure reconstruction, which unveiled the beauty of structural biology to me. Dr. Samantha Yost is my closest colleague and best friend. Thank you for listening to my whines about everything and giving me suggestions. Thank you for not being fed up with my silly English questions. Thank you for starting talking to me when I was totally unconfident with talking in broken English.

I would like to thank our previous lab members Ankita Basant, Alicja Cygan, Amoli Kulkarni, Ryan Levy, Yi Li, Brandon Schweibenz, Lynda Tuberty, Lexi Zatorski, and current members Jennifer Casiano, Kristina Edwards, Dr. Ashish Gupta, Myeisha Paskel, and Yuanyuan Wang. I would like to express gratitude to the students, faculty, and staff of Center for Advanced Biotechnology and Medicine and National Institutes of Allergy and Infectious Diseases/National Institutes of Health.

My graduate work is inseparable from my excellent collaborators. Dr. Anand Ramanathan, Dr. Swapnil Devarkar from Smita's lab are outstanding scientists to work with, who renders me a lot of help when I first started working on the project by myself. Thank Dr. Michael Gale from University of Washington, Ann Durbin and Dr. Lee Gehrke from Massachusetts Institute of Technology, Dr. Marco Binder from German Cancer Research Center, Dr. Jie Zheng and Dr. Patrick Griffin from the Scripps Research Institute for their influence and contribution to my thesis research.

I must thank my friends in the U.S. and China: Na Cai, Jia Ding, Manlu Guo, Yang Liu, Yuchen Wang, Jiaying Xu, Dr. Binxing Yu, Yijun Zhou and so many others. It is not easy to live in a country where I have no family and my friends' support help me make through this journey. I miss all of you and hope we could see each other very soon.

Last but most importantly, I would like to thank my family. My grandpa Zhenpei Chen, my aunts Jie Chen, Hua Chen and uncle Peng Chen and everyone in our big family, thank you for

taking care of my parents when I am far away from home. And my dearest and best parents, Yan Chen and Shouye Wang, thank you for giving me life twenty eight years ago, thank you for giving me such a loving family, thank you for teaching me to be good person, thank you for supporting me when I was experiencing the hardest time, thank you for believing me that I can do it, and thank you for loving me. This is not easy for us, but we made it. I desperately look forward to the days we reunion and I can take up the responsibilities to take care our family. This is not typically what we say to each other, but I want to say: Mom and Dad, I love you.

TABLE OF CONTENTS

LIST OF TABLE

LIST OF FIGURES

INTRODUCTION

1. Innate Immunity

The human immune system acts via two traditional components: the innate immunity and the adaptive immunity each with a different function and role. The recognition of pathogens and activation of the innate immune responses decides the launch status of the adaptive immunity. The innate immune system is the first line of defense against pathogens (1). The recognition of pathogens is mediated by germline-encoded receptors, meaning the specificity of each receptor is genetically predetermined. Despite the heterogeneous nature of pathogens and their high rate of genomic mutation, the innate immune receptors are still able to recognize them by focusing on specific, highly conserved structures that are present in large groups of microorganisms. These structures are called pathogen-associated molecular patterns (PAMPs) (2)(3). The receptors that recognize PAMPs are called pattern recognition receptors (PRR) (4). After infection, factors such as antimicrobial peptides and phagocytes, and signaling pathways are triggered immediately. Activation of these factors and pathways turns on the production of pro-inflammatory cytokines, type I interferons [IFN-alpha and IFN-beta (IFN α/β)] or interferon stimulated genes (ISGs) (5). The production of type I IFN triggered by viral infection can induce gene transcription which ultimately establishes the antiviral states in infected cells and uninfected bystander cells (6)(7)(8).

2. Pattern Recognition Receptors

PRRs are classified to five families based on protein domain homology: Toll-like receptors (TLRs), C-type lectin receptors (CLRs), NOD-like receptors (NLRs), RIG-I-like receptors (RLRs) and AIM2-like receptors (ALRs) (9). TLRs and CLRs are membrane-bound on the cell surface, surveying pathogens in the extracellular space and within endosomes. TLRs can

recognize pathogens on the cell surface with PAMPs derived from bacteria, fungi, protozoa and pathogens in the endocytic compartments. The major ligands of CLRs are from fungi and certain types bacteria. NLRs, RLRs and ALRs are unbound, located in the cytoplasm, surveying intracellular pathogens. NLRs recognize the components of bacterial outer membranes or cell walls. The RLRs and ALRs detect viral RNAs and DNAs respectively derived from pathogenic gene expression or replication which usually occur in the cytosol (or nucleus).

3. RIG-I-like Receptors (RLRs)

RLRs located in the cytoplasm can sense viral RNAs from actively replicating viruses and induce the production of ISGs, type I IFN and pro-inflammatory cytokines. Viral RNAs can be viral genomes or viral replication intermediates. This family of receptors consists of three members: Retionic acid-inducible Gene I (RIG-I), Melanoma Differentiation-Associated protein 5 (MDA5) and Laboratory of Genetics and Physiology 2 (LGP2) (3)(10)(11). All three members have a central ATPase containing DExD/H box helicase domain (Figure 1). The N terminal domain of RIG-I and MDA5 contains a tandem of two caspase activation and recruitment domains (CARDs), named as CARD1 and CARD2, which are vital in signaling transduction. They also have a C terminal repressor domain (RD) within the C-terminal domain (CTD). LGP2 has a CTD but lacks CARDs, consistent with its inability to transduce signals. The helicase domain together with CTD functions in ligand binding. RIG-I and MDA5 have very similar domain organization but they sense different types of viruses (12). RIG-I is a sensor of hepatitis C virus (HCV), influenza virus, vesicular stomatitis virus, Sendai virus, rabies virus and Japanese encephalitis virus, while MDA5 detects picornaviruses and noroviruses (13)(14). They have some overlap and redundancies in recognizing viruses, such as reovirus and dengue virus (15). LGP2 was not characterized in sensing a particular viral RNA.

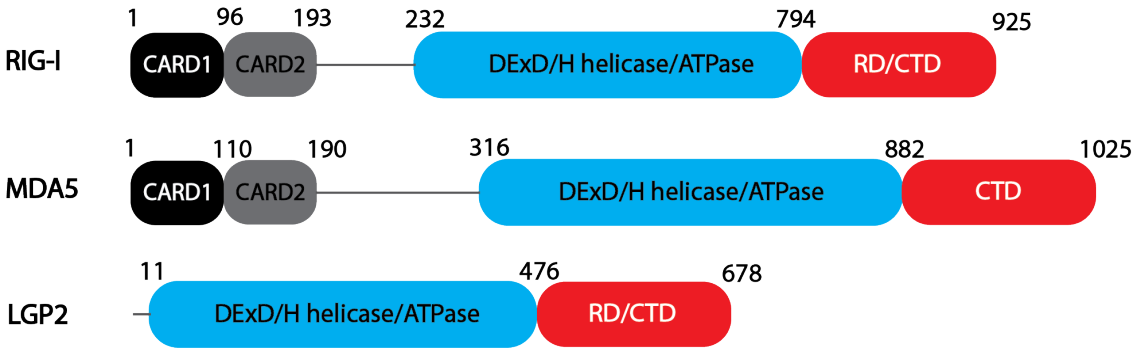

Figure 1. Schematic Domain Organizations of RIG-I-like Receptors. RIG-I, MDA5 and LGP2 sharing the SF2 helicase domain (blue) with ATPase activity and C-terminal domain (CTD, red). RIG-I and MDA5 contains two CARD domains (black and grey) on the N-terminus responsible for signaling transduction absent in LGP2.

3.a. RIG-I Recognition Characteristics

RIG-I is the most well studied member of RLRs, initially found by cDNA libraries screening for factors that activate IFN-β promoter in response to polyriboinosinic-polyribocytidylic acid [poly(IC)] that mimics viral RNAs (16). To gain understanding of the discrimination mechanisms of cellular/self RNA versus viral/non-self RNA by RIG-I, Hornung *et al.* and Pichlmair *et al.* first determined the properties of RIG-I ligand reporting that a free 5'-triphosphate on RNA is essential to activate RIG-I related immune responses (17)(18). Later Schlee *et al.* and Schmidt *et al.* found that a base paired region in proximity to the 5'-triphosphate on RNA either from secondary RNA structures such as hairpin or panhandle conformations is required for RIG-I signaling (19)(20). The importance of a RNA blunt-end conformation was emphasized in optimal activation of RIG-I (21). RNA secondary structures resulting from sequence composition may also affect the stimulatory potential of 5'-triphosphorylated RNA. HCV genomic ssRNA is composed of polyuridine motifs with interspersed C nucleotides (poly-U/UC motifs) and a 5'-triphosphate. Deletion of the poly-U/UC

motif or C nucleotides and the length of U-Core motif abrogated the stimulatory activity of HCV genomic RNA (22)(23)(24). 5'-diphosphate, 5'-monophosphate double-stranded RNA (dsRNA), viral 3'-untranslated region (UTR) and short dsRNAs generated by RNase L cleavage are also reported to activate RIG-I (25)(26)(27). Although the properties of RIG-I ligands have not been thoroughly described (28), it is commonly agreed that a blunt-end dsRNA in the range of 10 to 20 nucleotides bearing a free 5'-triphosphate is the best PAMP ligand of RIG-I (29) and cellular RNAs usually do not carry an exposed 5'-triphosphate.

3.b MDA5 Recognition Characteristics

MDA5, a cytoplasmic sensor for viral dsRNAs, is encoded by *IFIH1* gene, activates the same signaling cascade via MAVS as RIG-I by recognizing long dsRNA (>2000 bp) without bulges (30)(31)(32). This long dsRNA can be a replicative form of viruses as most self RNAs only contain short dsRNA regions within 5'- or 3'- UTRs. MDA5 functions in a dsRNA internal binding manner, requiring the formation of oligomers of MDA5 along dsRNA that cooperate multiple 2CARDs into close proximity enabling their assembly to filament (33)(34). Interestingly, MDA5 shows comparable affinities to ssRNA and dsDNA, a robust stimulatory activity is not induced by them as dsRNA is necessary for filament formation. Monomeric MDA5 binds dsRNA with low affinity and the affinity is increased significantly under the circumstance of protein-protein interaction along dsRNA.

3.c. LGP2 Recognition Characteristics

LGP2 is the most mysterious member of RLRs. It is reported that LGP2 is both a positive and negative regulator in antiviral responses (35)(36). Studies showed that overexpression of LGP2 interferes with viral recognition by RIG-I and MDA5 (11)(37)(38). Transfection of LGP2 and

RIG-I into cells at a ratio of 1:1 decreased RIG-I signaling by about half. The signaling was further reduced to nearly background level at a ratio of 5:1 (39). Virus-induced gene activation is significantly inhibited by LGP2 overexpression; however, LGP2 knockout mice shows an increased susceptibility to certain RNA viruses (40). Other gene disruption of LGP2 also show its role as a positive regulator of the innate immune system (41)(42)(43). LGP2 has a positive role in facilitating MDA5 signaling, evidenced enhancement of MDA5 signaling by LGP2 (44) and the discovery of a picornavirus-derived MDA5 agonist through interaction with LGP2 (45). Furthermore, LGP2 is reported to bind both dsRNA and ssRNA in a 5'ppp independent manner and preferentially binds 5'ppp dsRNA over other RNAs (46)(47). LGP2 is incapable of signaling itself, but evidence implies that LGP2 helps MDA5 load near RNA temini so that MDA5-dependent signaling is augmented while RIG-I dependent signaling is inhibited (48)(49). Nevertheless, no consensus about LGP2 binding preference and function has been reached.

4. Structural Mechanisms of RIG-I Activation

4.a RIG-I Domain Organization

RIG-I contains three major domains: the CARDs, helicase domain and RD domain. The central DEAD-box RNA helicase domain is composed of two Rec A-like domains, Helicase 1 (Hel-1), Helicase 2 (Hel-2) and a family specific large Helicase 2 insertion (Hel-2i) (Figure 2) (50)(51). The helicase domains, Hel1 and Hel2, are involved in the formation of active site for ATP binding and hydrolysis. Together with RIG-I CTD, they forms the RNA recognition module (52)(53)(54).

Figure 2 Schematic Domain Organization of RIG-I. RIG-I has two CARDs domains (black and grey) on N-terminal, a central helicase domain divided into Hel-1 (blue), Hel-2 insertion (Hel-2i, green), Hel-2 (yellow) and a C-terminal RD domain (red) connected to helicase domain by a bridge linker (orange).

4.b RIG-I Activation Model

Overexpression of the CARDs of RIG-I itself is enough to trigger an immune response (16). In the absence of PAMP RNA, RIG-I keeps CARDs in a signal-off state by masking them with Hel-2i (52), known as the RIG-I autoinhibition state. In this state, RD is highly flexible and disordered in the full length structure (PDB ID 4A2W). PAMP RNA is sensed by RD, causing CARDs release from Hel-2i, which is then freed to interact with the RNA along with RD (51). With the help of ATP binding and hydrolysis, the activated RIG-I exhibits a large conformational change causing Hel and RD to embrace the RNA as a ring (50). Subsequently, the released CARDs are ubiquitinated with Lys63-linked polyubiquitin or bound to unanchored chains (55)(56)(57)(58), triggering signaling through downstream adapter Mitochondria Antiviral Signaling protein (MAVS) (Figure 3). Notably, RIG-I is phosphorylated in resting cells to prevent premature activation and dephosphorylated rapidly when cells are stimulated with viral RNAs (59)(60)(61)(62).

Both *in vivo* and *in vitro* studies reported the occurrence of RIG-I oligomerization, induced by relatively long RNAs (63)(64). This hypothesis was evidenced by gel filtration analysis of RIG-I in complex with 5'ppp RNA of various lengths. Some have observed RIG-I oligomerization by band shift in native gel electrophoresis (63)(65). Studies also showed that RIG-I CTD can dimerize. However, these results are doubted by J Louber *et al.* because they

failed to identify the oligomerization of RIG-I by *in vitro* biochemical methods or by *in vivo* pull-down assay (66). The 'loose' oligomerization of RIG-I by incubating RIG-I with dsRNA at least 46bp long has been observed (67). The importance of ATP hydrolysis in RIG-I oligomerization was emphasized, and a model of ATP hydrolysis driving RIG-I oligomerization on RNA was proposed. Furthermore, clear oligomer formation of RIG-I was seen in the presence of poly(I:C) with the application of fluorescent fusion proteins and fully quantitative FRET imaging (68). It is stated that a correct dimer or oligomer might be a prerequisite for optimal signal transduction (69). Apparently, the exact function and necessity of oligomerization in RIG-I activation process is still elusive and requires high-resolution studies.

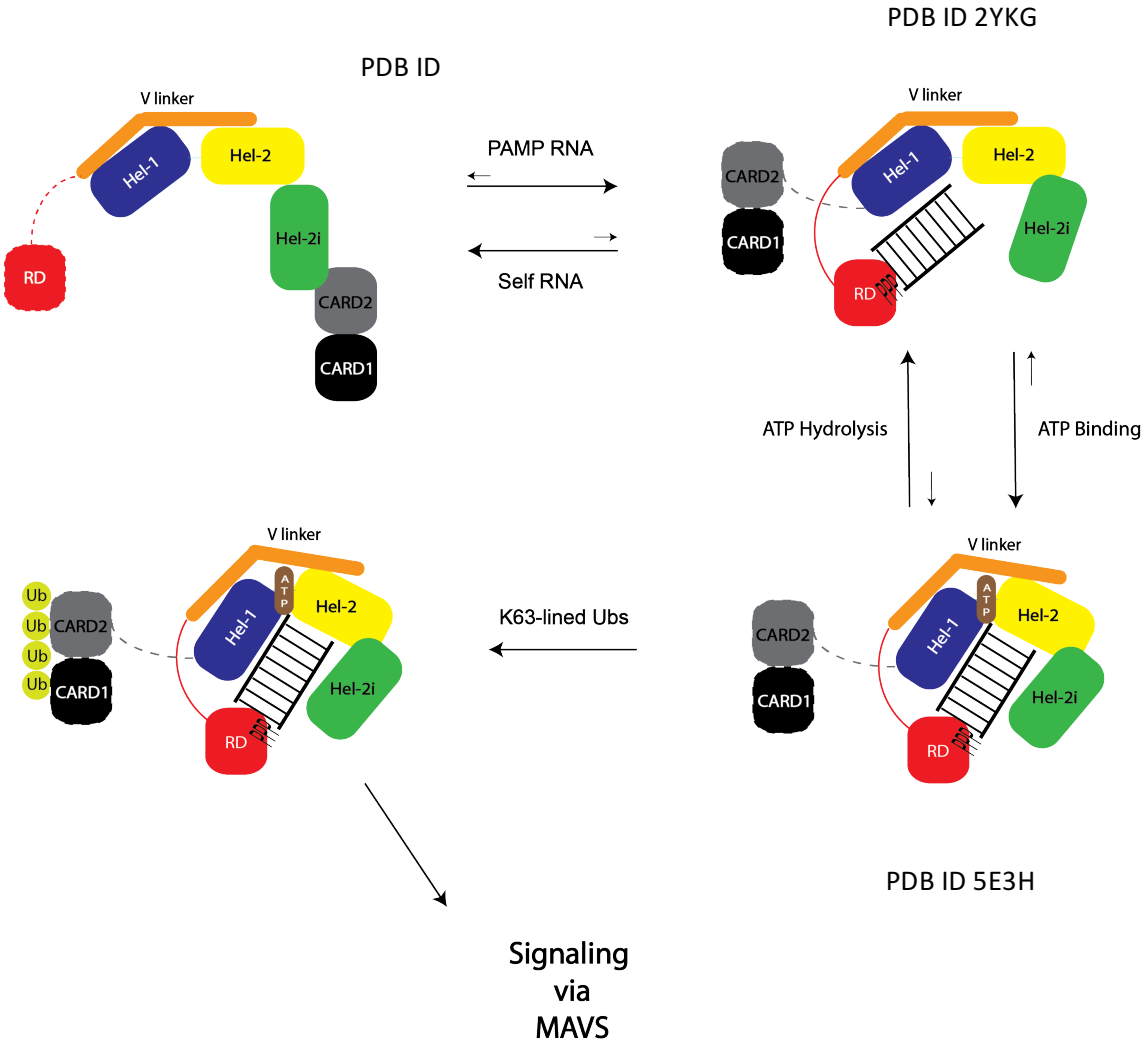

Figure 3. RIG-I Activation Model. RIG-I is autoinhibited by CARD2 internally interacting Hel-2i in the absence of PAMP RNA. When RD senses PAMP RNA, RIG-I adopts conformational change to form a ring structure around PAMP RNA and release CARDs. RIG-I is fully activated by hydrolyzing ATP and CARDs becomes ubiquitinated, eligible for transducing signals via downstream partner MAVS.

5. Capping Structures on RNAs

Cellular, self RNAs do not activate RIG-I because eukaryotic or cellular RNAs are modified post-transcriptionally, distinguishing them from viral RNAs. In prokaryotes, the 5' end

of many mRNAs is a triphosphorylated purine corresponding to the residue that initiated transcription. In contrast, eukaryotic RNAs like messenger RNAs (mRNAs) are modified with a 'cap' structure at the 5' end (Figure 4). There are multiple types of caps. The simplest one called 'cap-0' is the addition of a 7-methyl guanosine (m7G) which is bound to the terminal 5'-end nucleotide with a 5'-5' triphosphate bridge (referred as m7Gppp). This structure protects mRNAs from phosphatases and 5'-3' exonucleases. Moreover, the methyl group on the guanosine confers a positive charge that plays an important role in its specific recognition by specialized proteins. In some other mRNAs, the 5' end is further modified with 2'-O-methylation of the first nucleotides ribose, termed as 'cap-1'. An additional methylation modification occurred on the second nucleotide ribose results in a more extensively modified 'cap2' (70)(71)(72)(Figure 4). Such caps stabilize the 3'-5' bond between 2'-O-methylated first nucleotide and the next in the mRNA chain against hydrolysis by alkali or RNase. Notably, the complexity of the caps moves up as one moves up in the evolutionary scale. For example, yeast only has cap-0 in mRNAs while human mRNAs have cap-1 and cap-2 modifications.

Due to the importance of cap structures in facilitating translation (73), viruses that rely on host cell machinery to replicate have evolved ways to synthesize cap structures in order to utilize necessary cellular proteins (74)(75). They either use enzymes encoded in their genome to synthesize caps to their genomes and/or transcripts, or directly 'steal' caps from cellular RNAs. As a result, different viruses have different types of caps on their RNAs. This renders the possibility that some viruses are able to evade cellular immune defenses, such as detection by RIG-I.

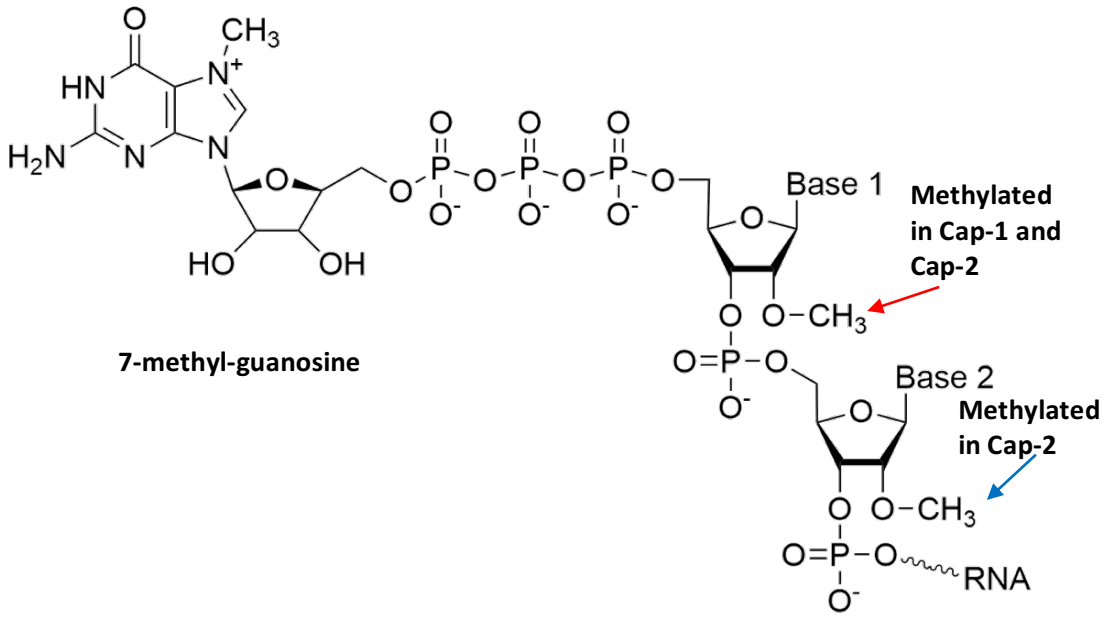

Figure 4. 5' Cap Structures on Eukaryotic mRNAs. Three cap structures are shown as indicated. Cap-0 contains the m7Gppp moiety, cap-1 contains m7Gppp and 2'-O-methylation of the first nucleotide (red arrow), and cap-2 has an extra 2'-O-methylation of the second nucleotide on the 5' end (blue arrow).

6. RIG-I-related Autoimmune Disease: Singleton-Merten Syndrome

If self RNAs are not correctly protected or RLRs lose autoinhibition ability due to genetic reasons, RLR-related immune response can cause autoimmune diseases. Singleton-Merten syndrome (SMS) is an autosomal-dominant multi-system disorder characterized by early and severe dental dysplasia, aortic calcification, glaucoma, psoriasis, skeletal abnormalities and other clinical findings. Recently, two mutations, c.1118A>C [Glu373Ala (E373A)] and c.803G>T [Cys268Phe (C268F)], in gene *DDX58* encoding RIG-I were identified associated with atypical SMS which does not cause dental anomalies (76). The two residues C268 and E373 belong to SF2 helicase domain ATP-binding motifs I and II (Figure 5), respectively, and lead to a gain-of-function phenotype (77). Studies have shown these SMS mutations result in constitutive

signaling activity of RIG-I due to its inability to discriminate self and non-self RNAs (78)(79)(80). A similar mutation was found in MDA5 as well, but not in LGP2 thus far (81).

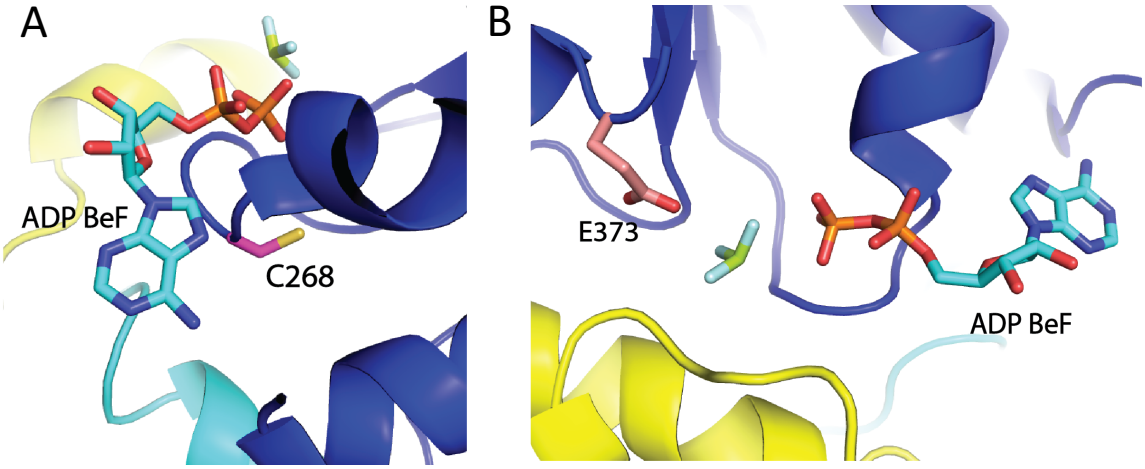

Figure 5. RIG-I Residues Related to Singleton-Merten Syndrom. Residue C268 (A) and E373 (B) are sitting in the ATP-binding pocket of RIG-I (PDB ID 5E3H) (50).

7. Rationale

The RIG-I signaling pathway is critical for early detection of viral RNA to initiate an antiviral response. Failure to elicit the early innate immune response can lead to serious systemic infections. Viruses employ an array of immune evasive mechanisms to avoid detection by RIG-I detection. For example, many viruses mimic cellular RNAs by incorporating the 5'm7Gppp structure on their genomes. This study is to discover RNA characteristics important for RIG-I recognition, to better understand immune evasive mechanisms of viruses and shed light on the process of RIG-I CARDs activated signal transduction. Determining the role of LGP2 in RIG-I activation and signaling will benefit in the complete understanding of RLRs functioning against pathogens. RIG-I is a therapeutic target, and compounds that activate innate immunity may serve as general antiviral agents of new infectious diseases or drug resistant variants and can be used in vaccine development, while inhibitors can be used for treating autoimmune

disorders stemming from unregulated activation of immune system. LGP2 serves as a regulator, which is a potential therapeutic target. It is possible that we could design compounds that affect LGP2 in order to regulate RIG-I signaling pathway. Therefore, the mechanistic knowledge gained from these studies will assist ongoing approaches to developing RIG-I and LGP2 based therapeutics.

MATERIALS AND METHODS

Chapter I. The Ligand Preferences of RIG-I

1. Oligo Sequences for RIG-I Studies

RNAs were chemically synthesized and HPLC purified by Bio-Synthesis Inc., TriLink BioTechnologies, or IDT (APPENDIX I). The synthetic RNAs were analyzed for purity by mass spectrometry and HPLC. The lyophilized RNA was resuspended in 20 mM potassium phosphate buffer pH 7.0. Duplex RNAs were prepared by mixing complementary ssRNAs in a 1:1.1 ratio, heating to 95°C for 1 min, and slow cooling to 4°C The concentration was determined in 7 M guanidinium HCl using the NanoDrop spectrophotometer at A260.

2. Recombinant Protein Expression and Purification

2.a. Full-length RIG-I, RIG-I Helicase-RD and full-length RIG-I H830A, H830A/V886A, E373A, C268F mutants Expression and Purification

Human wild type full-length RIG-I (1-925) and RIG-I Helicase-RD (232-925) were expressed in pET28 SUMO vector. Human full-length RIG-I (1–925) and Helicase-RD (232–925) were expressed in *Escherichia coli* strain Rosetta (DE3) (Novagen) as soluble proteins. The soluble fraction of protein was purified from the cell lysate using a Ni^{2+}- nitrilotriacetate (Qiagen) column or HisTrap FF column (GE Healthcare). The recovered protein was then digested with Ulp1 protease to remove the 6xHis–SUMO tag and further purified by hydroxyapatite column (CHT-II, Bio-Rad) and heparin sepharose column (GE Healthcare). Finally, purified protein was dialyzed against 50 mM HEPES (pH 7.5), 50 mM NaCl, 5mM $MgCl_2$, 5 mM DTT, 10% glycerol overnight at 4°C, snap frozen in liquid nitrogen, and stored at - 80°C. Full-length RIG-I H830A, H830A/V886A, E373A, C268F mutants were purified in a similar manner.

2.b 1-228 RIG-I CARDs preparation

Protein construct was expressed in pGEX 6P-1 GST vector. Human RIG-I CARDs (1–228) was expressed in *Escherichia coli* strain Rosetta (DE3) (Novagen) as soluble proteins. The soluble fraction of protein was purified from the cell lysate using a GST column (GE Healthcare). The recovered protein was then digested with Precission protease to remove the GST tag and further purified by Q FF column (GE Healthcare). The recovered protein was passed through Superdex 75 gel filtration column against 25 mM Tris-HCl (pH 8.0), 50 mM NaCl, 5 mM DTT. The purified protein was snap frozen in liquid nitrogen after 10% glycerol added, and stored at - 80°C.

3. RNA Binding and ATP Hydrolysis Assay

The ATP hydrolysis rates were measured at constant RIG-I (5 nM) and increasing RNA concentration (1 nM – 1 µM) in the presence of 1 mM ATP (spiked with [γ-32P] ATP). A time course (0-60 min) of the ATPase reactions was performed in Buffer A at 37°C. The reactions were stopped at desired time points using 4 N HCOOH and analyzed by PEI-Cellulose-F Thin-layer chromatography (TLC) (Merck) developed in 0.4 M potassium phosphate buffer (pH 3.4). The TLC plates were exposed to a phosphorimager plate, imaged on a Typhoon phosphor-imager, and quantified using ImageQuant software. The ATPase rate was determined from the plots of [Pi] produced versus time and dividing the rate of hydrolysis by RIG-I concentration. The ATPase rates were then plotted as a function of RNA concentration and fitted to hyperbolic equation (Equation 1) or quadratic equation (Equation 2) to get the binding affinity ($K_{d,app}$) and the maximal ATPase rate (k_{atpase}), where observed ATPase rate = k_{atpase} x [PR]/[Pt] ; [Pt] is total protein concentration.

$$[\mathrm{PR}] = \frac{[S]}{Kd,app+[S]} \qquad \text{(Equation 1)}$$

$$[\mathrm{PR}] = \frac{([Pt]+[Rt]+Kd,app)-\sqrt{([Pt]+[Rt]+Ka,ppp)^2-4[Pt][Rt]}}{2} \quad \text{(Equation 2)}$$

4. Protein-RNA Complex Crystallization and Data Collection

4.a Preparation of Helicase-RD-HP RNA Complexes

The5'OH HP RNA oligonucleotide (IDT), 5'ppp HP RNA oligonucleotide (BioSynthesis) and Cap-0 HP RNA oligonucleotide (TriLink) were resuspended with DNase and RNase-free water before use. The resulting HP RNAs were mixed with purified Helicase-RD in a RNA:protein molar ratio of 1.2:1, incubated on ice for 30 min, and then purified by size-exclusion chromatography (Superdex 200, GE Healthcare) with an elution buffer of 50 mM HEPES (pH 7.5), 50 mM NaCl, 5 mM $MgCl_2$, 5 mM DTT.

4.b RIG-I Helicase-RD-5'ppp 24mer HP RNA Complex

Crystals of native complex were grown by the hanging-drop vapor diffusion method at 20° C. Aliquots (2 µL) of 10 mg/ml of Helicase-RD–5'ppp HP RNA complex in 50 mM HEPES (pH 7.5), 50 mM NaCl, 5 mM $MgCl_2$, 5 mM DTT were mixed with 2 µL of reservoir solution containing 23% (w/v) PEG 3350, 0.2 M KSCN, 100 mM MOPS (pH 7.8). Crystals of RIG-I Helicase-RD-5'ppp HP RNA crystals were transferred into crystallization solutions plus 5% (v/v) (2R,3R)-(−)-2,3-butanediol and then flash-frozen to 100K for data collection.

Data was collected from a single crystal diffracted to 3.2 Å at X25 beamline of the National Synchrotron Light Source at the Brookhaven National Laboratory (BNL). The crystallization and data collection of this complex was done by Dr. Fuguo Jiang.

4.c RIG-I Helicase-RD-5'OH 24mer HP RNA Complex

Crystals of native complex were grown by the hanging-drop vapor diffusion method at 20° C. Aliquots (2 µL) of 10 mg/ml of Helicase-RD–5'OH HP RNA complex in 50 mM HEPES (pH

7.5), 50 mM NaCl, 5 mM $MgCl_2$, 5 mM DTT were mixed with 2 µL of reservoir solution containing 23% (w/v) PEG 3350, 0.3 M KSCN, 100 mM MOPS (pH 7.8). Crystals of RIG-I Helicase-RD-5'OH HP RNA crystals were transferred into crystallization solutions plus 5% (v/v) (2R,3R)-(−)-2,3-butanediol and then flash-frozen to 100K for data collection.

Data was collected from a single crystal diffracted to 2.6 Å at F1 beamline of the Cornell High Energy Synchrotron Source (CHESS). The crystallization and data collection of this complex was done by Dr. Fuguo Jiang.

4.d RIG-I Helicase-RD-Cap-0 24mer HP RNA complexes

Crystals of native complex were grown by the hanging-drop vapor diffusion method at 20° C. Aliquots (2 µL) of 8 mg/ml of Helicase-RD–Cap-0 HP RNA complex in 50 mM HEPES (pH 7.5), 50 mM NaCl, 5 mM MgCl2, 5 mM DTT were mixed with 2 µL of reservoir solution containing 20% (w/v) PEG 3350, 0.2 M NaSCN, 100 mM MOPS (pH 7.8), 3.5% (v/v) 2,2,2-trifluoroethanol. Crystals appeared after 1-2 days and grew to a maximum size of 0.15 × 0.15 × 0.5 mm over the course of six days. RIG-I Helicase-RD-Cap-0 HP RNA crystals were transferred into crystallization solutions containing 15% (v/v) glycerol and 10% (v/v) ethylene glycol as cryoprotectant and then flash-cooled at 100 K for data collection.

Data was collected from a single crystal diffracted to 3.3 Å at 8.3.1 beamline of the Advanced Light Source at University of California at Berkeley.

5. Structure Determination and Refinement

5.a RIG-I Helicase-RD-5'ppp 24mer HP RNA Complex Structure

The collected data were integrated and scaled with iMosFLM (82)(83) and SCALA from ccp4 suites (84), showing a space group of $P2_12_12_1$. Phases were determined by molecular

replacement using 5E3H structure (50). The structure was further refined with manual building and adjustment using Coot (85) and Phenix (86). The final refinement model consists of six complexes in one asymmetrical unit with R_{work}/R_{free} factors 0.22/0.27, 97.1% Ramachandran favored amino acid residues. Atomic coordinates and structure factor amplitudes have been deposited in the Protein Data Bank (PDB ID 5F9H).

5.b RIG-I Helicase-RD-5'OH 24mer HP RNA Complex Structure

The collected data were integrated and scaled with iMosFLM (82)(83)and SCALA from ccp4 suites (84), showing a space group of $P2_12_12_1$. Phases were determined by molecular replacement using 5E3H structure (50). The structure was further refined with manual building and adjustment using Coot (85) and Phenix (86). The final refinement model consists of six complexes in one asymmetrical unit with R_{work}/R_{free} factors 0.20/0.26, 95.3% Ramachandran favored amino acid residues. Atomic coordinates and structure factor amplitudes have been deposited in the Protein Data Bank (PDB ID 5F9F).

5.c RIG-I Helicase-RD-Cap-0 24mer HP RNA Complex Structure

The collected data were integrated and scaled with iMosFLM (82)(83) and SCALA from ccp4 suites (84), showing a space group of $P2_12_12_1$. Phases were determined by molecular replacement using 5E3H structure (50). The structure was further refined with manual building and adjustment using Coot (85) and Phenix (86). The m7G modification was manual built in structure file referred to previous cap RNA structures. The final refinement model consists of six complexes in one asymmetrical unit with R_{work}/R_{free} factors 0.22/0.28, 93.1% Ramachandran favored amino acid residues. Atomic coordinates and structure factor amplitudes have been deposited in the Protein Data Bank (PDB ID 5F98).

6. Limited Trypsin Proteolysis

Limited proteolysis with trypsin (Roche) was performed using 120 µg of purified full-length RIG-I in the absence or presence of HP RNAs. The samples were incubated with trypsin at a protein: protease mass ratio of 100:1. The reaction mixtures were maintained on ice and aliquots were removed at 0, 15, 30, 60, and 120 min. The aliquot reaction was quenched by the addition of sodium dodecyl sulfate polyacrylamide gel electrophoresis (SDS-PAGE) loading buffer and analyzed by SDS-PAGE.

7. Small Angle X-ray Scattering (SAXS)

SAXS data of RIG-I in complex with 5'ppp, 5'OH, Cap-0 HP RNA were collected at G1 beamline at CHESS using a Finger Lakes CCD X-ray detector system. The sample-to-detector distance was 1450mm to make scattering vectors q range from 0.007 to 0.7 $Å^{-1}$, where $q = 4\pi\sin\theta/\lambda$ (2θ is the scattering angle and $\lambda = 1.244$ Å). Complex preparation is same as above and flow through buffer from sample concentration was used in buffer subtraction. BioXTAS RAW (87)(88) and ATSAS (89)were applied to process and analyze scattering data. Radius of gyration (R_g) was calculated by Guinier Plot at low q region ($q < 1.3/R_g$). P(r), the probability distribution of distances of atoms within the macromolecule, and the maximum atom pair distance D_{max} were generated by GNOM algorithm. Kratky plots were generated by BioXTAS RAW. The low resolution 3D *ab initio* reconstruction of protein-RNA complex molecule envelopes was carried out by a Python script written by Dr. Matthew Miller integrating DAMAVER, SUPCOMB and DAMMIF programs.

8. Cell-based IFN-β Reporter Signaling Assays

HEK293T cells were grown in 6-well plates to 60% confluence and cotransfected with firefly luciferase reporter plasmid (pLuc125 / 2.5 µg), Renilla luciferase reporter plasmid (pRL-TK / 500 ng), and a plasmid carrying either the wt RIG-I gene, the H830A RIG-I mutant gene or an empty plasmid under the constitutively active CMV promoter (pcDNA3.1 / 2 µg). The firefly luciferase gene is under the interferon β promoter and the Renilla luciferase plasmid is under the constitutively active TK promoter. The plasmid transfections were carried out with X-tremeGENE HP DNA Transfection Reagent (Roche). Cells were replated in 96-well plates the next day at 2 x 104 cells/well density and transfected with each of the RNA ligands (700 nM final concentration in 110 µL) using Lipofectamine transfection reagent (Life Technologies). After 20 hours the activities of firefly and Renilla luciferases were measured sequentially with the Dual-Luciferase reporter assay (Promega). Data was collected in quadruplicate sets and the relative luciferase activities were calculated. The error bars represent the standard error of the mean (SEM).

9. Anti-RIG-I CARDs Antibody Generation

The antibody was generated with a commercial available MonoExpress custom monoclonal antibody production service from GenScript Biotechnology. Approximately 3 mg purified RIG-I CARDs protein was sent to GenScript to initialize the project. The project was composed of three phases including Phase I Immunization, Phase II Cell fusion and Phase III Subcloning. Samples were received and analyzed by Enzyme-Linked Immunosorbent Assay (ELISA) after each phase.

9.a Antibody Screening by ELISA

ELISA 96-well microplate was coated with purified antigens overnight at 4°C by rigorously shaking. The plate was washed three times with phosphate buffer saline with Tween 20 (PBS-t) before blocked with 5% bovine serum albumin (BSA). Samples from each phase were applied as primary antibody. Goat-anti-mouse antibody was used as secondary antibody. The microplate then was treated with Pierce TMB substrates (Thermo Scientific) and 2 M sulfuric acid subsequently. Color change was read and analyzed by plate reader (Molecular Devices) at λ= 450 nm.

9.b Antibody Purification

Monoclonal antibody secreted by hybridoma cells maintained in suspension culture was purified over a Protein G column (GE Healthcare). The pH of antibody was adjusted with 1 M Tris HCl pH 9.0. The antibody was then dialyzed against 20 mM Sodium Phosphate pH 7.0 and 10 mM EDTA and digested with Papain for 3 hours at 37°C to generate Fab and Fc fragments. The product was passed through Protein A (GE Healthcare) chromatography to eliminate Fc fragments. The recovered protein was further purified with Mono Q column (GE Healthcare).

10. RIG-I Dimerization Determination

Purified full-length RIG-I E373A and C268F mutants were mixed with Stem RNAs at a protein: RNA ratio of 3:1 on ice for 30min. The mixture was passed through a size exclusion column Superdex 200 Increase 10/300 (GE Healthcare) in line with a Multi-Angle Light Scattering (MALS) detector (DAWN-EOS Wyatt technology) (SEC-MALS). Data were analyzed with the ASTRA software (90).

Chapter II. LGP2 Studies

1. Oligo Sequences for LGP2 Studies

RNAs were chemically synthesized and HPLC purified by Bio-Synthesis Inc., TriLink BioTechnologies, or IDT (APPENDIX II). The synthetic RNAs were analyzed for purity by mass spectrometry (Appendix) and HPLC. The lyophilized RNA was resuspended in 20 mM potassium phosphate buffer pH 7.0. Duplex RNAs were prepared by mixing complementary ssRNAs in a 1:1.1 ratio, heating to 95°C for 1 min, and slow cooling to 4°C The concentration was determined in 7 M guanidinium HCl using the NanoDrop spectrophotometer at A260.

2. Recombinant LGP2 Expression and Purification using Escherichia coli System

Protein constructs were expressed in pET28 SUMO vector. Human full-length LGP2 (1–628) was expressed in *Escherichia coli* strain Rosetta (DE3) (Novagen) as soluble proteins. The soluble fraction of protein was purified from the cell lysate using HisTrap FF column (GE Healthcare). The recovered protein was then digested with Ulp1 protease to remove the 6xHis–SUMO tag and further purified by Q column (GE Healthcare). The recovered protein was passed through Superdex 200 gel filtration column against 50 mM Sodium Phosphate (pH 8.0), 300 mM NaCl, 5 mM DTT. The purified protein was snap frozen in liquid nitrogen after 10% glycerol added, and stored at - 80°C.

3. LGP2 Expression in Mammalian Cells

HEK293T cells were grown in 6-well plate to 30-35% confluence and transfected with plasmid pcDNA 3.1 myc LGP2, pJG His LGP2, pcDNA 3.1 gp140 and pcDNA 3.1 mouse LGP2.

4. Western Blotting

Media was removed and cells lysed with 120 µL standard SDS loading buffer in 48 hours post-transfection. 12 µL samples were separated on 4-12% SDS gradient gels (Bio-Rad) and transferred to nitrocellulose membranes using a Trans-Blot SD Semi-Dry Transfer Cell (Bio-Rad) in 25 mM Tris, 192 mM glycine pH 8.3, 0.025% SDS, and 10% methanol for 2 hours at 0.3 Amp. Membranes were blocked for 1 hour at room temperature in 5% skim milk in 0.05% Tween-20 in PBS and incubated with primary antibody overnight at 4°C. Anti-myc, anti-His and anti-human LGP2 antibodies were used at 1:2000, 1:2000 and 1:1000 dilutions.

5. ATP Hydrolysis Assay

5.a ATP Hydrolysis V_{max} Experiment

The ATP hydrolysis rates were measured at constant LGP2 (100 nM) and RNA/DNA substrates concentration (2 µM) in the presence of 1 mM ATP (spiked with [γ-32P] ATP). A time course (0-60 min) of the ATPase reactions was performed in Buffer A [50 mM MOPS-Na (pH 7.4), 5 mM $MgCl_2$, 5mM DTT, 0.01% Tween 20] at 37°C. The following steps were performed as described in Materials and Methods Chapter I.

5.b ATPase Competition Assay

The ATP hydrolysis rates were measured at constant RIG-I (10 nM or 25 nM), RNA (10 nM or 25 nM) and increasing LGP2 concentration (0 – 50 nM or 150 nM) in the presence of 1 mM ATP (spiked with [γ-32P] ATP). A time course (0-60 min) of the ATPase reactions was performed in Buffer A [50 mM MOPS-Na (pH 7.4), 5 mM $MgCl_2$, 5mM DTT, 0.01% Tween 20] at 37°C. The following steps were performed as described in Materials and Methods Chapter I.

6. Fluorescence Anisotropy and Intensity Titration Assay

Fluorescence anisotropy measurements were carried out using FluoroMax-4 spectrofluorimeter (Horiba JobinYvon) in Buffer A at 25 °C mounted with Glen-Thomson calcite prism polarizers in an L-format scheme. Fluorescein labeled RNA or DNAs (5 nM) were titrated with increasing LGP2 concentration with excitation at 570 nm and emission at 547 nm for DY547 or Cy3, excitation at 495 nm and emission at 515 nm for fluorescein. The mixed solution of RNA or DNA and LGP2 was incubated in a 3-ml cuvette for ~5 min before taking measurements of fluorescence anisotropy to reach an averaged value of fluorescence anisotropy. The observed fluorescence anisotropy (robs) contributed both by free RNA or DNA (with anisotropy r_f) and from protein-bound RNA or DNA (with anisotropy r_b) was plotted as a function of LGP2 concentration and fit to Equation 2 and 3 (In Method Chapter I) to obtain the equilibrium dissociation constant, K_d.

$$r_{obs} = r_b f_b + r_f(1 - f_b) \quad \text{(Equation 3)}$$

where f_b is the fraction of RNA or DNA in the form of LGP2-RNA/DNA complex, f_b = $[PR]/[R_t]$ ([PR] is the complex concentration and $[R_t]$ is the RNA concentration in total) (90)(91)(92).

EXPERIMENTAL RESULTS

Chapter I. Ligand Preferences of Innate Immune Receptor RIG-I

1. Structural Basis for m7G recognition in capped RNA by RIG-I

1.a ATPase activity of RIG-I in the presence of 5'ppp, 5'OH, Cap-0 24mer Hairpin RNAs

Studies have shown that 5'ppp dsRNA is the best characterized ligand for RIG-I, and the 5' triphosphate protected capped RNA did not activate RIG-I (2006). However, the crystal structure of RIG-I Helicase-RD in complex with 5'ppp hairpin (HP) RNA revealed the detailed environment of RIG-I binding to 5' end of RNA (Figure 7B Center). It is obvious that the big open pocket close to triphosphate moiety is spacy enough to accommodate modifications such as a m7G. Previous studies on capped RNA utilized in vitro transcription method to generate capped RNA, and it is known that T7 RNA polymerase adds unknown amounts of non-templated nucleotides to RNA. In order to understand the relationship between RIG-I and modifications on RNA 5'end thoroughly, we first analyzed binding affinities and ATP hydrolysis rate of RIG-I in complex with 5'ppp HP RNA, 5'OH HP RNA and Cap-0 HP RNA in collaboration with Dr. Smita Patel's lab from Rutgers Medical School. The results were fit to the 1:1 binding model to acquire the RNA dissociation constant ($K_{d,\ app}$) and the maximal ATPase turnover rate (k_{atpase}). The $K_{d,\ app}$ of 5'OH HP RNA binding to RIG-I is ~40nM, whereas 5'ppp HP RNA exhibits a 20-fold higher affinity binding to RIG-I ($K_{d,\ app}$ ~2nM) (Figure 6 and Table 1). Surprisingly, the Cap-0 HP RNA shows comparable high binding affinity with RIG-I as the 5'ppp HP RNA ($K_{d,\ app}$ ~2nM). Moreover, RIG-I's ATPase activity is stimulated by all three HP RNAs. This indicates that the adding of m7G cap on the 5'ppp group does not affect the binding affinity or the ATPase activity of RIG-I.

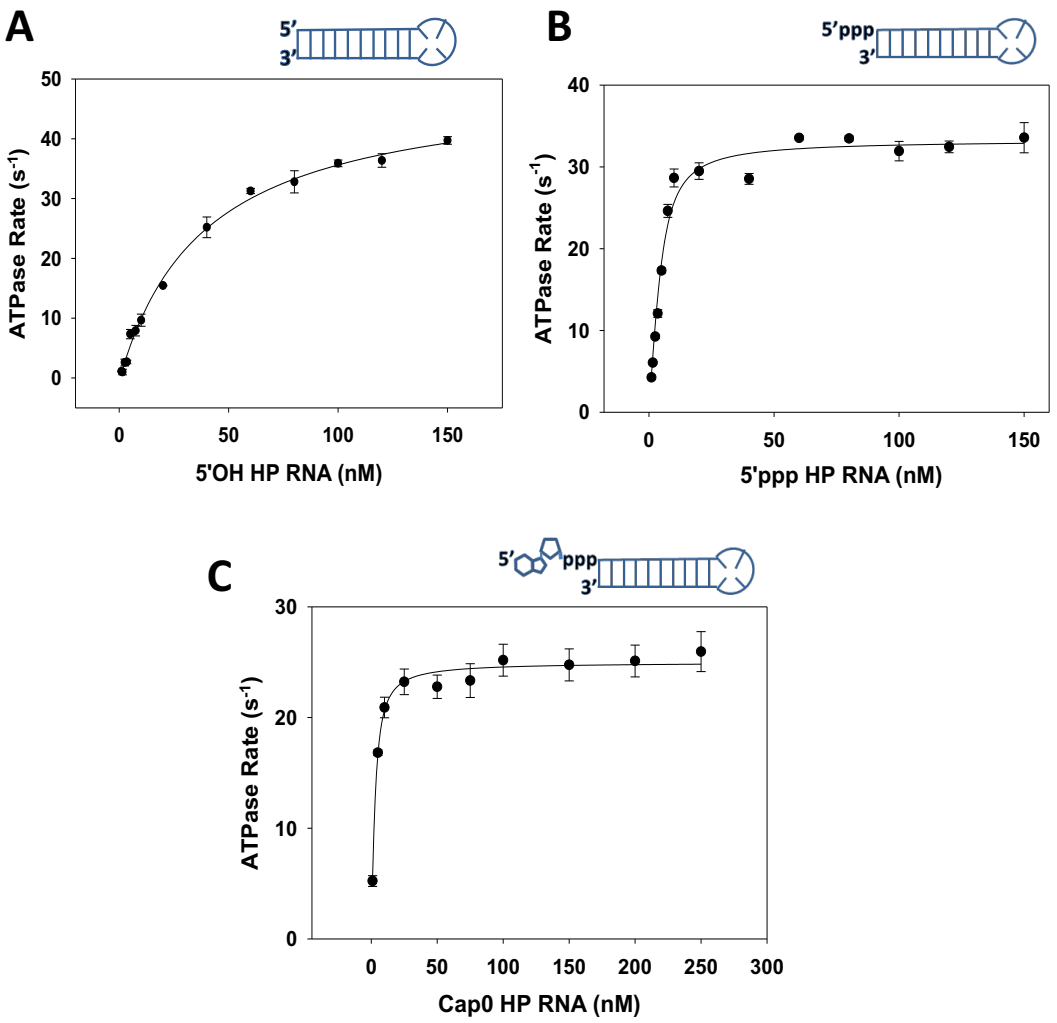

Figure 6. K_d and ATP Hydrolysis Rate of the RIG-I-RNA Complexes. The ATP hydrolysis rate of RIG-I measured at 37°C in buffer A is plotted against increasing concentrations of 5'OH (A), 5'ppp (B) and Cap-0 (C) HP RNA.

Table 1 RNA Binding and ATPase Activity of WT RIG-I and Helicase-RD

	WT RIG-I		Helicase-RD	
RNA Ligand	$K_{d,app}$(nM)	k_{atpase} (s^{-1})	$K_{d,app}$(nM)	k_{atpase} (s^{-1})
5'OH HP RNA	38.5 ± 4	49 ± 1	0.4 ± 0.3	63 ± 1
5'ppp HP RNA	1.8 ± 0.9	33 ± 0.9	0.75 ± 0.3	48 ± 1
Cap-0 HP RNA	1.7 ± 0.5	25 ± 0.4	0.08 ± 0.04	36 ± 0.4
5'ppp ssRNA	N.B.	N.B.	35 ± 5.5	0.9 ± 0.03
Cap-0 ssRNA	N.B.	N.B.	14 ± 4.4	0.3 ± 0.03

1.b Crystal Structures of RIG-I Helicase-RD with 5'OH, 5'ppp, and Cap-0 HP RNAs

Three structures of RIG-I Helicase-RD in complex with HP RNA, identical in sequence and bearing 5'OH, 5'ppp, or Cap-0, respectively were determined by X-ray crystallography (Figure 7 and Table 2). The three crystals all have the symmetry of space group $P2_12_12_1$ and have six complexes in one asymmetric unit, yielding six independent views of the complex. The six views of each complex contribute to an overall identical structure. Interestingly, all three structures are nearly identical, such that α carbon atoms have a root mean square deviation (rmsd) less than 0.7 Å. This indicates that the triphosphate and m7G moieties do not perturb the overall structure of RIG-I Helicase-RD.

By comparing our Helicase-RD-5'ppp HP RNA structure with the previously reported structures of Helicase-RD bound to 5'ppp 8-bp HP RNA (PDB ID 4AY2), we found that there is a conformational difference in the helicase domain with a rmsd of 3.8 Å (Figure 6A). The helicase domain of 4AY2 is more closely similar to the free duck RIG-I structure (PDB ID 4A2W) (rmsd of 2.8 Å) (Figure 8), whereas the rmsd of our structure with 4A2W is 6.2 Å. Furthermore, the helicase domain of 4AY2 has fewer interactions with the RNA compared to 5F9H even though

human RIG-I was used in both cases. This discrepancy probably resulted from the disulfide bond in the Hel2i of 4AY2, different crystallization conditions, or different crystal packing arrangement.

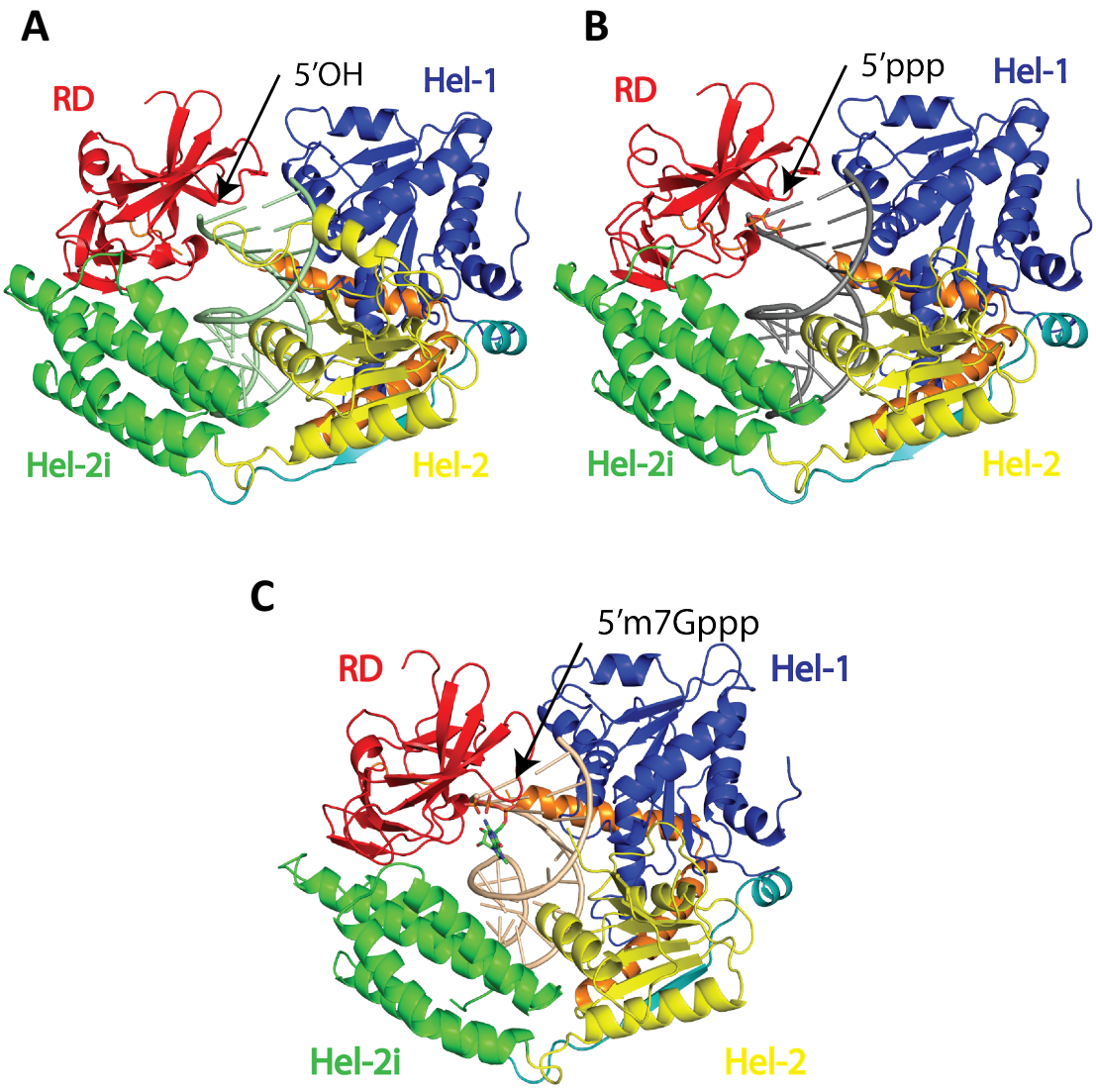

Figure 7. Overview of Crystal Structures of the RIG-I-RNA Complexes. Crystal structures of RIG-I Helicase-RD in complex with 5'OH HP RNA (PDB ID 5F9F) (A), 5'ppp HP RNA (PDB ID 5F9H) (B), and Cap-0 HP RNA (PDB ID 5F98) (C). The color code is corresponding to Figure 2.

Table 2 Data Collection and Refinement Statistics for RIG-I Helicase-RD in Complex with 5'OH, 5'ppp, Cap-0 HP RNAs.

PDB ID	5F9H	5F9F	5F98
5' end	PPP	OH	m7Gppp
Location	BNL (X25)	CHESS (F1)	ALS (8.3.1)
Detector	Pilatus 6M	ADSC Q270	ADSC Q315
Wavelength	1.100	0.918	1.116
Resolution range	46.2-3.2 (3.4-3.2)	30.0-2.6 (2.7-2.6)	49.4-3.3 (3.4-3.3)
Space group	$P2_12_12_1$	$P2_12_12_1$	$P2_12_12_1$
Unit cell parameters	111.2, 174.8, 309.3	111.5, 174.3, 308.3	111.2, 174.2, 308.8
Total reflections	1,110,358	2,156,243	1,268,139
Unique reflections	99,666	166,166	90,827
Redundancy	11.1 (10.6)	13.0 (9.5)	14.0 (11.8)
Completeness (%)	99.5 (99.6)	90.6 (80.3)	99.8 (99.7)
Mean I/sigma (I)	9.6 (2.4)	13.0 (2.4)	7.1 (1.9)
R_{merge}	0.28 (1.11)	0.15 (1.02)	0.56 (1.95)
R_{meas}	0.29 (1.16)	0.16 (1.07)	0.60 (2.12)
R_{pim}	0.09 (0.35)	0.04 (0.33)	0.21 (0.81)
R_{work}	0.22 (0.31)	0.20 (0.29)	0.22 (0.29)
R_{free}	0.27 (0.36)	0.26 (0.38)	0.28 (0.36)
Number of atoms			
All	33,603	34,918	32,719
Protein	30,480	31,642	29,503
RNA	3,108	3,036	3,204
Other	15	114	12
Water	0	126	0
RMS bonds (Å)	0.004	0.002	0.002
RMS angles (°)	0.74	0.58	0.54
Ramachandran favored (%)	97.1	95.3	93.1
Ramachandran allowed (%)	2.8	4.6	6.8
Ramachandran outliers (%)	0.1	4.6	6.8
Clashscore	0.1	0.1	0.1
Average B-factors ($Å^2$)			
All atoms	66.2	55.1	57.1
Protein atoms	65.5	54.9	56.4
RNA atoms	72.6	57.3	63.3
Other	49.6	78.5	41.8
Water atoms	NA	34.5	NA

Data for highest resolution range shell are shown in parentheses.

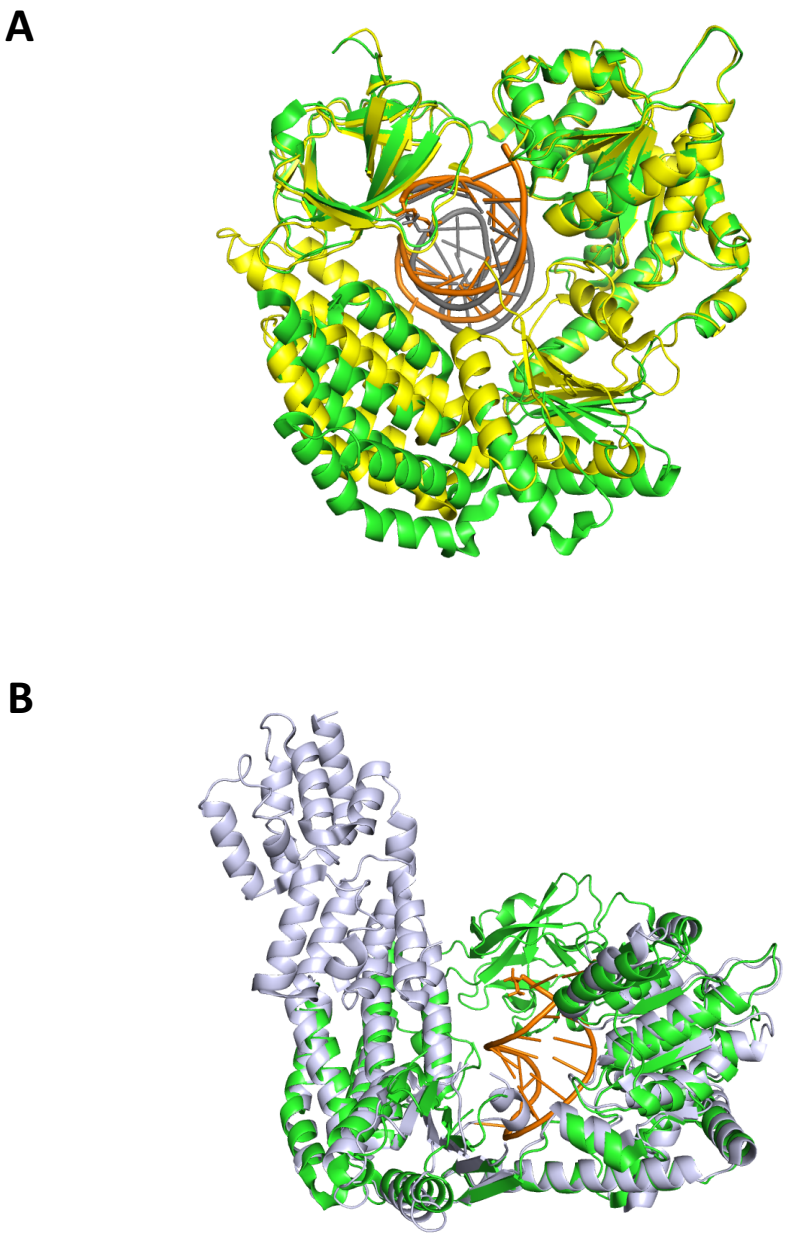

Figure 8. Structure Comparison of RIG-I in Different Conformations. (A) Structure superimposition of 5F9F (yellow) and 4AY2 (green) showing the helicase domain in 4AY2 sitting further away from RNA compared to 5F9F. (B) The helicase domain of 4AY2 (green) is more closed to unliganded RIG-I structure (4A2W, grey) by superimposition.

1.c Conformational Change in Helicase Motif Iva Accommodates 5'ppp and Cap-0 dsRNA

Although the three complexes share overall identical crystal structures, one remarkable difference attracted our attention. The helicase motif IVa, located in the Hel-2 region of RIG-I (residues 664-685) and highly conserved in the SF2 family of helicases (93) adopts an extended loop structure followed by a short alpha helix in the HelRD-5'OH HP RNA structure (Figure 9), whereas it is disordered in the absence of RNA (4A2W) or presence of 5'ppp (5F9H) or Cap-0 RNAs (5F98). The alpha helix is approximately perpendicular to the RNA axis and the loop region of this motif is in proximity to the blunt end of RNA. This loop would clash with the 5'ppp and m7G moieties if it sits in the same position according to superposition of the three structures (Figure 10). Therefore, disruption of motif IVa creates a cavity between RD and Hel-2i which accommodates the 5'ppp and cap-0 modifications. Limited proteolysis by trypsin also showed a more protected state of RIG-I-5'OH HP RNA complex compared to complex with 5'ppp HP RNA and Cap-0 HP RNA (

Figure 11). Deletion of this region results in in capability of RIG-I signaling (Figure 12), which indicates its importance for RIG-I function even though it is disordered in the 5'ppp and Cap-0 HP RNA structures. The corresponding loop in MDA5 is involved in interacting with the major groove of dsRNA, the deletion of which leads to defects in MDA5's ATPase and signaling function.

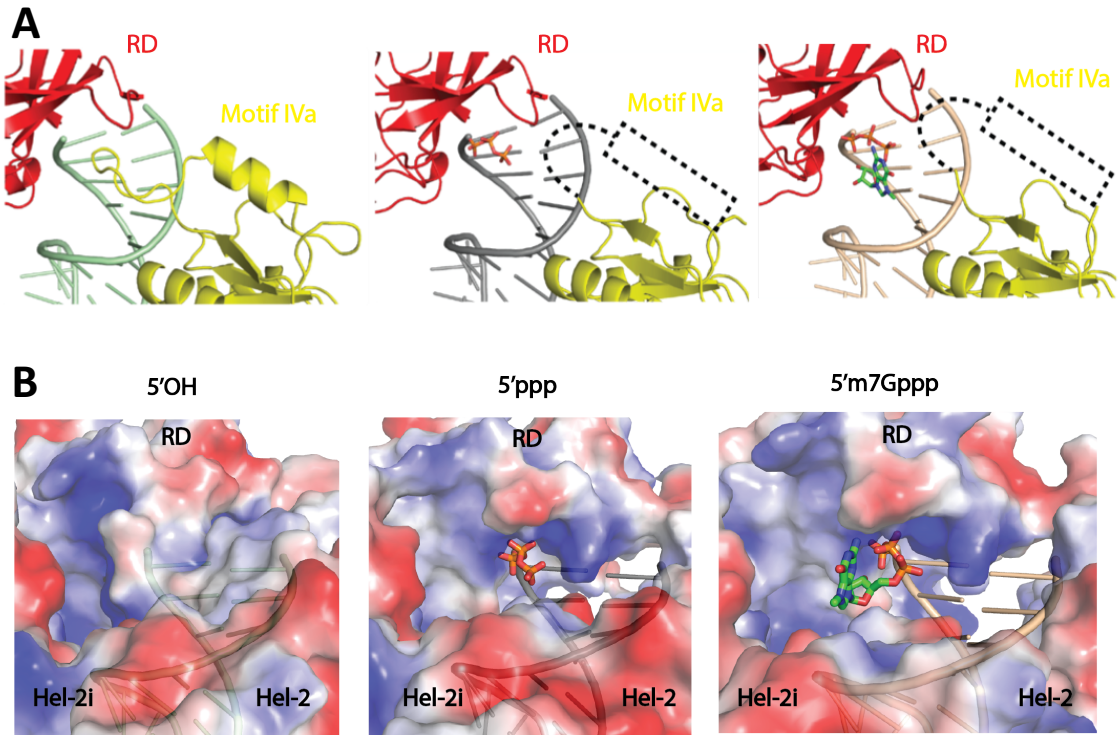

Figure 9. The Conformational Change of Helicase Motif IVa in Three Structures. (A) Magnified view of Hel-2 and RD interaction with 5'OH HP RNA (Left), 5'ppp HP RNA (Center), and Cap-0 HP RNA (Right). The Hel-2 loop-helix region (664-685) in the helicase motif Iva is ordered in the presence of 5'OH and disordered (dashed line) in the presence of 5'ppp and Cap-0. (B) Molecular surface of Helicase-RD in the presence of 5'OH HP RNA (Left), 5'ppp HP RNA (Center), and Cap-0 HP RNA (Right) colored for electrostatic potential. The view is identical to (A). Disruption of the Hel-2 loop and helix creates a pocket for the ppp and m7G moieties.

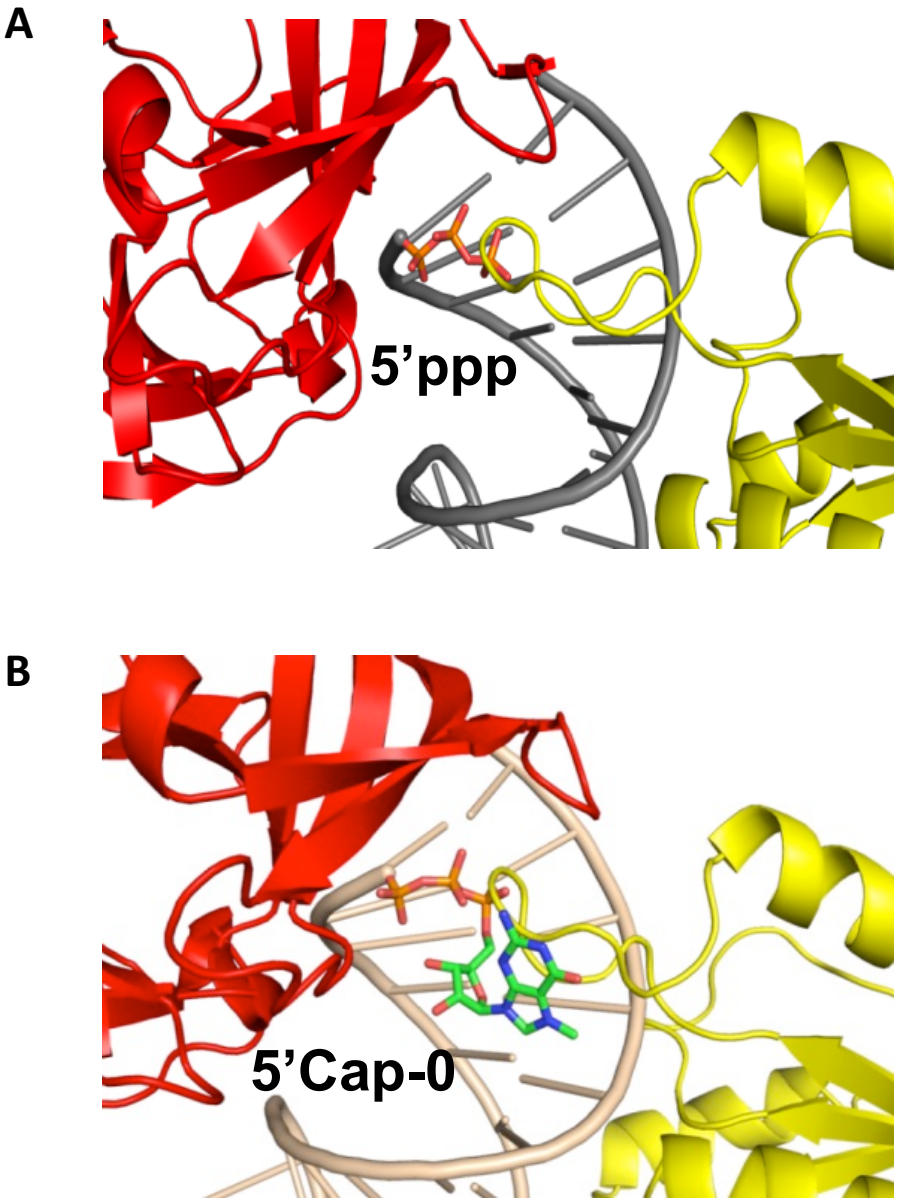

Figure 10. Superimposition of Motif IVa in 5’OH Structure with 5’ppp and Cap-0 HP RNAs. Crystallographic structure of Helicase-RD with 5'OH HP RNA overlayed on the Helicase-RD-5'ppp HP RNA structure (A) and Helicase-RD-Cap-0 HP RNA structure (B) showing the steric clash of Hel2 extended loop-helix (673-685) formed in presence of 5'OH with the 5'ppp and m7Gppp moiety of 5'ppp and Cap-0 HP RNA respectively.

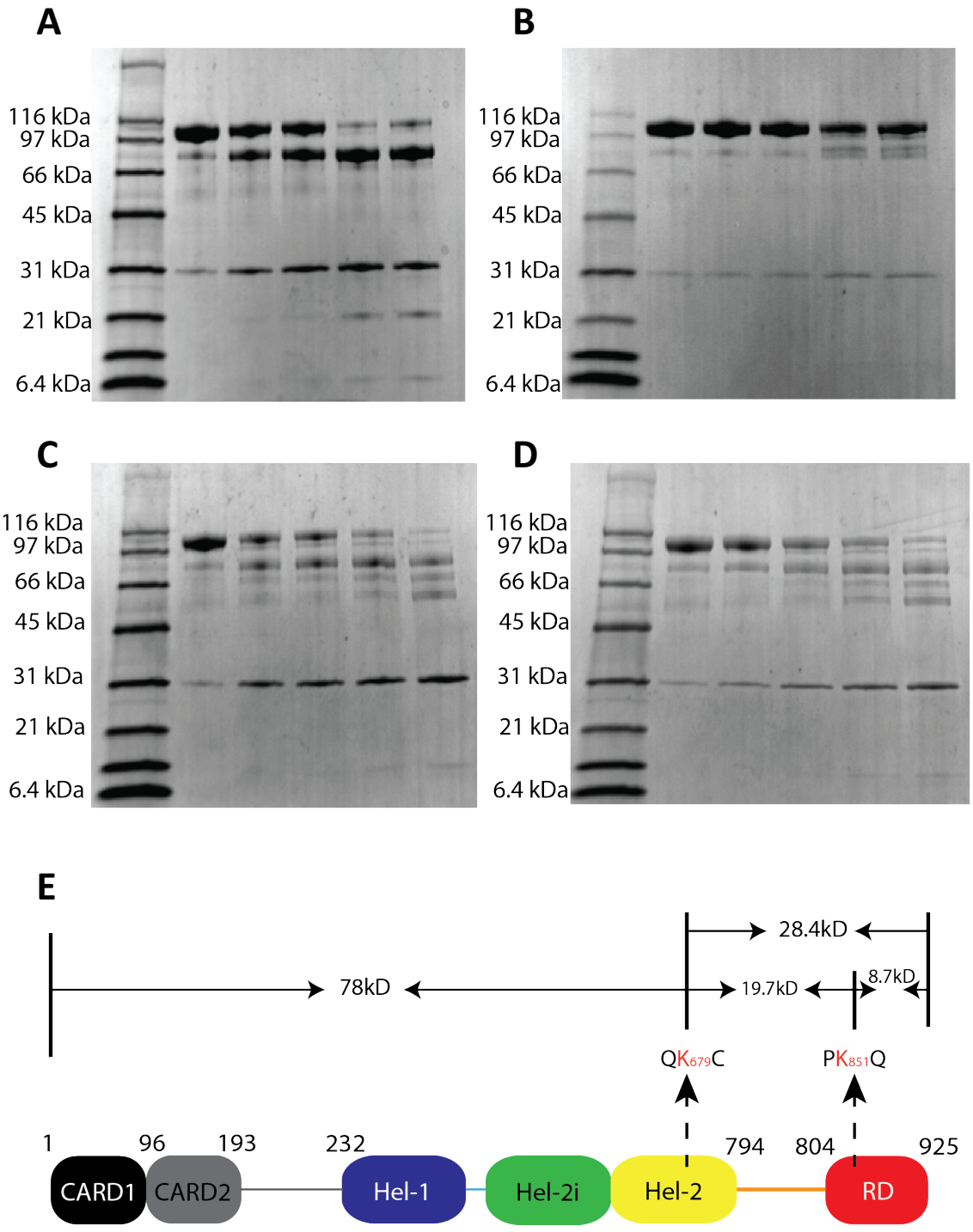

Figure 11. Trypsin Limited Proteolysis of FL RIG-I with and without Different RNAs. (A) FL RIG-I without RNAs (B) FL RIG-I with 5'OH HP RNA (C) FL RIG-I with 5'ppp HP RNA (D) FL-RIG-I with Cap-0 HP RNA (E) Schematic map of RIG-I trypsin digestion sites and sizes of predicted products.

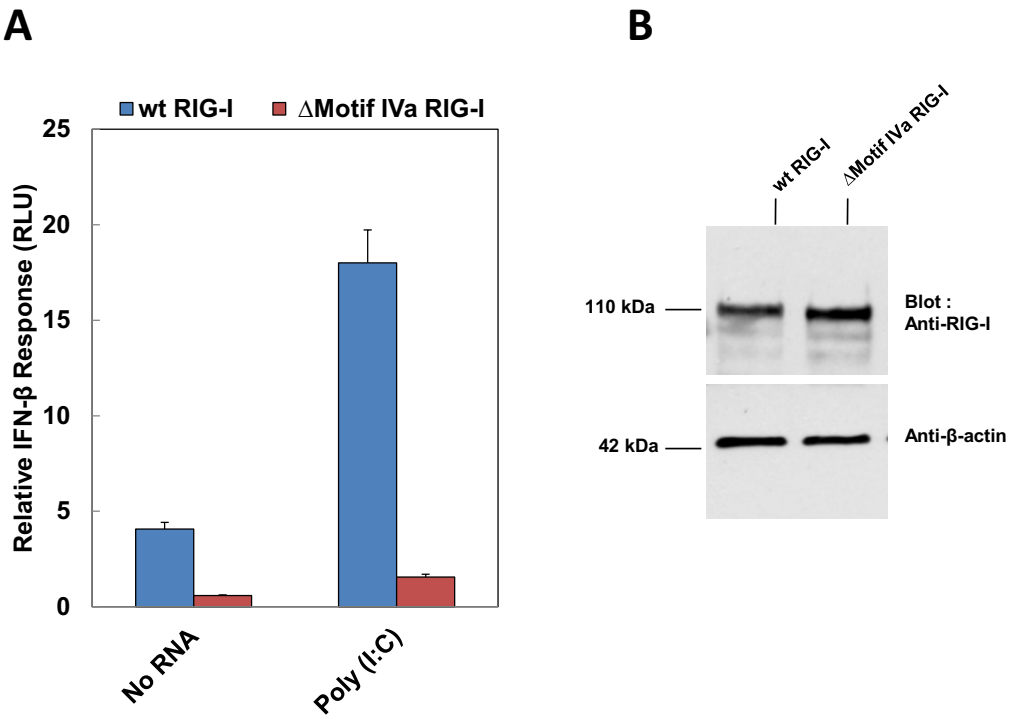

Figure 12. The Deleterious Signaling Effect of Deletion of Motif IVa in RIG-I. (A) IFN response of WT RIG-I and the Motif IVa deletion mutant (Δ673-685) for Poly(I:C) as well as their respective background signal is shown (B) Western blots for WT RIG-I and the Motif IVa deletion mutant (Δ673-685) as well as their respective loading controls (β-actin) are shown. Assay performed by Dr. Swapnil Devarkar.

1.d RIG-I Accommodates the m7G Cap

The HP RNAs in three structures only show an rmsd of 0.6 Å for similar backbone atoms indicating essentially identical conformations (Figure 13A). The triphosphate moiety is recognizable in all copies of the 5'ppp and Cap-0 HP RNA based on the electron density and superimpose well (Figure 13B). In contrast to triphosphate, the position of m7G in Cap-0 HP RNA is relatively unpredictable. The riboses of m7G have interpretable density although their positions vary. However, only three out of six complexes in the asymmetric unit show

discernable density for the bases (Figure 14). This is possibly resulted from crystal packing. Furthermore, the positions of three bases with density are quite different, indicating that the base is highly flexible. And no conserved interactions with the m7G moiety are observed (Figure 15). Interactions with triphosphate moiety in both 5'ppp and Cap-0 structures are conserved as reported before (Figure 16, Figure 17). However, in contrast to structures of RD with 5'pp 12-bp dsRNA (PDB ID 3NCU) and Helicase-RD with 5'ppp 8-bp HP RNA (PDB ID 4AY2), the gamma phosphate is in close proximity to K858 in both 5'ppp and Cap-0 HP RNA structures. This interaction was reported in the structure of RD with 5'ppp 14bp dsRNA (PDB ID 3LRN). To conclude, RIG-I can accommodate m7G modification without specific interactions that were emphasized in cap binding proteins, such as eIF4E. Taking all together, the structural data agrees with the biochemical analysis that RIG-I treats 5'ppp and Cap-0 HP RNA equally.

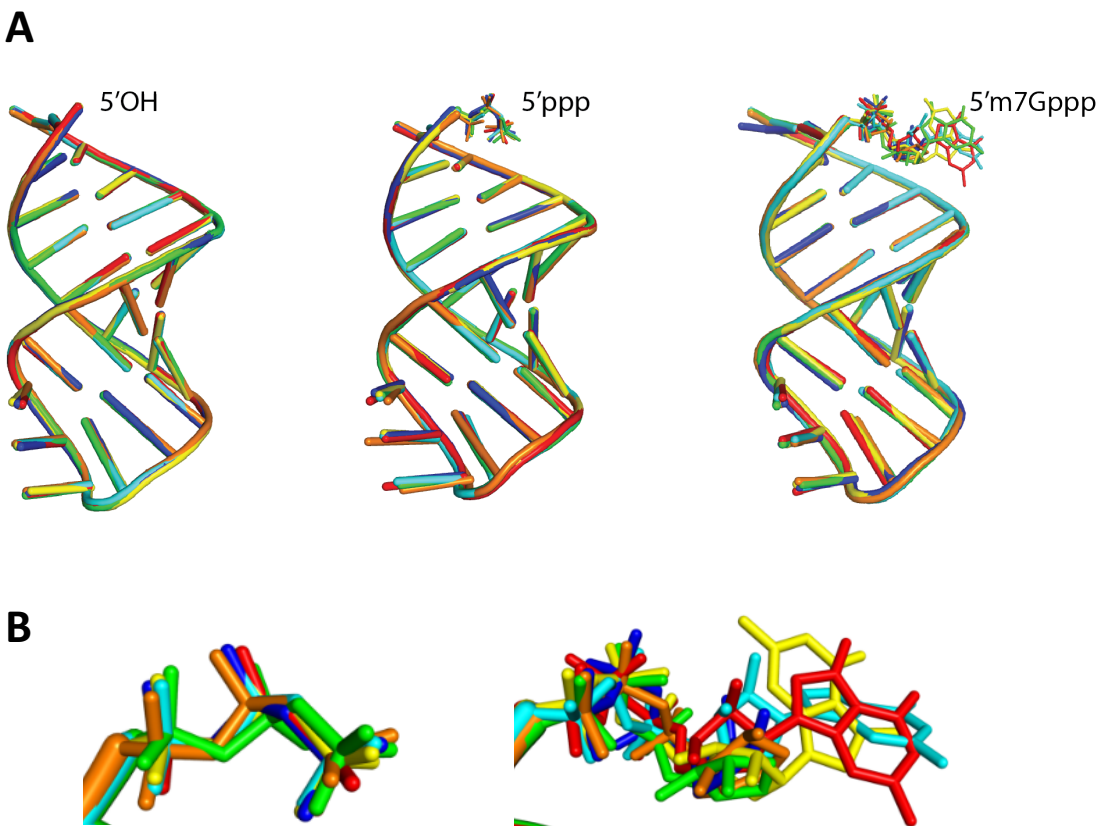

Figure 13. Superimposition of HP RNAs from Six Complexes in One Asymmetrical Unit. (A) Superimposition of 5′OH HP RNA (Left), 5′ppp HP RNA (Center), and Cap-0 HP RNA (Right). (B) Magnified view of the overlaid 5′ppp (Left) and m7Gppp (Right) moiety from A.

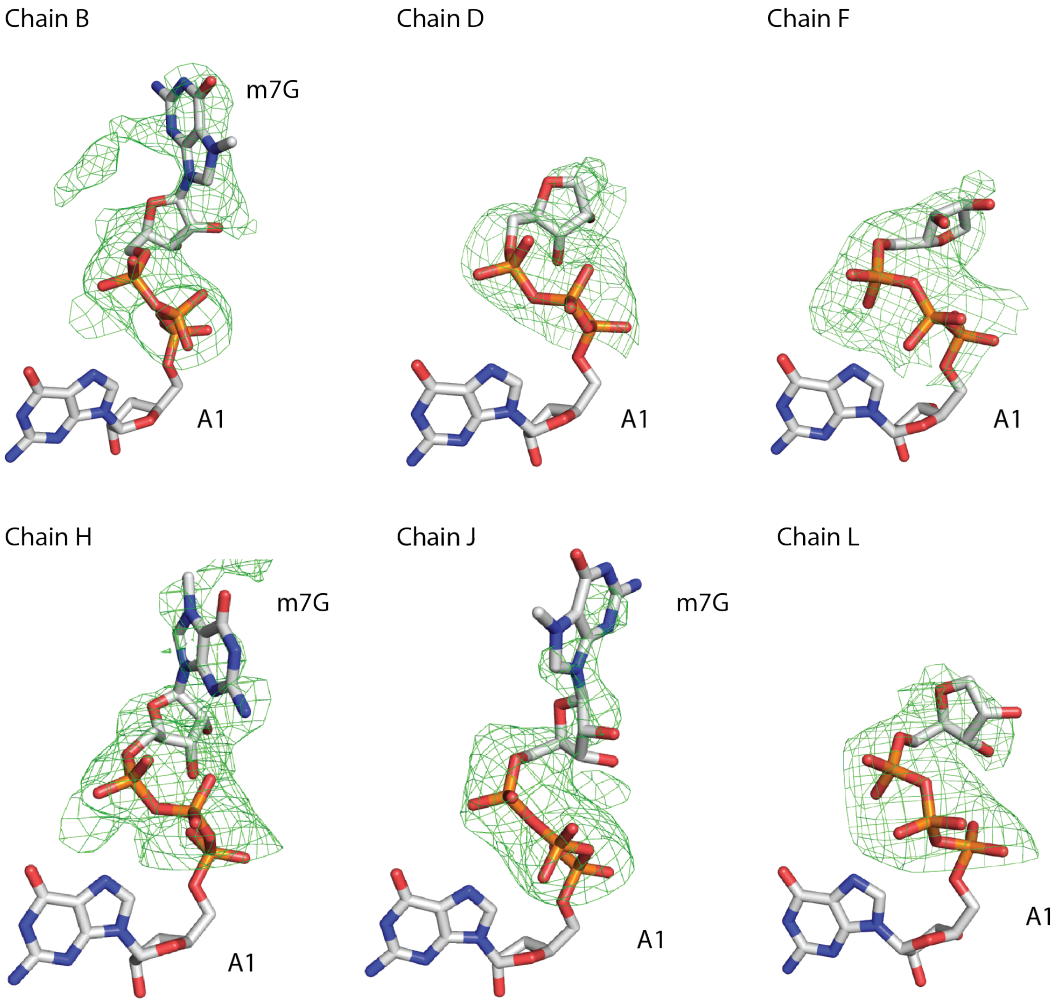

Figure 14. Fo-Fc Omit Density Map of m7Gppp Moieties in One Asymmetric Unit. F_o-F_c omit density map calculated without the triphosphate, ribose and m7G moieties; and overlaid with the 5' end of the RNAs from the model. The first adenine of the double-stranded portion (A1), which was included in the model, is shown for orientation purposes. The map is contoured at 2.3σ.

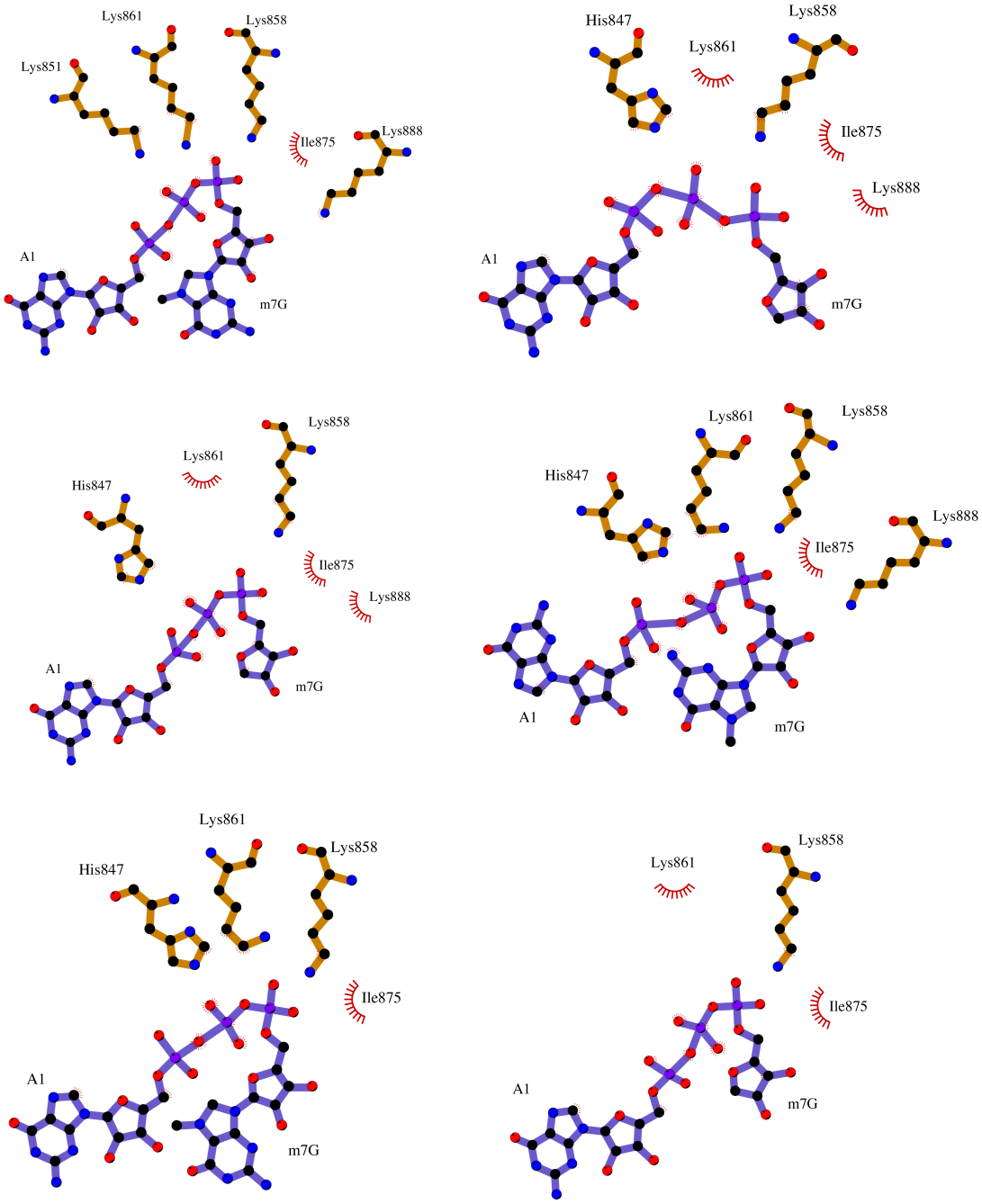

Figure 15. Schematic Diagram of Conversed Interactions to 5' End. RIG-I Helicase-RD residues within 3.6 Å of 5' end of the RNA for all six complexes in the asymmetric unit are highlighted. RIG-I Helicase-RD contacts the triphosphate without any specific interactions with m7G base. Given the conformational flexibility of the caps in the six complexes, certain triphosphate contacts are further than 3.6 Å, and therefore are not shown.

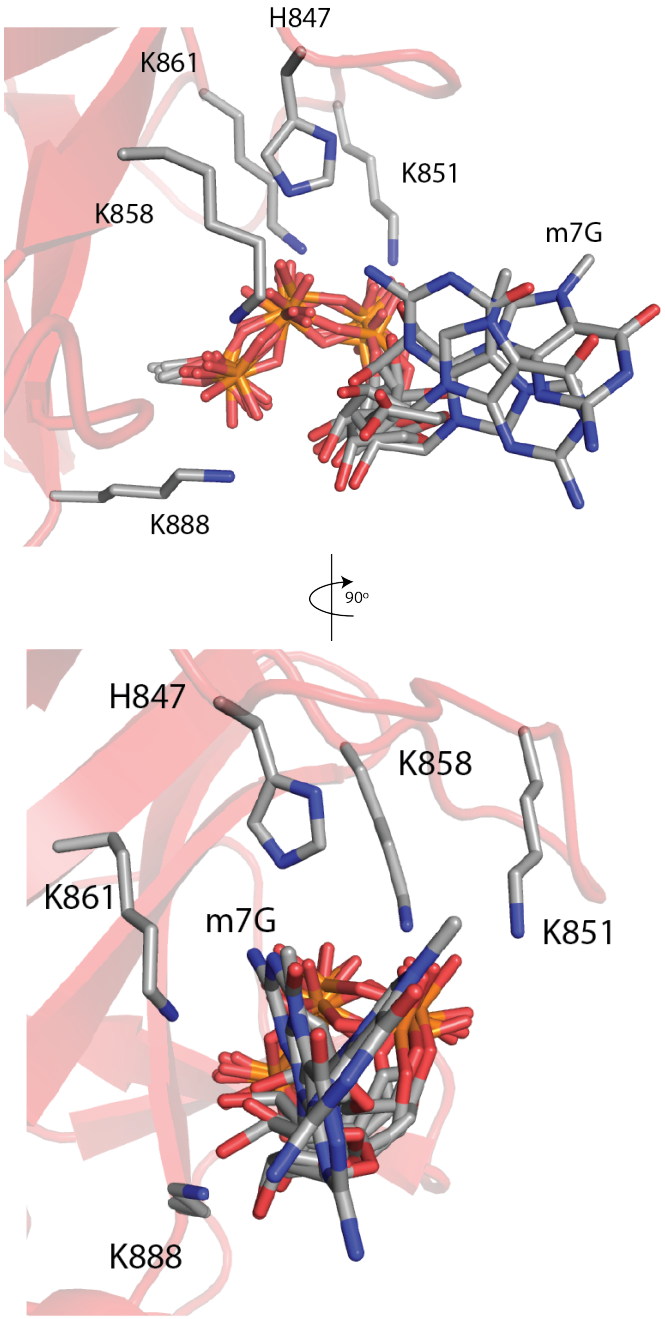

Figure 16. Interactions of RIG-I with the 5'm7Gppp Modifications.
Superimposition of the m7Gppp moiety from the six complexes of the asymmetric unit is shown. Highlighted are conserved contacts within 4 Å of the m7Gppp moiety. The view at bottom is rotated 90° around a vertical axis.

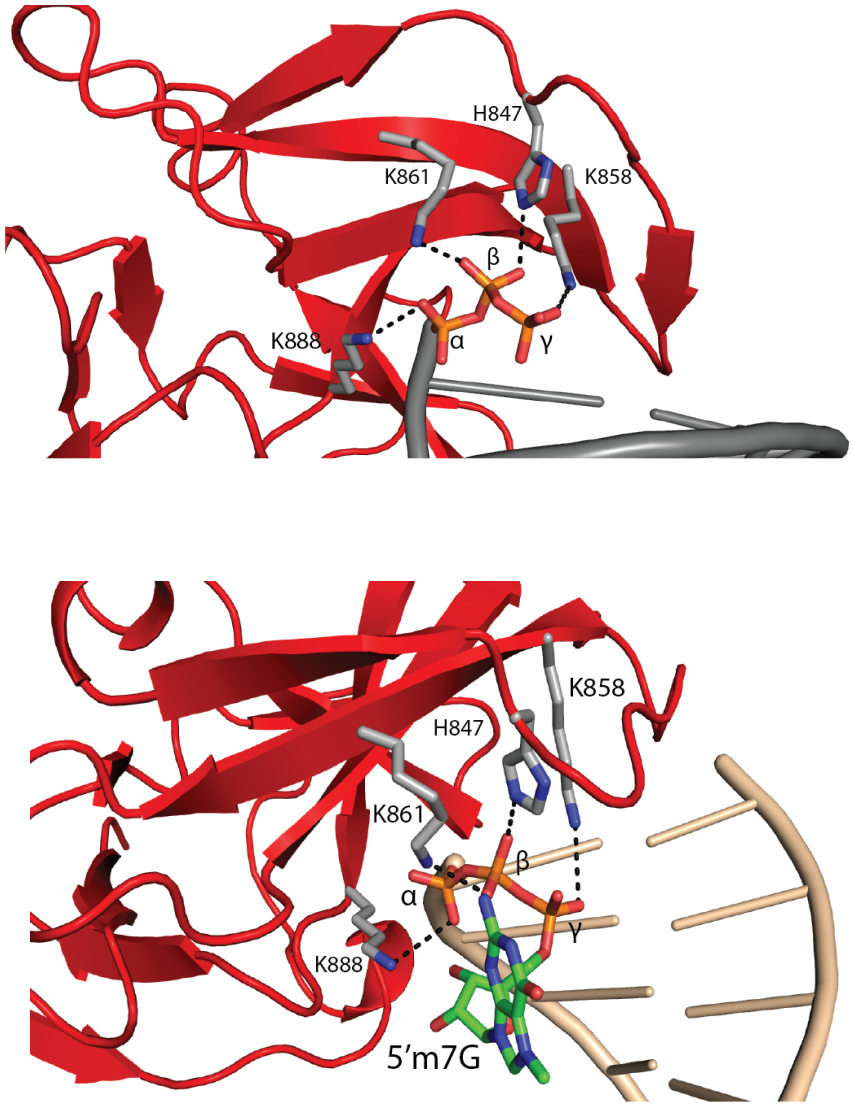

Figure 17. Interactions of RIG-I with the 5'ppp and 5'm7Gppp Modifications. Magnified view of the protein contacts of the 5'ppp moiety in the 5'ppp HP (Top) and Cap-0 HP (Bottom) RNA structures.

2. Mechanism for 2'-O-methylation Discrimination by RIG-I

2.a 2'-O-methyaltion Effect

m7G modification is not the critical point of RIG-I discrimination. Keeping cap structures in mind, we noticed that the 2'OH of the first nucleotide ribose at the 5' end of RNA is very close to histidine 830 (H830) (Figure 18). In eukaryotes, the higher the organism is, the more complicated form of cap structures it has, meaning higher eukaryotes usually carry cap1 or cap2 in RNAs which contain additional 2'-O-methylation of the first and second nucleotide ribose. Due to the limit space between 2'OH and H830, the 2'-O-methylation would clash with the histidine residue. Therefore, we decided to determine the effects of 2'-O-methylation of the first nucleotide ribose of the 5'ppp and Cap-0 HP RNAs on the binding affinity and ATPase activity of RIG-I. Consistent with our prediction, The 5'ppp HP RNA with 2'-O-methylation (5'ppp 2'-OMe) showed an about 20-fold lower binding affinity ($K_{d,app}$=40 nM) and two fold lower ATPase hydrolysis rate (k_{atpase} = 12s^{-1}) compared with 5'ppp HP RNA (Figure 19). 2'-O-methylated Cap-0 (Cap-1) HP RNA exhibit a dramatically 200-fold decrease in binding affinity ($K_{d,app}$ = 425 nM) and two-fold lower ATPase turnover rate (k_{atpase} = 15 s^{-1}) (Figure 19and Table 3). The significant difference in binding affinities indicates a synergistical effect between m7G and 2-O-methylation to lower RNA binding affinity.

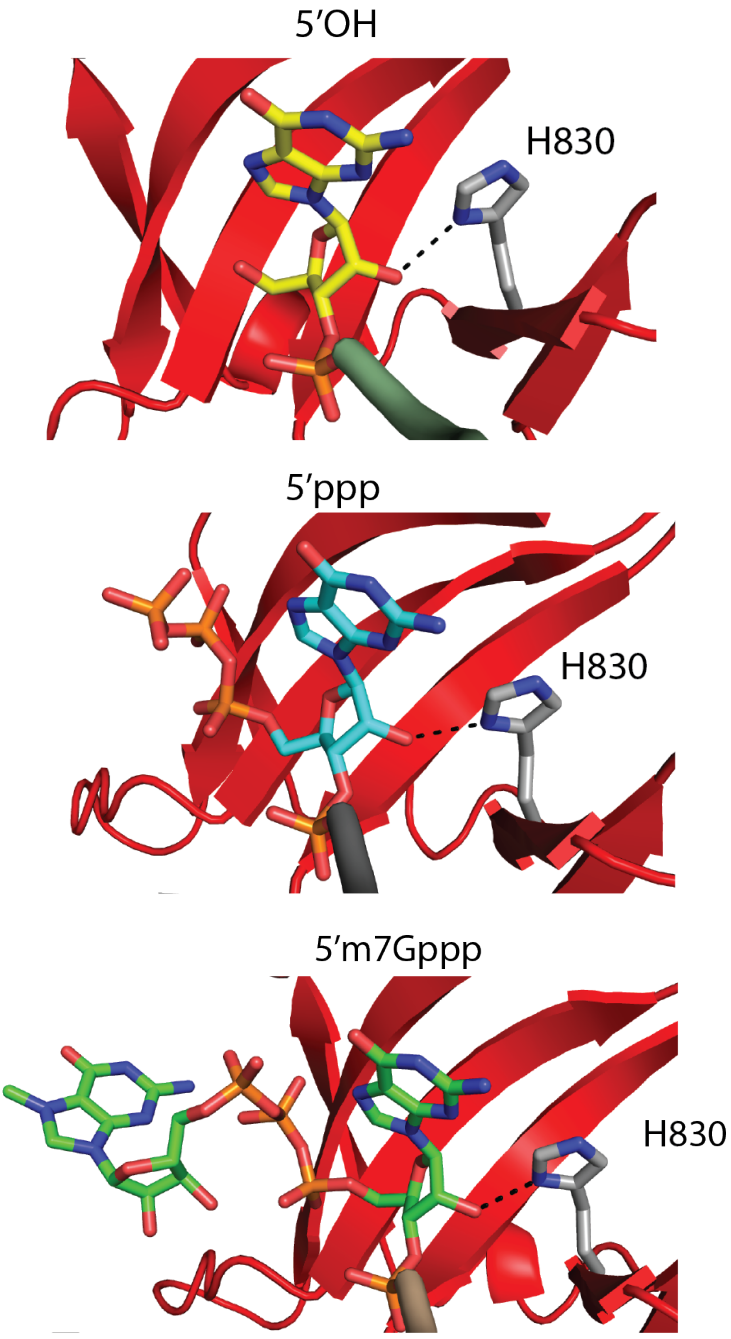

Figure 18. Interaction of the 2′-OH of the First Nucleotide with H830. The interaction is conserved in structures of 5′OH (Top), 5′ppp (Middle), Cap-0 (Bottom) HP RNAs.

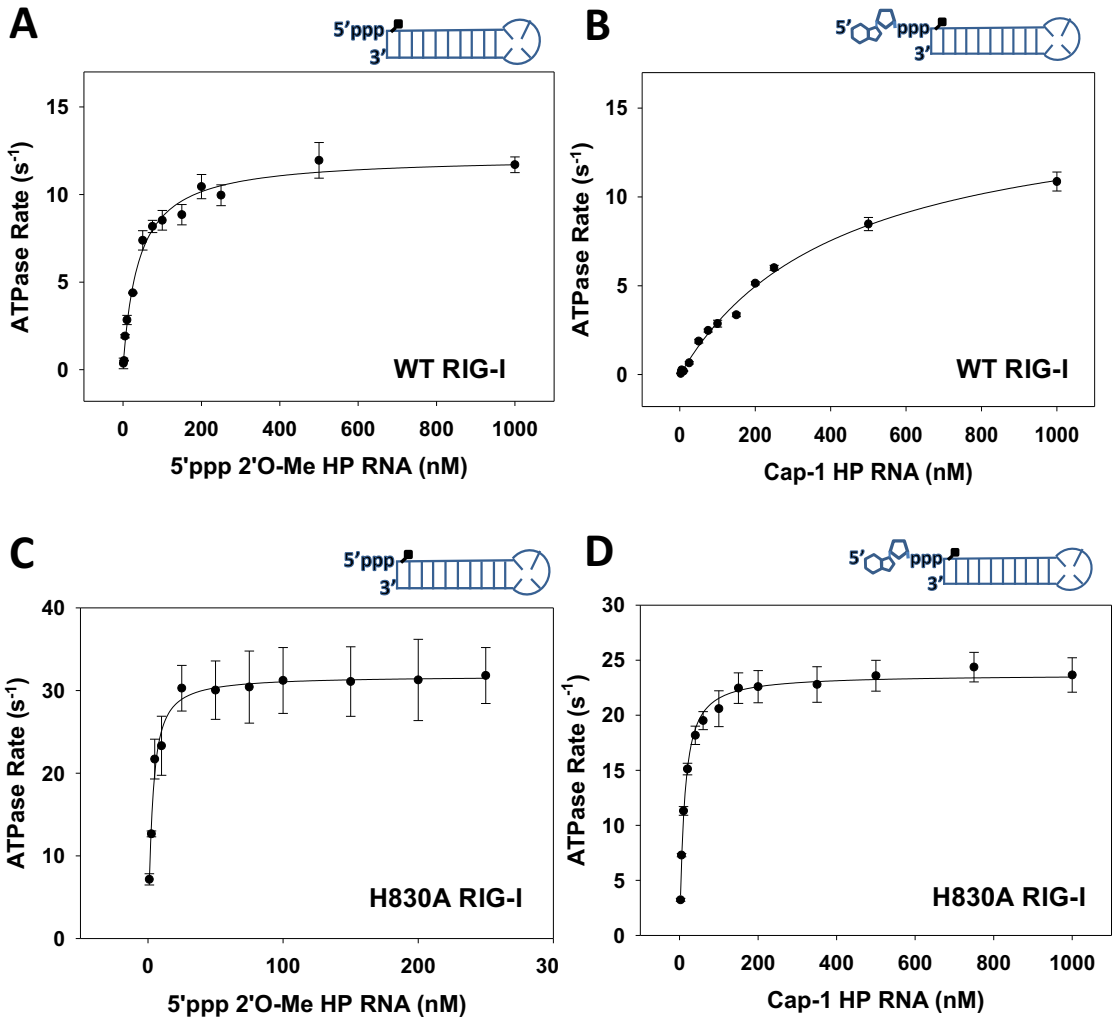

Figure 19. K_d and ATP Hydrolysis Rate of RNA Complexes with WT and H830A RIG-I. The ATP hydrolysis rate of WT RIG-I is plotted against increasing concentrations of 5'ppp 2'-OMe HP RNA (A) and Cap-1 HP RNA (B). The ATP hydrolysis of RIG-I H830A is plotted against increasing concentrations of 5'ppp 2'-OMe HP RNA (C) and Cap-1 HP RNA (D).

Table 3 The measured $K_{d,app}$ and k_{atpase} values of WT RIG-I and H830A RIG-I for the indicated RNAs is presented.

	WT RIG-I		H830A RIG-I	
RNA Ligand	$K_{d,app}$(nM)	k_{atpase} (s^{-1})	$K_{d,app}$(nM)	k_{atpase} (s^{-1})
5'ppp HP RNA	1.8 ± 0.9	33 ± 0.9	1.6 ± 1.9	34 ± 1
5'ppp 2'-OMe HP RNA	40 ± 6	12 ± 0.4	2.3 ± 0.7	32 ± 0.5
Cap-0 HP RNA	1.7 ± 0.5	25 ± 0.4	1.9 ± 0.5	22 ± 0.4
Cap-1 HP RNA	425 ± 50	15 ± 0.7	9.5 ± 2	24 ± 0.3

2.b H830A in Biochemical Assays

2'-O-methylation shows a significant effect on RIG-I binding and ATPase activity, which is effective through the interaction, probably H830. Next, we decided to determine the role of H830 by mutating this histidine to an alanine. The reason of this mutagenesis is that alanine has very small side chain which potentially provide more space for the methylation of 2'OH since we predicted the steric hindrance is the cause of lower binding affinity. As we expect, in contrast to WT RIG-I, H830A showed similar binding affinities with 2'-O-methylated HP RNAs (5'ppp 2'-OMe HP RNA and Cap-1 HP RNA) and unmethylated ones (Table 3). The ATPase turnover rate reached wild-type level. Accordingly, H830A mutation rescues the effect of 2'-O-methylation. We also noticed that V886 is close to the 2'OH group of the first 5' end nucleotide ribose. However, H830A V886 double mutant did not enhance rescue effect (Figure 20). As a result, H830 serves as the primary sensor for 2'-O-methylation on the first nucleotide ribose in Cap-1 RNAs.

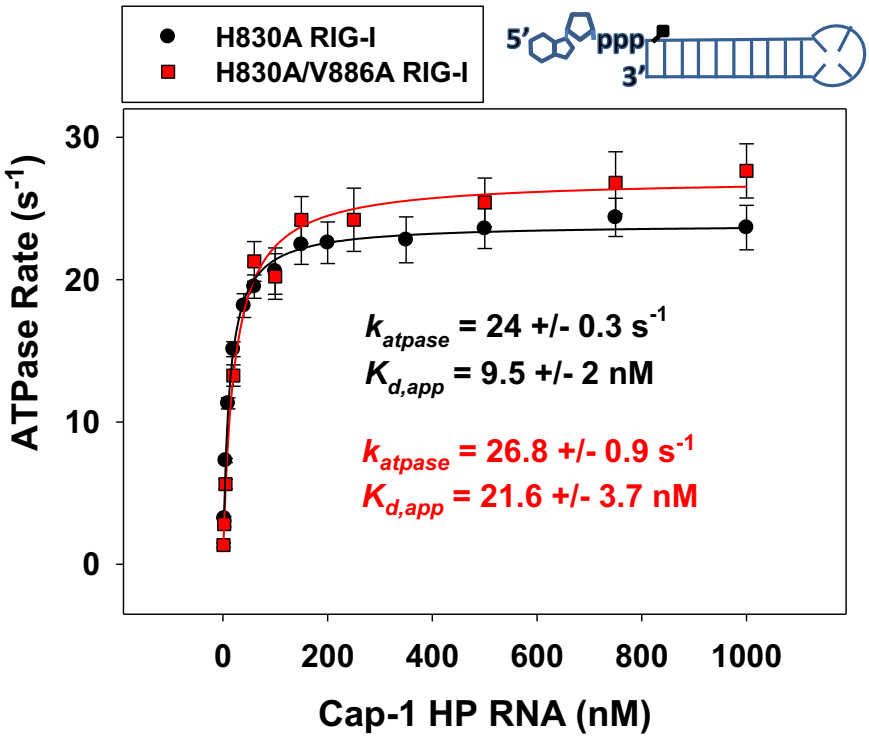

Figure 20. Binding and ATPase Activity of H830A RIG-I and H830A/V886A RIG-I for Cap-1 HP RNA. The data depicted above is from radiometric ATPase assay wherein a fixed concentration of protein is titrated with increasing concentration of RNA. The curves are fit to the quadratic equation to obtain the k_{atpase} and $K_{d,app}$ values. Error bars are from the time courses of the ATPase rate measurements at each RNA concentration.

2.c Cell-base Signaling Assay

In order to confirm the results from biochemical and structural studies in cellular environment, we tested dsRNA with different 5' end modifications with cell-based signaling assays in HEK293T cells. Studies showed longer RNAs can induce a more robust cell signaling response. The dsRNAs are 27bp long, with various 5' end modifications on one end and a three-nucleotide 5' overhang (5'ovg) on the other end to prevent unwanted binding and signaling. No detectable signal was shown in mock-transfected (empty plasmid) cells after RNA stimulation (Figure 21A). In the case of RIG-I ectopic expression, there is a background signal even in the absence of RNAs, which was subtracted from the signal produced. As low as 5 nM 5'ppp dsRNA

is able to stimulate observable response in cells expressing WT RIG-I based on cellular titration assay (Figure 21B). Cap-0 dsRNA induced similar signaling response. The 5'ppp dsRNA and Cap-0 dsRNA follow an almost identical trend in concentration dependency. These results illustrate that Cap-0 dsRNA can activate RIG-I.

Contrary to Cap-0, Cap-1 dsRNA did not show the high capability of activating RIG-I. The signaling response is substantially low even though 700 nM Cap-1 dsRNA was added. The low signal activity is probably produced by 5'ovg on the other end because 5'ovg dsRNA showed an identical low signaling response. Furthermore, the signaling response of 5'ppp HP RNA was abrogated when a methyl group was added on the 2'OH group of the first nucleotide (Figure 22). All these results are consistent with our biochemical and structural results, demonstrating 2'-O-methylation is the critical modification for RIG-I discrimination but not Cap-0.

Cells expressing H830A RIG-I showed a similar concentration dependency as WT RIG-I in cell-based assays when activated by 5'ppp dsRNA and Cap-0 dsRNA. In contrast to cells expressing WT RIG-I, 5'ppp 2'-OMe dsRNA and Cap-1 dsRNA can trigger signaling response in H830A RIG-I-expressing cells. Interestingly, Cap-0 dsRNA activates H830A mutant to a higher extent than WT RIG-I. Compared with WT RIG-I, H830A RIG-I has a twofold higher background signal when no RNA is added. This is probably due to activation by cellular RNAs since the expression levels of H830A and WT RIG-I are similar. A study also pointed that cellular RNAs activate H830A mutant and that MTr1, a Cap-1 methyltransferase enzyme, suppresses WT RIG-I activation by endogenous RNAs, but has no effect on H830A mutant.

To summarize, the biochemical, structural and cell-based studies together illustrate that H830 residue is crucial for discriminating Cap-0 and Cap-1 RNAs by RIG-I.

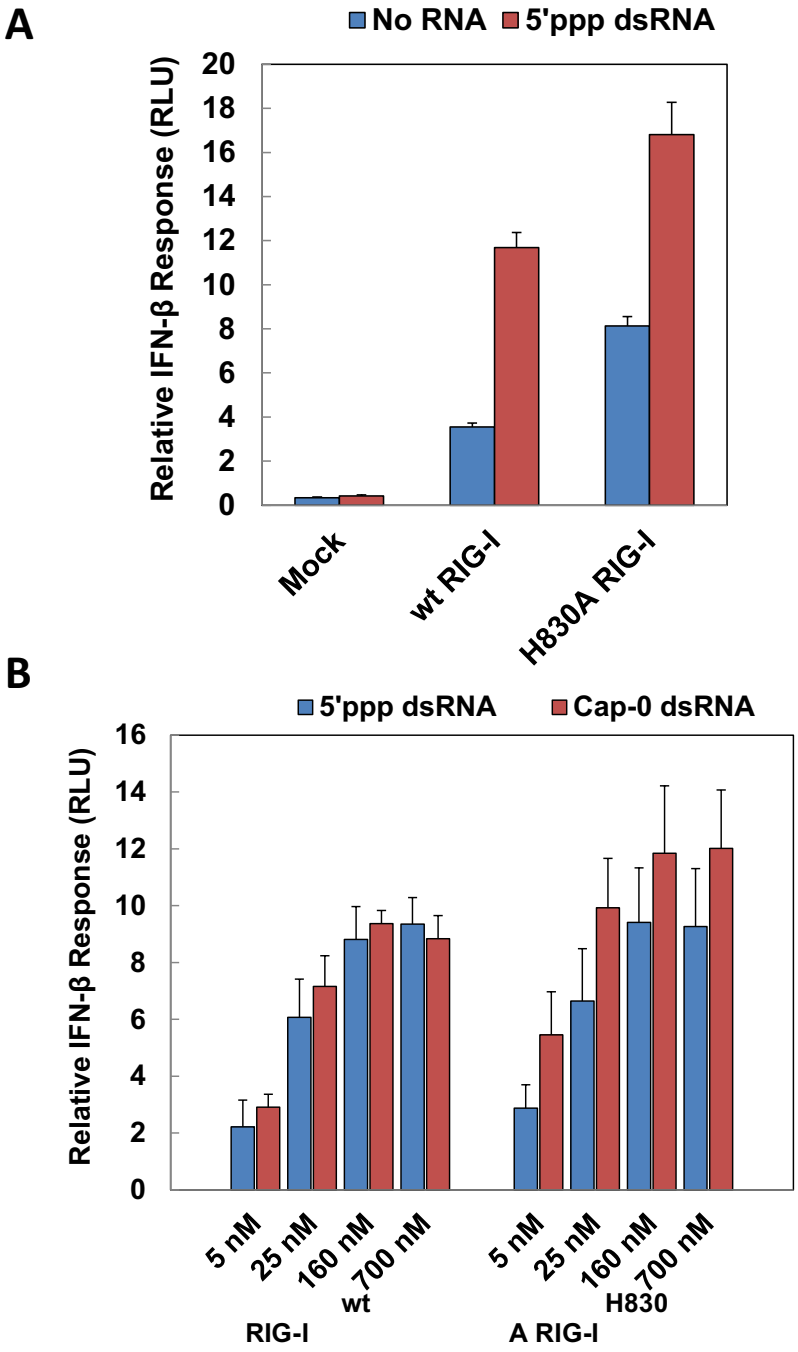

Figure 21. RIG-I Induced IFN Response Activated by RNAs with Different 5' end Modifications. (A) IFN response of mock transfected (empty plasmid), WT RIG-I, and H830A RIG-I for 5'ppp dsRNA as well as their respective background signal is shown. (B) The luciferase signal is plotted as the IFN-β response of WT RIG-I or H830A RIG-I transfected cells stimulated with various concentration of 5'ppp dsRNA (blue bars) and Cap-0 dsRNA (red bars).

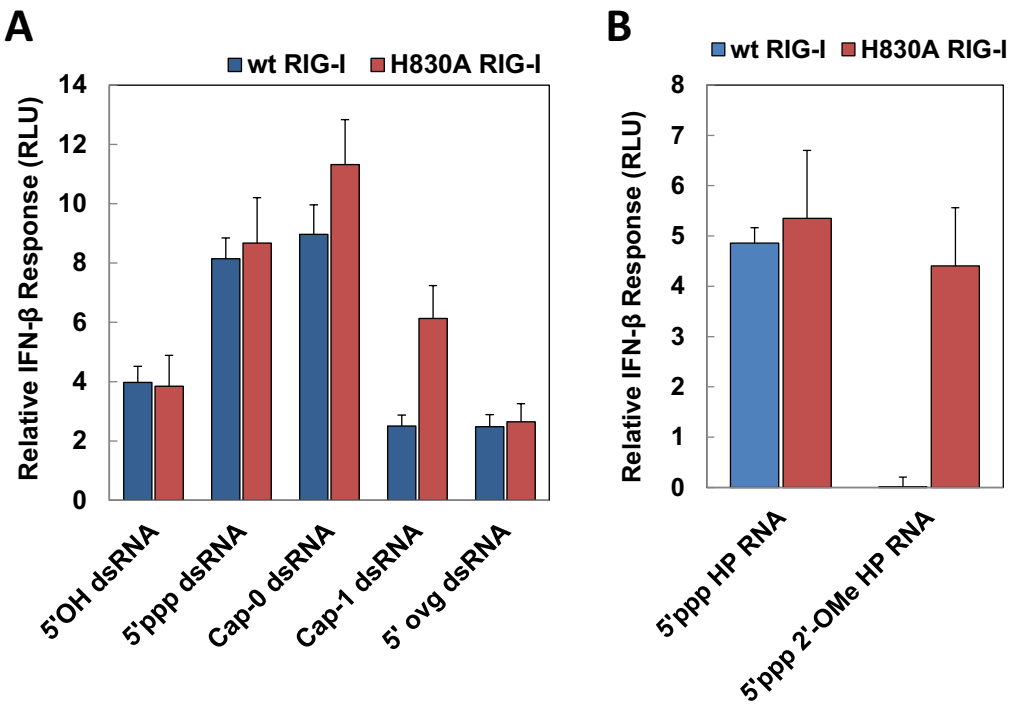

Figure 22. RIG-I Induced IFN Response Activated by RNAs with Different 5' end Modifications. (A) The luciferase signal is plotted as the IFN-β response of WT RIG-I (blue bars) or H830A RIG-I (red bars) stimulated with the indicated RNA ligand. (B) IFN response of WT RIG-I and H830A RIG-I for 5'ppp HP RNA and 5'ppp 2'-OMe HP RNA is shown.

2.d Small Angle X-ray Scattering study

Small angle X-ray scattering (SAXS) is a technique that records the scattering pattern (molecular transform) at a very small angle range (approximately 20 Å). It provides information about the shape and size of particles through two significant parameters: D_{max}, the maximum dimension of particles and radius of gyration (R_g) defined as square root of the sum of square of the distance of all atoms to the center of mass of the particle. The low binding affinity of RIG-I with Cap-1 HP RNA and possible steric clash with 2'-O-methylation give rises to the hypothesis

that RIG-I and Cap-1 form a more "open" conformation. We applied SAXS to test this hypothesis. SAXS data of FL RIG-I in complex with 5'OH HP RNA, FL RIG-I in complex with 5'ppp HP RNA and FL RIG-I in complex with Cap-1 HP RNA was collected and analyzed. The estimated overall size of a protein can be obtained by making Guinier Plot, which gives R_g. The other important parameter D_{max} is calculated from P(r) function (Figure 23A). FL RIG-I with 5'OH HP RNA has a R_g of 34 Å, D_{max} of 115 Å, which is similar to FL RIG-I with 5'ppp HP RNA, R_g of 32 Å, D_{max} 119 Å. Kratky Plots provide information on globularity and flexibility of a protein (Figure 21), a well folded globular protein showing "bell shape" at low q region. Three complexes exhibit an overall globular conformation with partial flexibility. The envelope structures of these two complexes are in a "Drumstick" shape, very alike overall according to superposition of them. However, FL RIG-I with Cap-1 HP RNA has larger parameters: R_g of 40 Å, D_{max} of 140 Å (Table 4). The envelope structures of three complexes was reconstructed with ATSAS package (Figure 24). By superposition, it is obvious that RIG-I in complex with Cap-1 HP RNA envelope structure is larger than the other two, indicating a more "open" and "loose" conformation and shape of this complex (Figure 25). The SAXS data is consistent with our hypothesis, but more detailed interaction between RIG-I and Cap-1 RNA is still required to fully understand the recognition process.

Table 4 Rg and Dmax of FL RIG-I in Complex with 5'OH, 5'ppp, and Cap-1 HP RNA

	R_g (Å)	**D_{max} (Å)**
FL RIG-I + 5'OH	34	115
FL RIG-I + 5'ppp	32	119
FL RIG-I + Cap-1	40	140

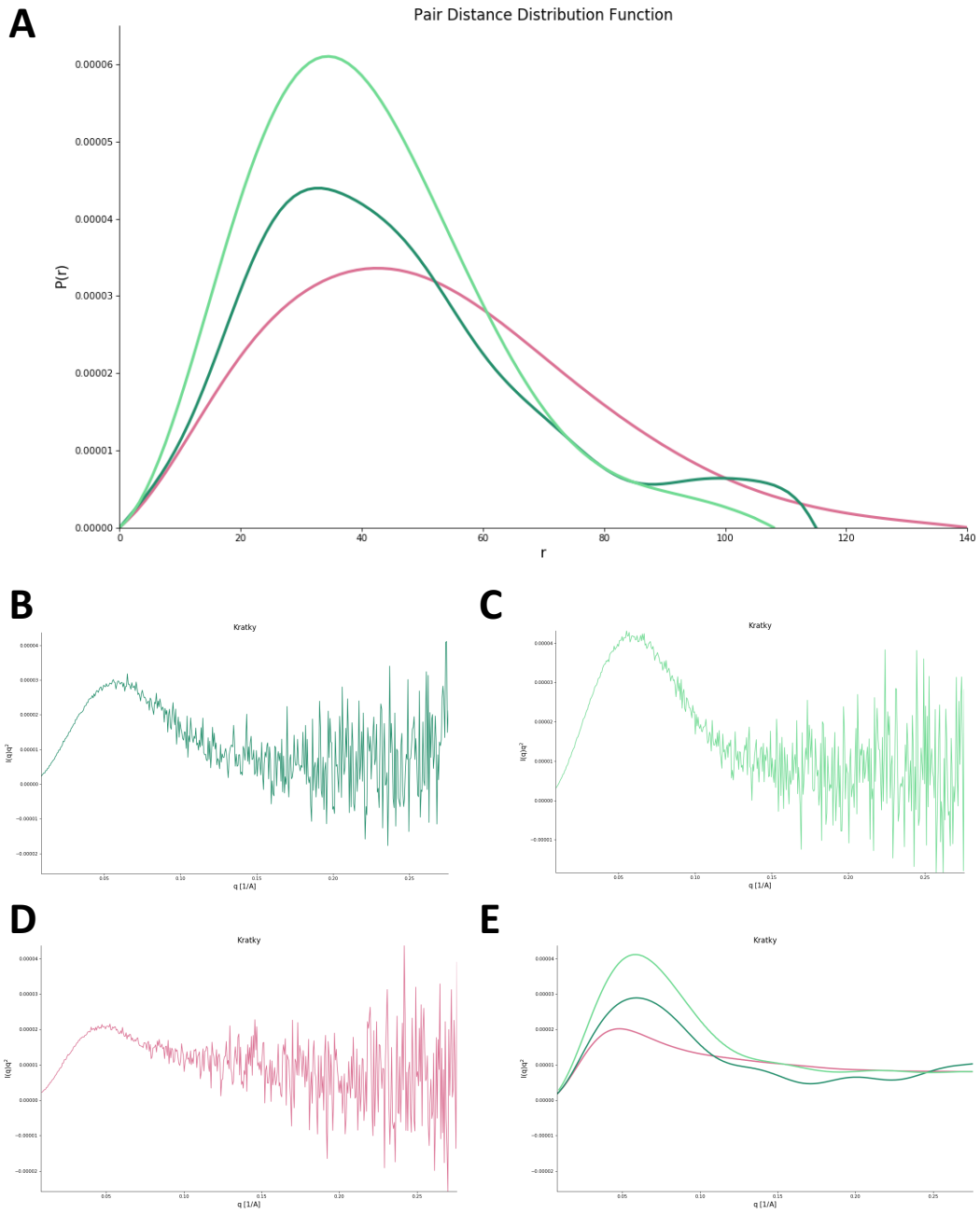

Figure 23. Pairwise Distance Distribution Function and Kratky Plots of RIG-I with Different RNAs. (A) Pairwise Distance Distribution Function shows R_g (r) plotted against the P(r) for RIG-I in complex with 5'OH HP RNA (dark green), 5'ppp HP RNA (light green) and Cap-1 HP RNA (pink). (B-D) Kratky Plots of scattering for RIG-I in complex with 5'OH HP RNA (B), 5'ppp HP RNA (C) and Cap-1 HP RNA (D). (E) Superimposition of the fit lines of Kratky Plots of three complexes.

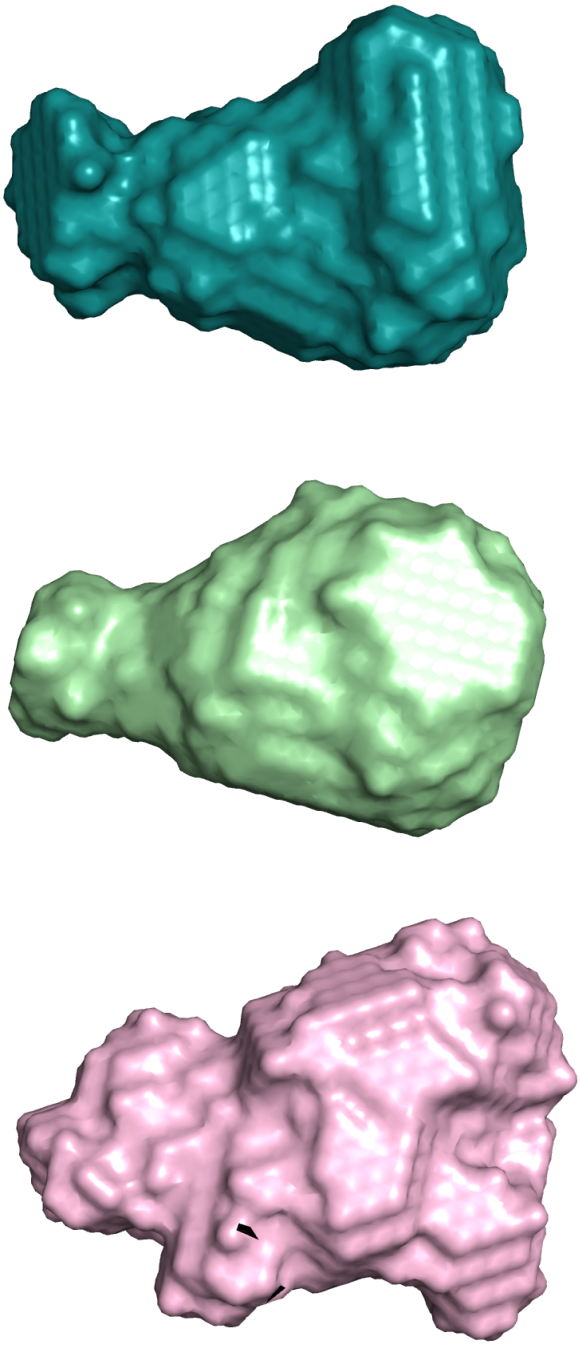

Figure 24. The Low Resolution 3D *ab initio* Envelope Structures of Three Complexes. Envelope structure of RIG-I with 5'OH (Top), 5'ppp (Middle), Cap-1 (Bottom) HP RNAs.

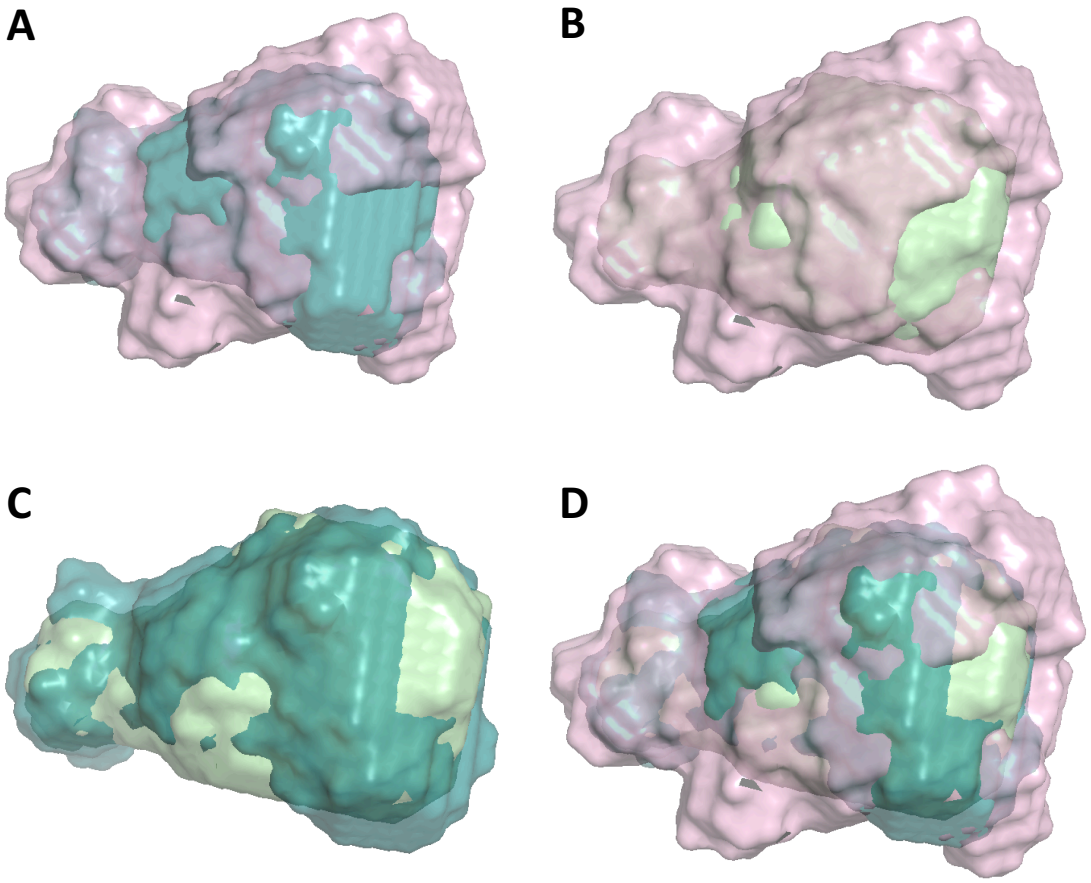

Figure 25. Superimposition of Envelope Structures of RIG-I with 5'OH, 5'ppp, Cap-1 HP RNAs. (A) Superimposition of Cap-1 and 5'OH HP RNA structures. (B) Superimposition of Cap-1 and 5'ppp HP RNA structures. (C) Superimposition of 5'ppp and 5'OH HP RNA structures. (D) Superimposition of all three structures.

2.e RIG-I Helicase-RD-Cap-1 HP RNA Crystallization Trials

RIG-I Helicase-RD in complex with Cap-1 HP RNA was also screened for crystallization studies. Interestingly, crystals appeared in crystallization screening kit PEG Ion (Hampton Research) B1 condition [20% (w/v) PEG 3350, 0.2 M NaSCN and 0.1 M HEPES pH 7.5] initially, same as Cap-0 HP RNA crystals (Figure 26A). However, it only diffracted to 8 Å the most probably due to its relatively loose conformation. Additives are broadly used reagents that can affect the solubility and crystallization of proteins. They can stabilize or create conformity by specific interaction with the proteins. The additives were screened with the Additive Screen Kit (Hampton Research) and a few conditions gave crystals different in morphology (Figure 26 B-G). These additives are 0.1 M ethylenediaminetetracetic acid disodium salt dihydrate, 30% w/v D-sorbitol, or 30% w/v trimethylamine N-oxide dihydrate, 0.1 M TCEP hydrochloride, 0.1 M CdCl2 hydrate and 0.5 M sodium fluoride.

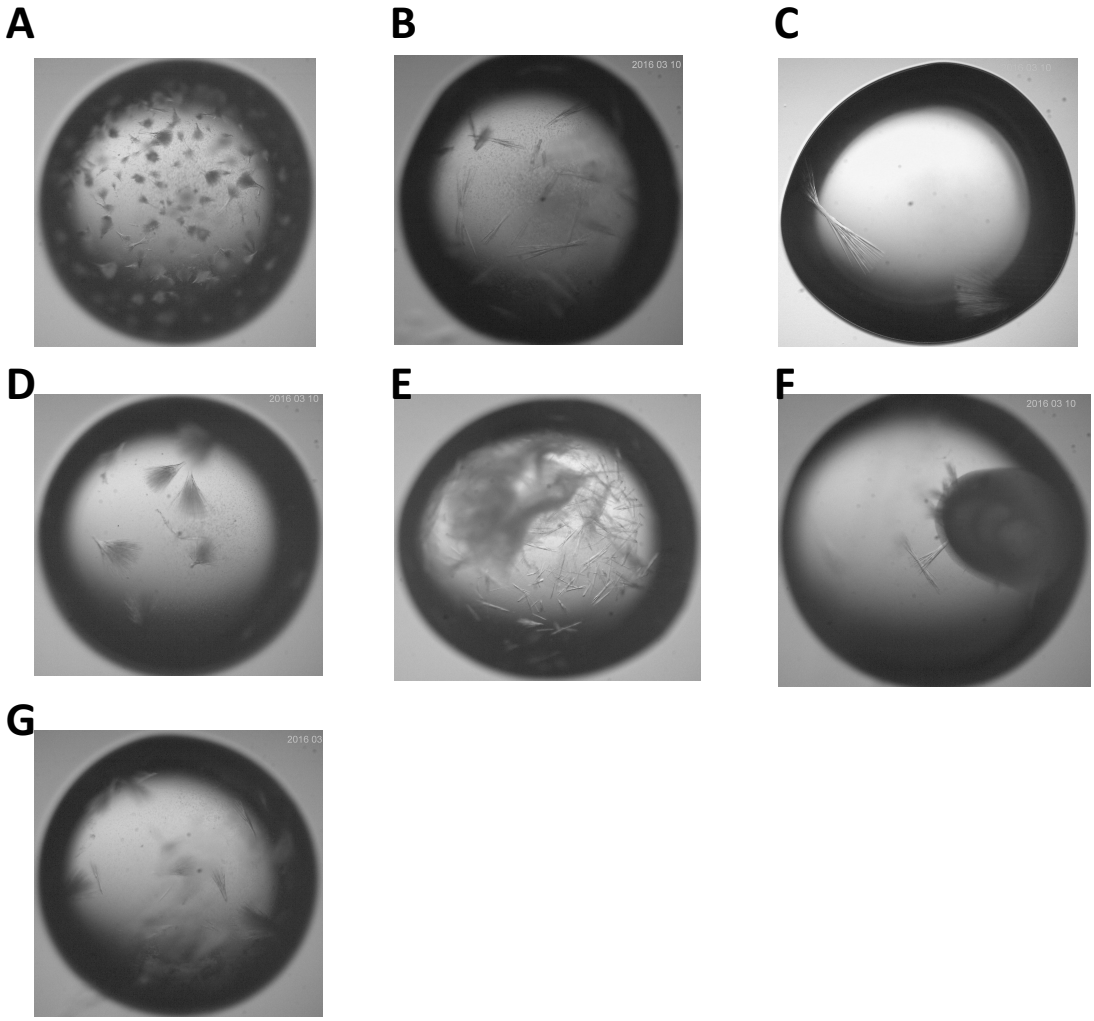

Figure 26. RIG-I Crystals of Helicase-RD-Cap-1 HP RNA Complex. (A) Crystals grow without additive. Crystals grow with 0.1 M Ethylenediaminetetracetic acid disodium salt dihydrate (B), or 30% w/v D-sorbitol (C), or 30% w/v Trimethylamine N-oxide dihydrate (D), or 0.1 M TCEP hydrochloride (E), or 0.1 M CdCl2 hydrate (F) or 0.5 M Sodium Fluoride (G).

3. RIG-I Monoclonal Antibody Generation and Purification

3.a Anti-RIG-I Monoclonal Antibody Generation

Based on the activation model, in the presence of PAMP RNA, RIG-I adopts a conformation wherein the helicase domain and RD form a ring structure around dsRNA. The CARDs are released from interacting with the helicase domain and become flexible and available for ubiquitination and downstream signaling. Due to its high mobility, it is difficult to capture a crystal structure of an activated FL RIG-I in complex with RNA. So we were looking for a method that can specifically fix CARDs, which in turn would benefit FL RIG-I-dsRNA complex crystallization. We generated monoclonal antibodies against RIG-I CARDs, using a commercial vendor (GenScript Biotechnology). Purified RIG-I 1-228 CARDs protein was used as antigen. Mice were immunized with the antigen and the serum from 9 mice were collected after 3rd boost. The serum was tested with ELISA. Each sample was tested with one antigen at three concentrations (5 ug, 2.5 ug, 1.25 ug), PBS-t, GST and HCV E2. PBS-t works as blank control. GST can counter select for samples that has residual GST which was used for purification. An unrelated protein (HCV E2) was used as negative control. Three antigens were used in the ELISA assay: CARDs, FL RIG-I, FL RIG-I in complex with 5'ppp HP RNA in order to select out the antibody that has high affinity to CARDs and capability to bind CARDs on "activated" RIG-I. The ideal candidates are supposed to show response to antigens but neither of the controls, especially not GST control and post-immunization samples show higher response than pre-immunization ones (examples showed in Figure 27, full results showed in APPENDIX III).

Three samples (#3085, #3086 and #3091) out of nine gave results as expected and continued to Phase II cell fusion step. We received supernatant of 56 cell lines after cell fusion. Tested with ELISA assay at similar setup as Phase I (examples showed in Figure 28, full results showed in APPENDIX III), 21 samples were picked for subcloning. They not only met the criteria

from Phase I, but also had slightly higher response against FL RIG-I-RNA complex than FL RIG-I alone, indicating that the antibodies bind the “activated” RIG-I better than the “autoinhibited” RIG-I. Nineteen subcloning cell lines were generated from Phase III, two lost. ELISA results showed they all met the criteria (full results showed in APPENDIX III).

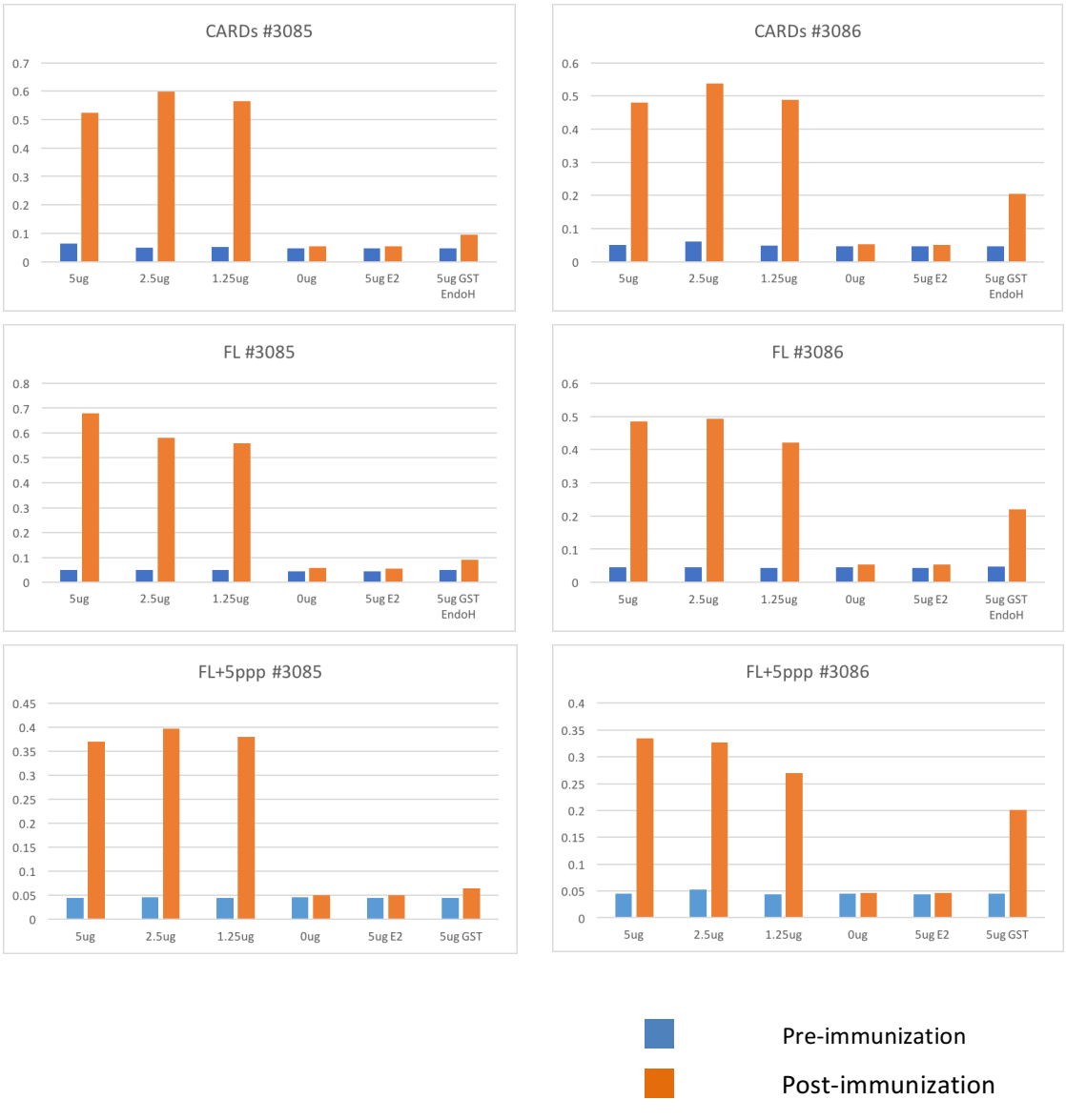

Figure 27. Examples of ELISA Criteria. Sample 3085 (Left panel) meets the criteria showing no response in pre-immunization or with negative controls. Sample 3086 (Right panel) is an example of failing samples. Blue bars represent pre-immunization samples and orange bars represent post-immunization samples.

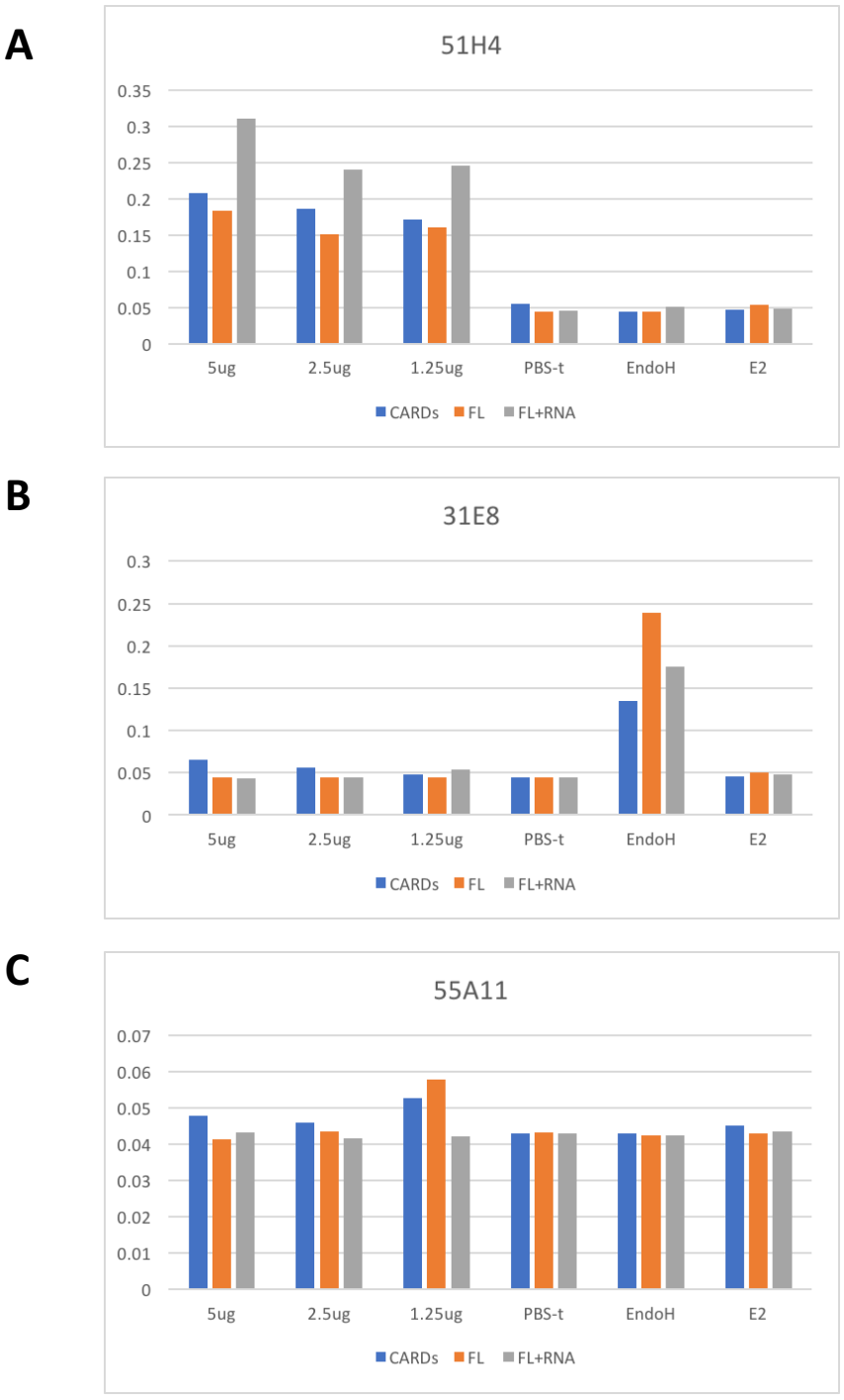

Figure 28. Examples of Phase II Samples. (A) An example of samples passed test with responses specific to antigens not controls. (B) A failure example responded to GST control. (C) A failure example showed no responses. Column colors represent different antigens used in coating plates. Blue represents CARDs, orange represents FL RIG-I, and grey represents FL RIG-I-5'ppp HP RNA complex.

3.b Anti-RIG-I mAb Purification

To further test the quality of the antibodies (Mw = 150 kDa), we picked 38H5-1 as the first sample. After about 10-day growth, the supernatant was collected, filtered and loaded onto a Protein G column (GE healthcare). The elution was analyzed by gel electrophoresis (Figure 29), which has two bands (50 kDa and 25 kDa) corresponding to the reduced products of the antibodies, heavy chain (HC) and light chain (LC) respectively. Next the antibody was digested with papain to cleave off Fc fragments such that Fab fragments can be isolated which contains the V regions responsible for binding antigens. The digestion efficiency is roughly calculated based on the results of 1.5 hour-digestion (Figure 30). Three bands (25 kDa and 50 kDa) were observed in reducing condition representing Fab HC (22 kDa), Fab LC (25 kDa) and Fc (28 kDa). Two bands were observed in non-reducing condition representing Fab (47 kDa) and Fc (56 kDa). The digestion products were passed through Protein A column (GE) to separate Fab fragments because the primary binding site of Protein A is on Fc region (Figure 31). The fractions containing Fab were further purified by Mono Q column (Figure 32).

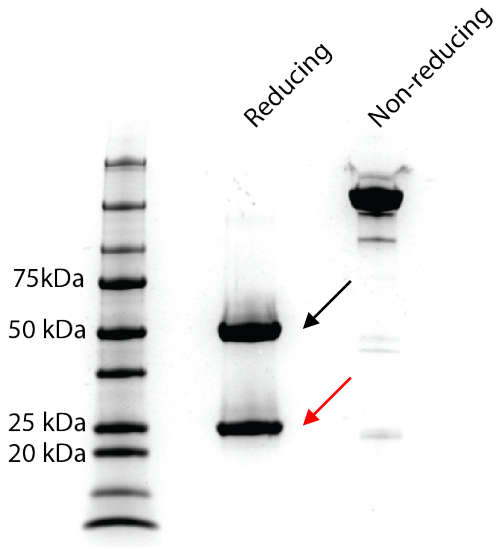

Figure 29. Purification of mAb 38H5-1 with Protein G Column. Heavy chain is denoted with black arrow and light chain is denoted with red arrows.

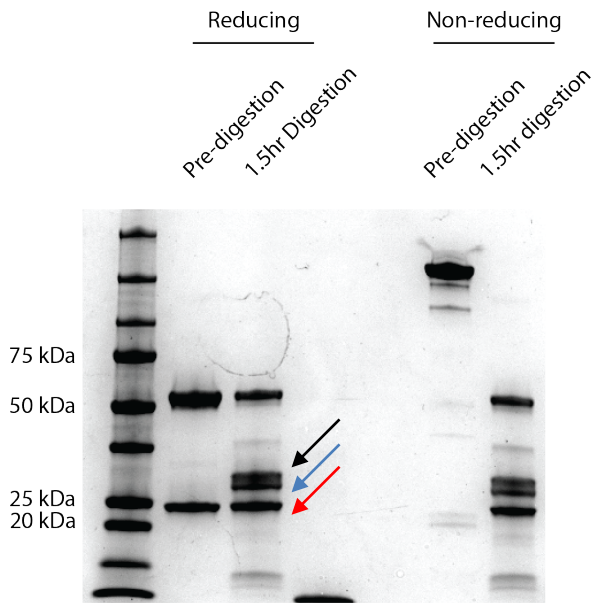

Figure 30. Papain Digestion of 38H5-1 mAb. Fc fragment is denoted with black arrow, Fab HC is denoted with blue arrow and Fab LC is denoted with red arrow.

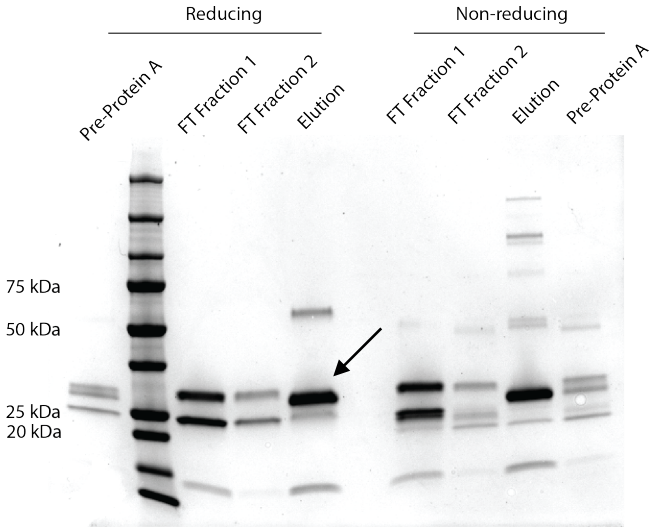

Figure 31. Purification of 38H5-1 mAb with Protein A Column. Fc fragment (black arrow) is eluted from the column and Fab fragment passed out in the FT.

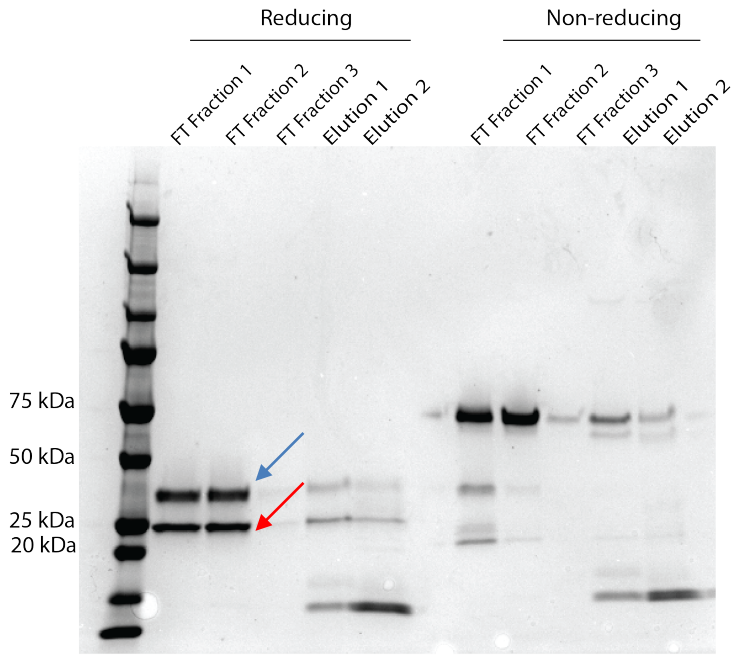

Figure 32. Purification of 38H5-1 mAb with Mono Q Column. Fab fragment is denoted with arrows.

3.c Anti-RIG-I mAb Quality Test

The quality of purified Fab was tested by incubated with FL RIG-I-RNA complex for 30min on ice and passed through size exclusion column. The chromatograph shift should be observed if the antibody and RIG-I-RNA form complexes compared to RIG-I-RNA. However, a shifted peak was not observed, instead, three peaks showed up, corresponding to FL RIG-I, antibody Fab and RNA when compared with these samples' individual chromatographic curves. This result indicates 38H5-1 clone dissembles RIG-I-RNA complex, the reason of which needs further investigation (Figure 33).

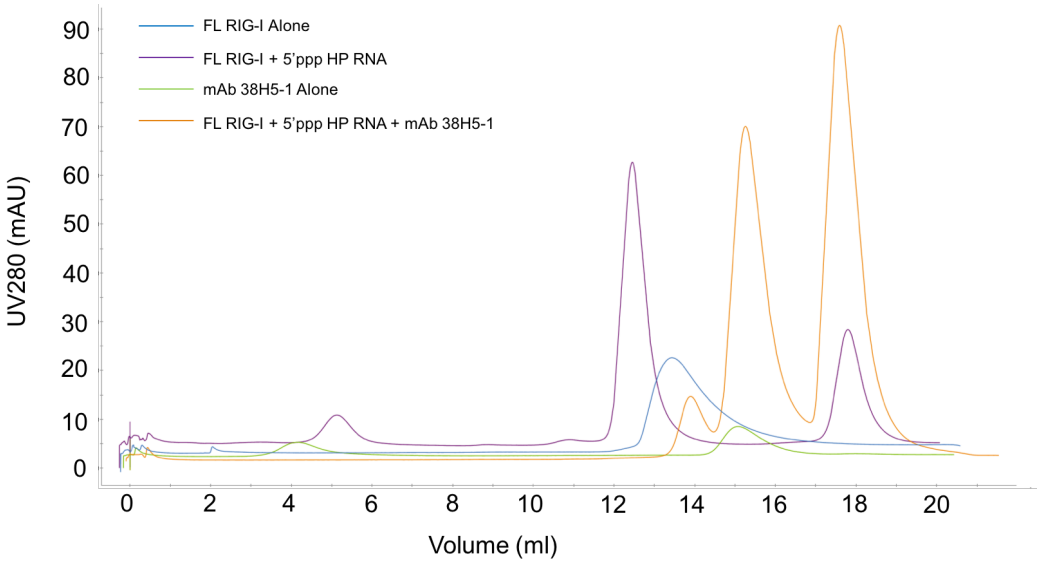

Figure 33. Anti-RIG-I mAb 38H5-1 Size Exclusion Test. The antibody was tested by incubated with FL RIG-I-5'ppp HP RNA complex and passing through size exclusion column (orange). FL RIG-I-5'ppp HP RNA complex (blue) and mAb 38H5-1 (green) were passed through size exclusion column as controls.

4. RIG-I Oligomerization Study

The role of oligomerization in RIG-I activation process is still vague and is probably related to the type of pathogens. ATP hydrolysis is important for RIG-I oligomerization (67). The barrier of studying the structures of RIG-I oligomerization lies in the active ATPase activity of RIG-I. We employed the mutants of full-length RIG-I residue 373 Glutamic acid to Alanine (E373A) and 268 Cysteine to Phenylalanine which are the cause of atypical Singleton-Merton Syndromes (SMS) due to its constant activity of RIG-I. Dr. Swapnil Devarkar, from Dr. Smita's lab designed two chimeric RNA/DNA stem oligo sequences of 26bp and 29bp long (refered as Stem26 and Stem29) that can induce RIG-I dimerization according to the biochemical assays. Then we tested the oligomerization potency of FL RIG-I C268F and E373A by Size Exclusion Chromatography (SEC) in line with Multi-Angle Light Scattering detector (DAWN-EOS Wyatt technology) (SEC-MALS) to identify the estimated Molecular Weight (Mw) of complexes the protein and stem oligos form. Only monomer was observed in the presence of Stem26 probably due to its short length. In

contrast, a fraction coming earlier than the monomer fraction was observed potentially containing the dimers. The calculated Mws of dimer and monomer are 234 kDa and 126 kDa, respectively. In the case of FL RIG-I C268F (Figure 34 and Table 5), the Peak 1 coming before 8 mL (void volume) in volume is considered as the aggregates and the Peak 2 and Peak 3 are very close to each other leading to a poor separation with apparent Mw of 168 kDa and 129.1 kDa, respectively. The second peak is probably a mixture of dimer and monomer. Notably, FL RIG-I E373A with Stem29 complexes show promising results (Figure 35and Table 5). Peak 2 has an approximate Mw of 228.1 kDa and Peak 3 is about 125 kDa. This result matches the predictions of dimer and monomer, making Peak 2 a promising candidate for RIG-I oligomerization study.

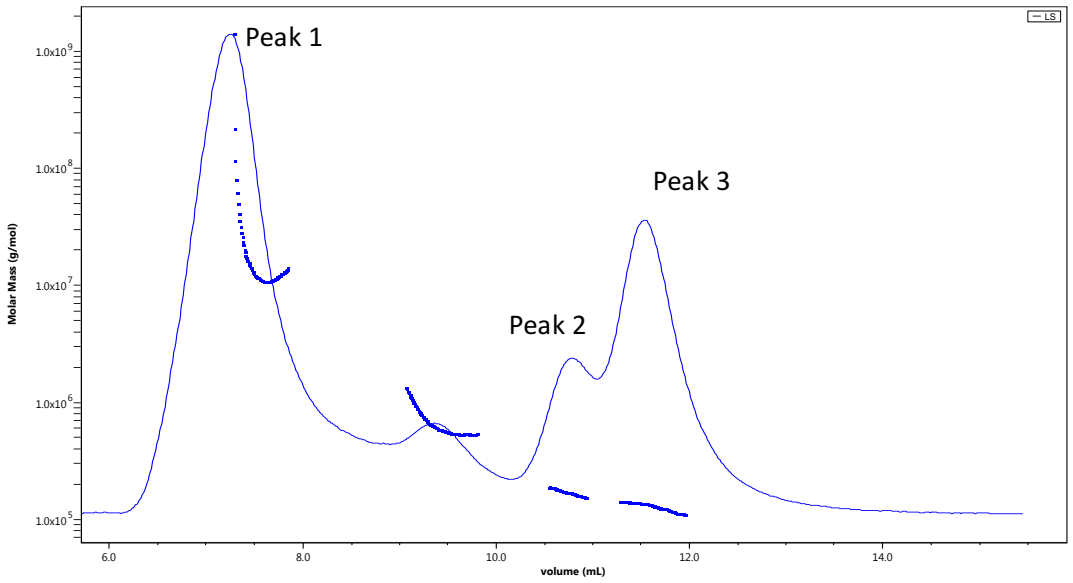

Figure 34. Oligomeric State of RIG-I C268F with Stem29 by SEC-MALS. Protein and oligo was incubated at ratio of 3:1. Peak 1 is the aggregates. Peak 2 (168 kDa) is probably a mixture of monomer and dimer. Peak 3 (129.1 kDa) is the monomer form of RIG-I C268F in complex with Stem29.

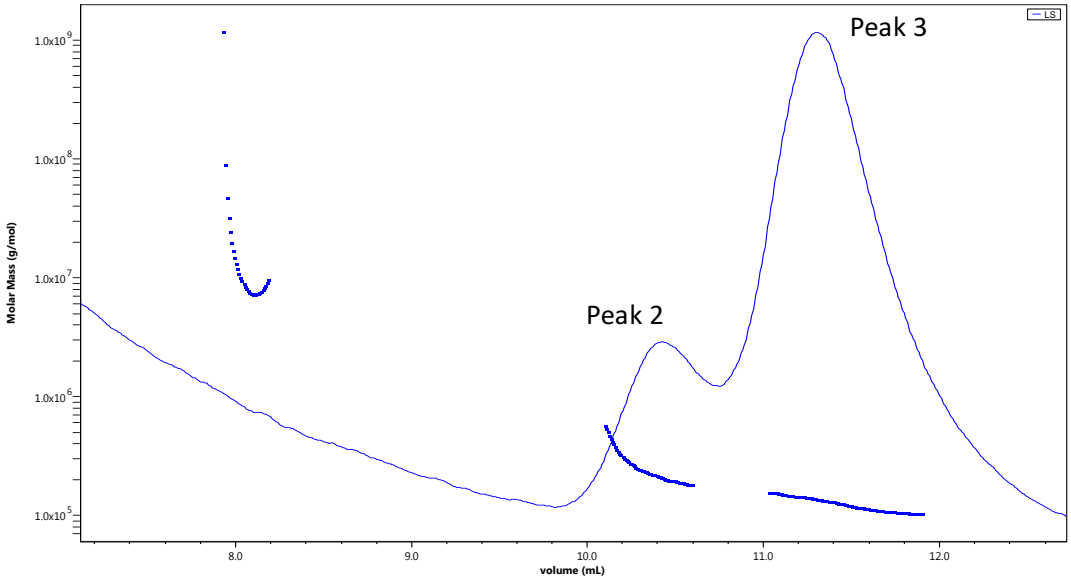

Figure 35. Oligomeric State of RIG-I E373A with Stem29 by SEC-MALS. Protein and oligo was incubated at ratio of 3:1. Peak 2 (228 kDa) probably contains dimerization form of the complex. Peak 3 (125 kDa) is the monomer form of RIG-I E373A in complex with Stem29.

Table 5 The Apparent Mw of Oligomeric State of RIG-I Mutants with Stem29 by SEC-MALS.

Mw (kDa)	Peak 1	Peak 2	Peak 3
FL RIG-I C268F with Stem29	637.4 ± 2.9%	168 ± 0.8%	129.1 ± 0.9%
FL RIG-I E373A with Stem29	N/A	228.1 ± 2.3%	125 ± 2.5%

Discussion

As an innate immune receptor specifically sensing viral RNAs, RIG-I has been studied extensively which could be a potential therapeutic target of viral infection. Scientists made profound efforts into understanding the ligand characteristics of RIG-I and its activation process. RNAs carrying a 5'-triphosphate (5'ppp) moiety and blunt-ended double-stranded (ds) RNAs are the best characterized PAMP ligands of RIG-I. RIG-I is surrounded by a great amount of cellular RNAs and the reason that it is not activated by cellular RNAs is due to the post-translational modification of the RNA 5'ends, such as 'cap' structures, including cap-0, cap-1 and cap-2. It was believed that the protection effect of m7G burying triphosphate from exposing to RIG-I and viral RNAs that do not have m7G bearing an exposed 5'ppp moiety would be recognition by RIG-I. However, we found dsRNAs with a 5'ppp end or Cap-0 showed similar binding affinities to RIG-I and similar ATP turnover rates. Crystal structures also showed an identical conformation of RIG-I Helicase-RD in complex with 5'ppp dsRNA and Cap-0 dsRNA. Besides, there are no conserved interactions with the m7G moiety. These results indicate that RIG-I can accommodate cap-0 modification which is not the critical property for RIG-I recognition.

Cellular RNAs are generally modified with cap-1 and cap-2 structure in higher eukaryotes. By analyzing the structure carefully, we noticed the interaction between RIG-I residue H830 and 2'-OH of the first nucleotide on the 5' end. And methylation of this 2'-OH resulted in a significant drop in RIG-I-RNA binding affinities and ATP hydrolysis rates. This histidine is conserved in different species. The mutation of H830A rescued the deleterious effect of cap-1. The results of cell-based assay agreed with the biochemical studies.

A similar scenario was observed with IFIT1 which is an IFN stimulated receptor specifically recognizing ssRNAs. IFIT1 recently was shown as a key player in the recognition of capped RNAs (94), such that it recognizes ssRNAs with 5'ppp and implicated in the recognition of

cap-0 RNAs but not cap-1 RNAs (95). RIG-I recognizes base paired RNAs with 5'ppp or Cap-0, but not short ssRNAs. This observation is consistent with structural studies of RIG-I and IFIT1 that show these molecules are tailored for binding base paired RNAs and ssRNAs, respectively (50)(51)(52)(53)(96)(97). Thus, it appears that the roles of RIG-I and IFIT1 are complementary to each other.

The 2′-O-methylation of 5′-end nucleotide is the essential modification to avoid recognition by RIG-I and residue H830 is the sensor for this modification on Cap-1 RNAs. RIG-I is found only in higher eukaryotes like humans and other vertebrates, and this coincides with the emergence of 2′-O-methyltransferases over the course of evolution (98). All human cellular mRNAs bear either Cap-1 or Cap-2 structures, and based on our findings such RNAs cannot activate RIG-I, regardless of single-stranded or double-stranded ends. A common feature of some of the most pernicious viruses like Ebola and Marburg virus is the evolution of capping mechanisms and 2′-O-methyltransferase activities, facilitating the viral RNA transcripts to closely mimic cellular Cap-1 RNAs. The viral titers of Yellow fever virus were drastically reduced in A549 and Vero cell lines when its 2′-O-methyltransferase activity was abrogated, and this effect was shown to be mediated by RIG-I (99). Thus, viral 2′-O-methyltransferase enzymes are prime targets for designing effective antiviral therapies.

Until now, no structures of FL RIG-I bound to RNAs are available probably due to the high flexibility of released CARDs. We generated cell lines producing antibodies against CARDs, which hopefully can stabilize the mobile domains making it possible for high resolution study of full-length RIG-I-RNA-antibody complex by X-ray crystallography or cryo-electron microscopy. Only a few cell lines have been tried and more need to be screened.

In order to understand the details about RIG-I oligomerization, RIG-I E373A and C268F was applied because of their constant ATPase activity. A stem RNA structure was used based on

our biochemical assays. According to SEC-MALS, RIG-I E373A with Stem29 is a promising candidate for RIG-I dimerization study, but a better separation may be needed.

Chapter II. LGP2

1. LGP2 Expression and Purification

1.a LGP2 Expression and Purification in Bacterial Culture

The wild-type cDNA encoding full-length LGP2 cloned in pcDNA 3.1 vector was originally received from Dr. Mike Gale and has been successfully cloned into pET28 SUMO, pGEX-6p-1 and pJG His vectors. pET28 SUMO LGP2 and pGEX-6p-1 LGP2 (APPENDIX IV Oligo Sequence of LGP2) were expressed in *Escherichia coli* strain Rosetta (DE3) and BL21 (DE3), and the protein expression levels were compared (Figure 34). Both recombinant protein showed a slight increase on expression after IPTG induction. Solubility tests indicate most of the protein is insoluble, precipitated in the pellet. Even though most protein is insoluble, we moved on to preliminary tests with the small soluble portion of LGP2. For pET SUMO LGP2, cell lysate was passed through HisTrap FF (GE) column and a small elution peak was collected and assumed the correct product based on SDS-PAGE gels (Figure 36). The candidacy of pGEX-6p-1 LGP2 was eliminated because nothing was eluted from GST column (GE), indicating no soluble LGP2. We also put effort into optimizing pET SUMO LGP2, including bacterial codon optimization, optimizing the human protein expression in bacterial host, lower temperature, reducing IPTG concentrations, inducing for shorter time. Unfortunately, we did not see a big difference can be achieved through these modifications. Series of chromatography including ion exchange column (Q FastFlow), hydroxyapatite column (Bio-rad), heparin affinity column and gel filtration column were employed to explore the best purification procedure. Q FF (GE) stood out due to its capability of separating LGP2 from impurities after SUMO cleavage by Ulp1 protease (Figure 36B, C). Finally, by passing through Superdex200 increase 10/30L column (GE Healthcare) we are able to obtain relatively pure LGP2 (Figure 37) which is confirmed by MALDI-MS (APPENDIX V). As a result, LGP2 is successfully purified from bacterial expression system.

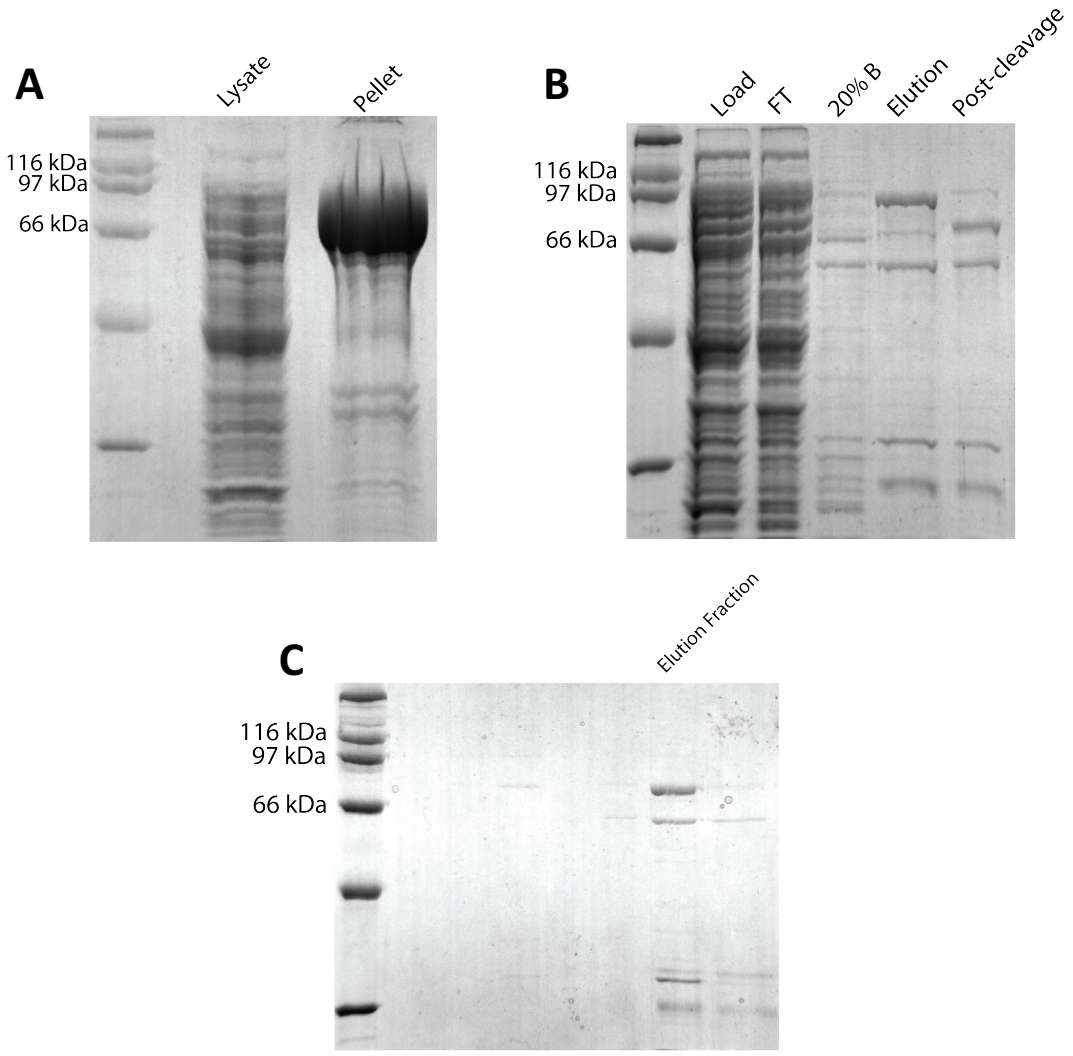

Figure 36. Solubility Test and Purification of LGP2. (A) Solubility test of LGP2 shows most protein is insoluble and a small portion is soluble. (B) This protein is initially purified from crude bacterial cell lysate using HisTrap column. Bacterial lysate is first loaded onto the column (Load) and flow-through (FT) is collected. The column is washed with 20%B to release nucleic acids. Bound SUMO-LGP2 is eluted with increasing concentrations of imidazole. The eluted protein is digested against Ulp-1 to cleave off the SUMO tag.

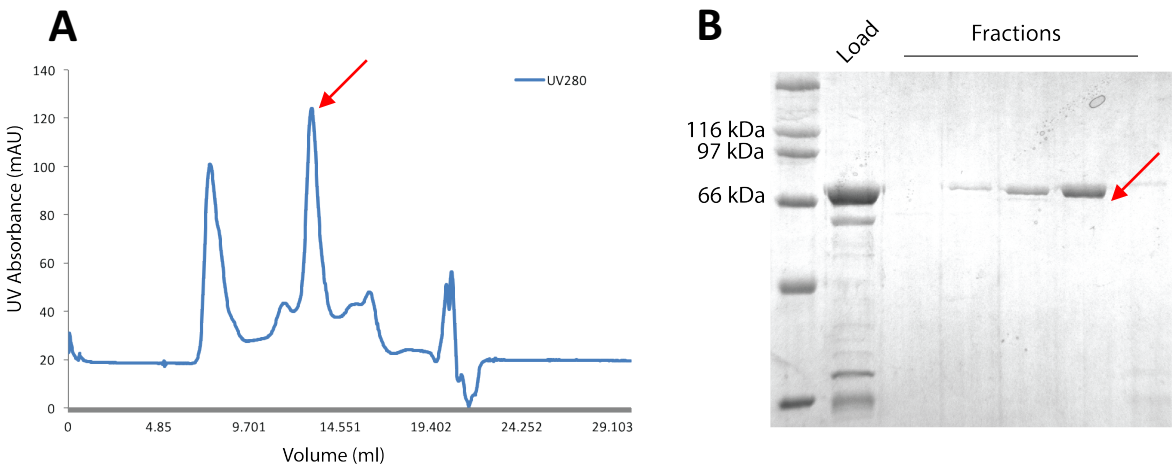

Figure 37. LGP2 Size Exclusion Chromatography Analysis. (A) Chromatogram of absorbance at 280nm of purified LGP2 from size exclusion chromatography. (B) SDS-PAGE analysis of fractions from size exclusion chromatography. Corresponding fractions are denoted with red arrows.

1.b LGP2 Expression in Mammalian Cells

Due to the low yield of LGP2 produced in bacterial expression system, mammalian expression system was tested for production of. HEK293T cells were transiently transfected with pcDNA 3.1 myc LGP2 and pJG His LGP2. LGP2 from both vectors expresses very well, detectable with anti-human LGP2 antibody (Figure 38). The western blot results show a good expression of LGP2 in mammalian HEK293T cells, which serves as a backup expression system to bacterial expression.

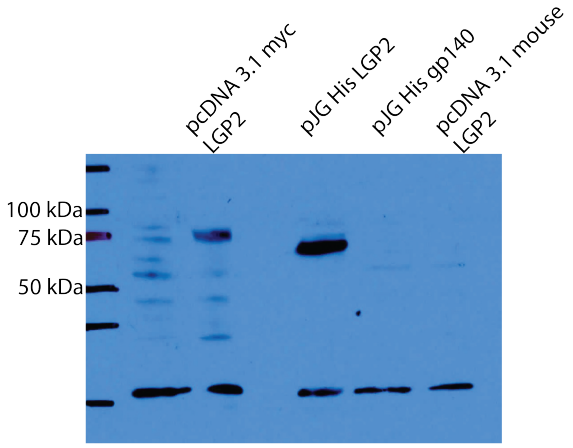

Figure 38. Mammalian Expression of LGP2. HEK293T cells were transiently transfected with different constructs and only human LGP2 was blotted by anti-human LGP2 antibody, indicating a good expression of LGP2 in mammalian cells.

2. LGP2 Function and Ligand Preference Study

2.a ATP Hydrolysis Assay

LGP2 does not have CARDs domain, resulting its incapability of transducing signals. However, it can bind ligand and hydrolyze ATP through its helicase domain and RD. Until now, the consensus of the types or properties of ligands that LGP2 recognizes and binds has not been reached yet. We screened a pool of ligands that are handy by ATPase assay, covering RNA and DNA, single-stranded or double-stranded, with or without secondary structures (Figure 39). As reported previously, LGP2 has a basal ATP hydrolysis activity, which is abrogated by Cap-0 dsRNA and 3'overhang (3'ovg) dsRNA. Unlike other studies, LGP2 did not show a stimulated ATP turnover rate in the presence of 5'ppp dsRNA, considering an almost 2-fold increase in the presence of polyI:C. 5'ovg dsRNA failed to induce an enhancement of LGP2 ATPase rate either. Surprisingly, 5'OH dsRNA accelerated LGP2 ATP hydrolysis rate to more than 2-fold compared

with no RNA, even higher than polyI:C. This is interesting because 5'OH dsRNA is considered as a PAMP-like ligand to RIG-I, indicating the potential regulation relationship between LGP2 and RIG-I. A more extensive screening showed the dsDNA with a fork structure can induce a higher ATPase rate of LGP2 than poly I:C, more than 3-fold compared with free LGP2. LGP2 exhibited slightly increased ATP turnover rate in the presence of some ligands, but incomparable with polyI:C. Then we determined the binding affinities of LGP2 with 5'OH dsRNA and the dsDNA with a fork structure (dsDNA fork) by fluorescence assay.

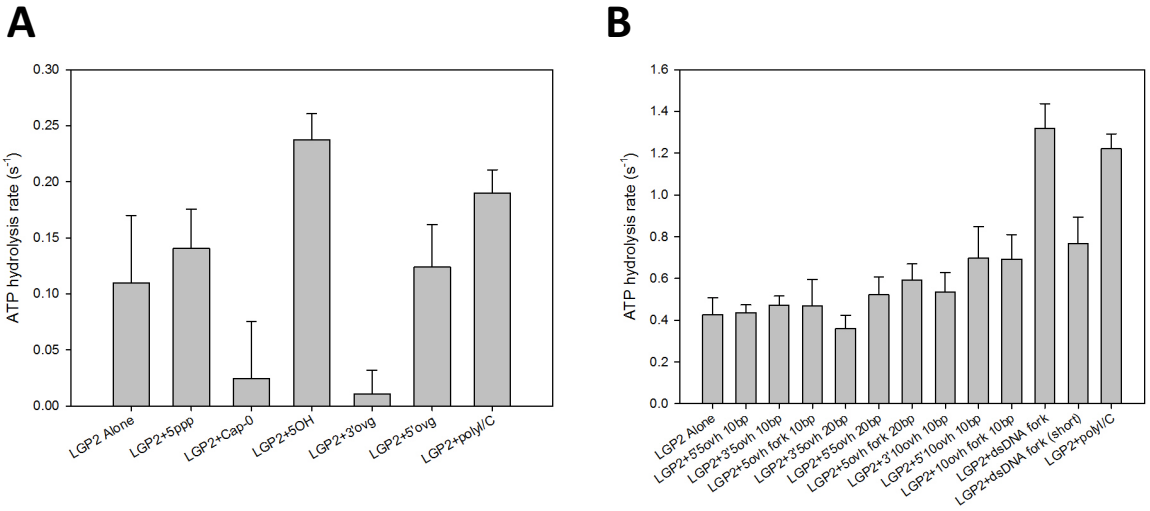

Figure 39. LGP2 Ligand Screening by ATPase Assay. The ATP hydrolysis rate of RIG-I measured at 37°C in buffer A with 100 nM LGP2 and 2 µM oligos.

2.b Ligand Binding Fluorescence Assay

In addition to ATPase activity, direct physical contact that can be measured as binding affinity is a significant parameter for characterizing ligand candidates. Fluorescence intensity and fluorescence anisotropy are employed to determine the binding affinities of LGP2 with fluorophore labeled nucleic acids (Figure 40 and Table 6). In contrast to RIG-I, LGP2 showed tighter binding to 5'OH 27bp dsRNA (K_d=13 nM) than the same 27bp dsRNA with a triphosphate

moiety on the 5'end (K_d=16 nM). Interestingly, LGP2 showed even higher binding affinity to a shorter 5'OH dsRNA with a length of 14bp (K_d=7 nM). In the case of 5'OH dsRNA, LGP2 prefers shorter length. Even though ATPase activity is high, the binding affinity of LGP2 for the 30bp dsDNA fork is relatively low (K_d=300 nM) compared to 5'OH dsRNA. This is probably resulting from frequently conformational change. In addition, we found that LGP2 binds to a 27bp dsRNA-DNA hybrid to a similar extent as 5'OH 14bp dsRNA, indicating that LGP2 does not need a 3' RNA strand and the 5' strand of RNA might be sufficient for LGP2 recognition and binding. This needs to be confirmed with 3'RNA and 5'DNA hybrid. ssRNA and ssDNA showed no binding to LGP2, consistent with previous reports (47).

Table 6 Binding Affinities of LGP2 with Different Oligos by Fluorescence Assays.

RNA	K_d (nM)	Cooperativity factor	Method
5'OH ds27 3'DY547	13.0±0.6	2.7±0.3	Fluorescence Intensity
5'ppp ds27 3'DY547	16.3±0.3	4.4±0.4	Fluorescence Intensity
stem RNA 3'DY547	16.5±1.3	N/A	Fluorescence Intensity
5'OH ds14 3'DY547	6.3±0.6	1.9±0.3	Fluorescence Intensity
ds27 RNA DNA hybrid 3'DY547	5.7±0.4	1.7±0.2	Fluorescence Intensity
ss10 polyU 3'Fluo	No binding	N/A	Fluorescence Intensity
ss10 dT DNA 5'Fluo	No binding	N/A	Fluorescence Intensity
ds30 DNA fork 3'Cy3	303±53	N/A	Fluorescence Anisotropy

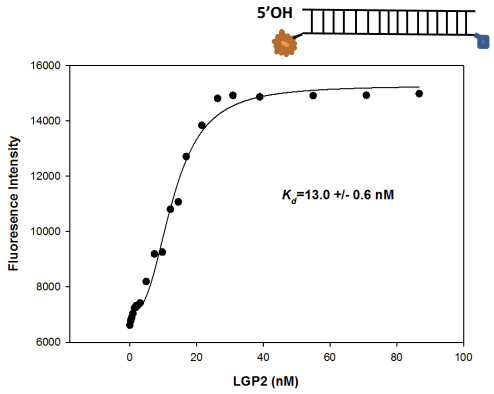
5'OH
Fluorescence Intensity
LGP2 (nM)
K_d=13.0 +/- 0.6 nM

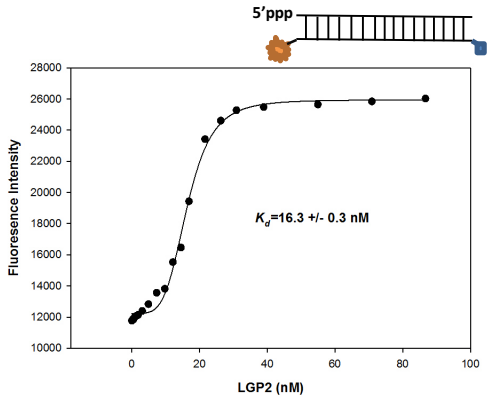
5'ppp
Fluorescence Intensity
LGP2 (nM)
K_d=16.3 +/- 0.3 nM

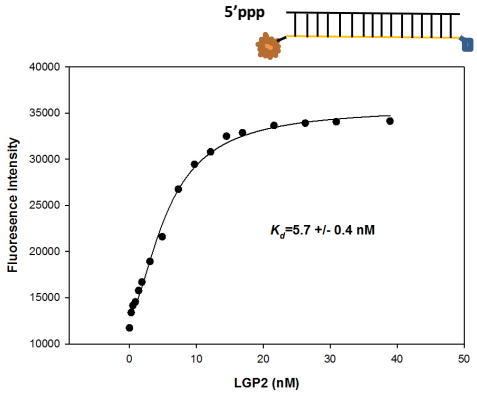
5'ppp
Fluorescence Intensity
LGP2 (nM)
K_d=5.7 +/- 0.4 nM

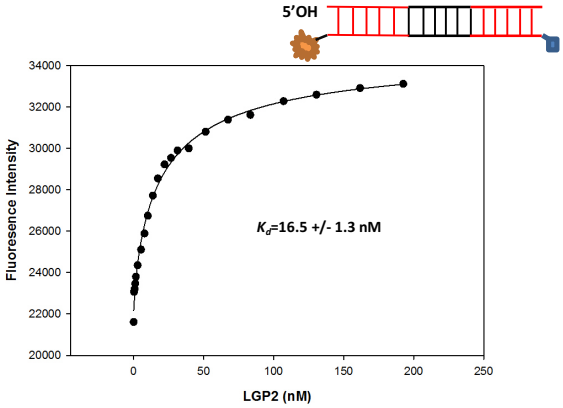
5'OH
Fluorescence Intensity
LGP2 (nM)
K_d=16.5 +/- 1.3 nM

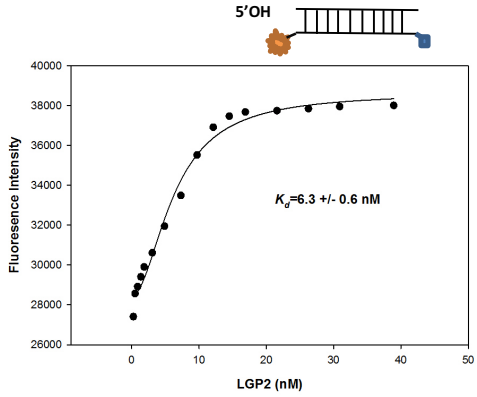
5'OH
Fluorescence Intensity
LGP2 (nM)
K_d=6.3 +/- 0.6 nM

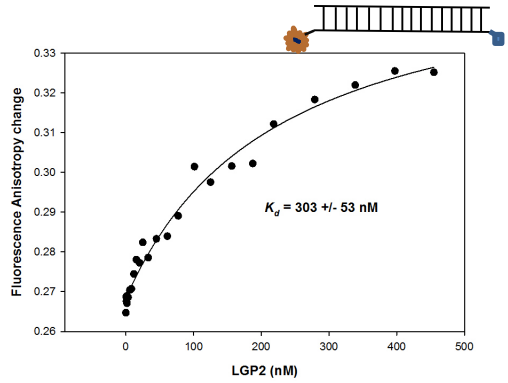
Fluorescence Anisotropy change
LGP2 (nM)
K_d = 303 +/- 53 nM

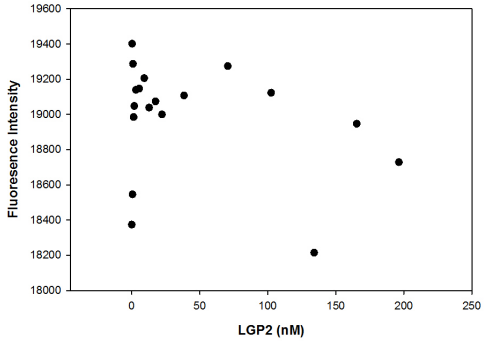
Fluorescence Intensity
LGP2 (nM)

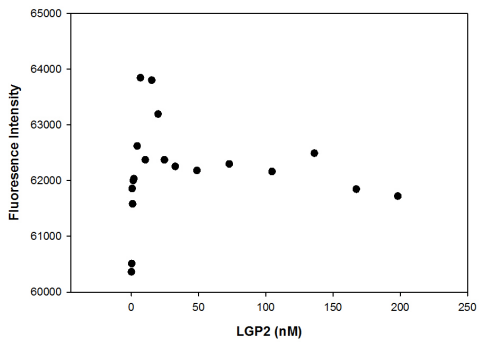
Fluorescence Intensity
LGP2 (nM)

Figure 40. Binding Affinities of LGP2 with Different Nucleic Acids by Fluorescence Assays. A fixed concentration of RNA or DNA is titrated by an increasing concentration of LGP2 (Details are described in Materials and Methods). The structures and modifications of oligos are shown in schematic form next to the graphs.

3. Relationship with RIG-I: ATPase Competition Assay

Based on the ligand screening assays, RIG-I and LGP2 bind to the same set of RNAs. In order to understand the roles of these two receptors in 5'OH dsRNA recognition, we set up an ATPase competition assay starting with a certain amount of FL RIG-I and RNA, and then titrating with increasing amount of LGP2. 5'ppp 14bp dsRNA was tested as a control, and FL RIG-I exhibited high ATPase activity with no LGP2 added, whereas LGP2 itself showed a normal slow ATP turnover rate. The ATPase rate slightly dropped with increase in LGP2 concentration. At equal concentration of RIG-I and LGP2 (10 nM), the ATPase rate remains high, indicating that the 5'ppp 14bp dsRNA preferentially binds to RIG-I (Figure 41A), otherwise there should be a more dramatic decrease in ATPase activity. However, at higher LGP2 concentrations, the ATPase rate decreased. Accordingly, RIG-I competes over LGP2 in binding 5'ppp dsRNA.

The opposite was observed with the 5'OH 14bp dsRNA (Figure 42). Compared to only RIG-I, the ATPase hydrolysis rate dropped significantly when LGP2 was added. At equal concentrations (25 nM), the ATPase rate was even lower than only LGP2, suggesting LGP2's high binding affinity to 5'OH dsRNA relative to RIG-I, and the possibility that LGP2 prevents RIG-I from binding to the 5'OH RNA (Figure 40A). The same results were observed with 40 nM of RIG-I and RNA (Figure 42B). This indicates that LGP2 has a stronger binding affinity for the 5'OH dsRNA than RIG-I. This conclusion is also applied to longer RNA, like 5'OH 27bp dsRNA. To conclude, 5'ppp dsRNA binds RIG-I preferentially in the presence of LGP2 while 5'OH dsRNA binds preferentially to LGP2 in the presence of RIG-I. This implies a potential role of LGP2 in RIG-

I regulation where it could serve as a coordinator to prevent activating RIG-I by non-PAMP RNAs mistakenly, which is highly possible in host cells.

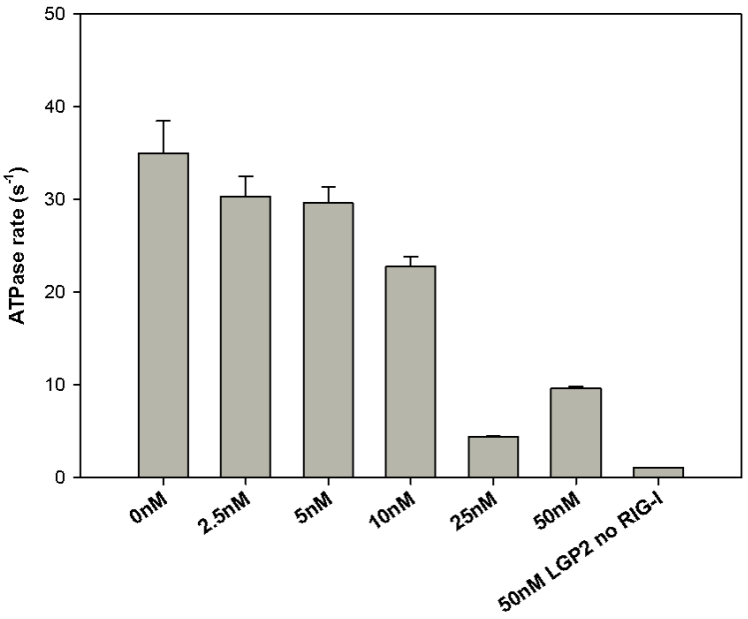

Figure 41. LGP2 and RIG-I Competition Assay in the Presence of 5'ppp dsRNA. The ATP hydrolysis rate of reactions starting with 10 nM FL RIG-I, 10 nM RNA and an increasing concentration of LGP2. At equal concentration, the ATP hydrolysis rate is not affected much, indicating a tighter binding of RIG-I and 5'ppp dsRNA compared to LGP2.

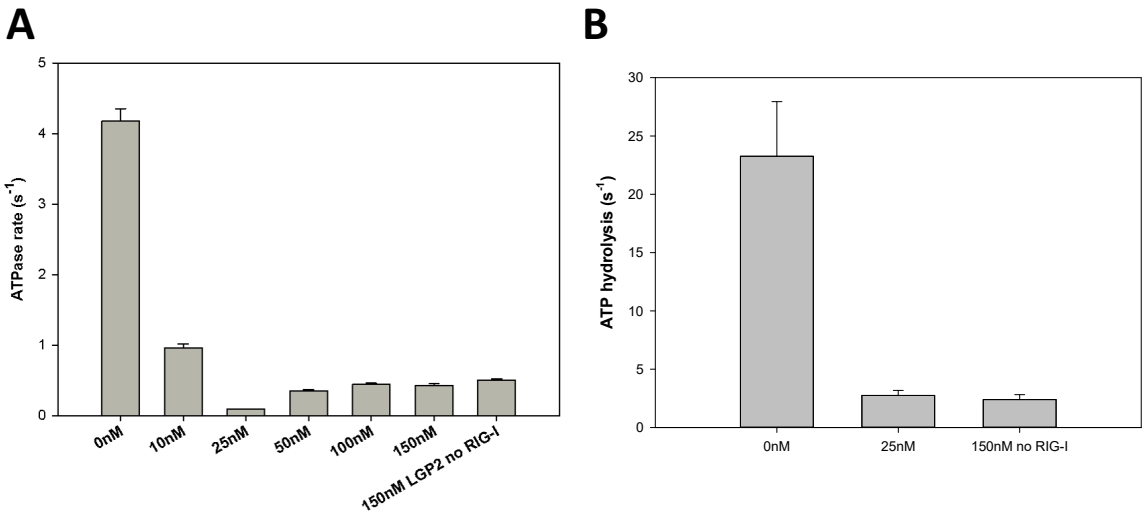

Figure 42. LGP2 and RIG-I Competition Assay in the Presence of 5'OH dsRNA. (A) The ATP hydrolysis rate of reactions starting with 25 nM FL RIG-I, 25 nM RNA and an increasing concentration of LGP2. At equal concentration, the ATP hydrolysis rate is greatly reduced, indicating a tighter binding of LGP2 and 5'OH dsRNA compared to RIG-I. (B) The ATP hydrolysis rate of reactions starting with 40 nM FL RIG-I, 40 nM RNA and an increasing concentration of LGP2. 25 nM LGP2 much less than RIG-I showed significant effect on ATP hydrolysis rate.

Discussion

LGP2, a member of RLR family, has a controversial role in regulating the other two members RIG-I and MDA5(36). This is partially due to the uncertainty of its binding preferences of ligands. Even though structurally LGP2 is similar to RIG-I Helicase-RD, the purification of LGP2 does not resemble that of RIG-I Helicase-RD. LGP2 is not as soluble as RIG-I in bacterial expression system which making it difficult to purify. Considering its low solubility, we started purification from recombinant bacterial cells overexpressing human LGP2 and tested the possibility of using mammalian expression at the same time. We managed to obtain a small amount of LGP2 with a few more steps of purification with a low yield from bacterial cells. In addition, LGP2 showed good expression in mammalian cells.

We tested LGP2's binding preferences by screening a pool of RNAs and DNAs via ATPase activity assay. LGP2 showed higher ATP hydrolysis rates in the presence of 5'OH dsRNA and dsDNA with a fork structure compared with polyI:C. However, a high ATP hydrolysis rate does not necessarily represents a high binding affinity. We applied fluorescence binding assays to measure the RNA binding affinities of LGP2(100). LGP2 does not bind to ssRNA or ssDNA but shows high binding affinity to 5'OH dsRNA, which is the PAMP-like ligand of RIG-I. As to the dsDNA fork, the binding affinity is relatively low, which may be explained by rapid binding dynamics due to rapid ATP hydrolysis that prevents LGP2 from staying bound to the DNA.

The interesting high binding affinity of LGP2 to 5'OH dsRNA implies its potential competitive role with RIG-I for RNA binding, which can explain why LGP2 negatively regulates RIG-I (63)(101). In contrast, the affinity of LGP2 binding the 5'ppp dsRNA is lower than RIG-I. We performed competition assays to determine the relative binding of LGP2 and RIG-I to these two ligands. Based on the results, 5'ppp dsRNA preferentially binds to RIG-I while LGP2 competes over RIG-I for binding to 5'OH dsRNA. This might imply that LGP2 can sequester non-optimal

ligands from RIG-I to prevent misactivation(102), which could be an additional mechanism of self and non-self discrimination by RIG-I.

CONCLUSION

RLRs are important in sensing viral infection and in stimulating the innate immune response to eliminate pathogens and establish antiviral state in host cells. As a result, a mechanistic understanding of self and non-self RNAs discrimination by RLRs is a critical question to answer. The most well-characterized member RIG-I can specifically recognize short blunt-ended dsRNA with 5'ppp modification. Our study revealed a significant mechanism of RNA discrimination by RIG-I. Unlike the previous hypothesis that the discrimination of self and non-self RNAs was due to the presence of the m7G moiety, which was thought to sterically hinder binding to RIG-I, dsRNAs with m7G show comparable binding affinity, ATPase, and cell signaling activity dsRNAs with a 5' triphosphate. Our structural studies provide the exact mechanism for binding of capped RNAs by RIG-I by providing insights into the nature of interactions between RIG-I and 5'm7Gppp moiety. Interestingly, RIG-I makes no specific interactions with the m7G, but instead accommodate its presence through the disordering of helicase motif IVa. The interactions of RIG-I with the ppp of the Cap-0 RNA were identical to that seen in the case of 5'ppp HP RNA, as evident in their respective structures.

Furthermore, the 2'-O-methylation of 5' end nucleotide is the essential modification to avoid recognition by RIG-I and residue H830 is the sensor for this modification on Cap-1 RNAs. The effect of 2'-O-methyaltion and crucial role of H830 are confirmed with biochemical and cell-based signaling assays.

These new insights can be used in the design of ligands or therapeutics to either stimulate or inhibit RIG-I activity, depending on the desired outcome. For example, the triphosphorylated dsRNA has high binding affinity and signaling activity; however, the triphosphate moiety can be easily degraded by cellular phosphatases. In cells, the m7G cap serves to increase the half-life of the RNA by circumventing 5'-end degradation. However, the

cap has additional roles in translation initiation, nuclear export, etc. The structure of RIG-I in complex with Cap-0 RNA will be useful for modeling of naturally occurring and designer chemical moieties on the 5'ppp that will increase the half-life of the RNA while preventing interactions with other cap-binding proteins (e.g., the translation initiation factor eIF4E). The moiety may itself serve a specific function, such as to act as an activator or inhibitor of another cellular protein, or target the RNA ligand to specific cell types. Similar to the m7G, RIG-I can accommodate 2-nucleotide 3'-overhangs such as those in siRNAs (103). The 5'ppp containing siRNAs have been used to knock down expression of specific oncogenes in cancer cells as well as stimulate RIG-I to induce apoptosis in the cancer cell (104). Conversely, it may be advantageous to design an RNA for a specific cellular function without stimulating RIG-I activity by modifying the 2′ position of the first base.

The progress in screening RIG-I antibody and identifying oligomerization would benefit the complete understanding of RIG-I activation process in the future and possibly help determine and select targets or checkpoints of RIG-I related signaling pathway.

The less characterized member of RLRs, LGP2 has an interesting competition role with RIG-I in binding 5'OH dsRNA, which is the PAMP-like ligand of RIG-I, but not the optimal ligand. This is consistent with the other observations of its negative regulation effect on RIG-I. The successful purification of this protein provides opportunities to extensively study the characteristics of its ligands and the relationship with other RLR members.

To summarize, the data presented here contributes to the goal of determining functions and properties of RIG-I and LGP2 in pathogen infection via biochemical, biophysical and cell-based methods. This would aid the understanding RLRs in innate immune responses and the discovery as well as the development of anti-viral drug or vaccine design.

APPENDIX I Oligo Sequences for RIG-I Studies

Sequence	RNA name	RNA end	Source
5’-pppGAAUAUAAUAGUGAUAUUAUAUUC-3’	5’ppp HP RNA	5’ppp	Biosynthesis
5’-(m7G)pppGAAUAUAAUAGUGAUAUUAUAUUC-3’	Cap-0 HP RNA	5'm7Gppp	TriLink
5’-GAAUAUAAUAGUGAUAUUAUAUUC-3’	5’OH HP RNA	5’OH	IDT
5'-pppAUACGUCCUGAUAGUUAGUAUCCAUCG-3'	5'ppp ssRNA	5’ppp	Biosynthesis
5'-AUACGUCCUGAUAGUUAGUAUCCAUCG-3'	5'OH ssRNA	5’OH	Biosynthesis
5'-(m7G)pppAUACGUCCUGAUAGUUAGUAUCCAUCG-3'	Cap-0 ssRNA	5'm7Gppp	Biosynthesis
5'-GCUCGAUGGAUACUAACUAUCAGGACGUAU-3'	complementary ssRNA	5’OH	Biosynthesis
5'-GCUAUACGUCCUGAUAGUUAGUAUCCAUCG-3'	5’ovg ssRNA	5’OH	Biosynthesis
5’-pppmGAAUAUAAUAGUGAUAUUAUAUUC-3’	5’ppp 2'O-Me HP RNA	5’ppp	Biosynthesis
5’-(m7G)pppmGAAUAUAAUAGUGAUAUUAUAUUC-3’	Cap-1 HP RNA	5'm7Gppp	TriLink
5'-(m7G)pppmAUACGUCCUGAUAGUUAGUAUCCAUCG-3'	Cap-1 ssRNA	5'm7Gppp	Biosynthesis
5’-pppCGUGAGACAU-3’Fl	5’ppp ss10 3’Fl RNA	5’ppp / 3’Fluorescein	Biosynthesis

APPENDIX II Oligo Sequences used in LGP2 Studies

Sequence	RNA/DNA name	RNA/DNA end	Source
5'-AUACGUCCUGAUAGUUAGUAUCCAUCG-3’	5’OH ds27 RNA	5’OH	Dharmacon
5'-pppAUACGUCCUGAUAGUUAGUAUCCAUCG-3’	5’ppp ds27 RNA	5’ppp	Biosynthesis
5'Bi-CGAUGGAUACUAACUAUCAGGACGUAU-3' DY547	Ss27 complementary RNA 5’biotin/3’DY547	5’biotin, 3’DY547	Dhamacon
5’-dAdTdAdCdGUCCUGAUAGUUAGUAUCdCdAdTdC-3’	Stem dsRNA ss26 RNA chimera	N/A	Dharmacon
5’-dCdGdAdTdGGAUACUAAC(Cy3)UAUCAGGAdCdGdTdA-3’	Stem dsRNA ss26 RNA chimera internal Cy3	Internal Cy3	Trilink
5’-CGUGAGACAUAdGdCdG-3’	5’OH ss14 3’ chimera	N/A	Dharmacon
5’-dCdGdCUAUGUCUCACG-3’Fl	Ss14 Complementary 5’ chimera 3’Fl	3’Fl	Dharmacon
5’-TTTTTTTTTTTTAGTTAGTATCCATCGAGC-3’	12ovg 18bp ss30 (DNA fork)	5’12ovg	IDT
5’Bi-GCTCGATGGATACTAACTATCAGGACGTAT-3’Cy3	Ss30 complementary DNA 5’biotin/3’Cy3	5’biotin, 3’Cy3	IDT
5’-UUUUUUUUUU-3’Fl	Ss10 polyU 3’Fl	3’Fl	Dharmacon
5’Fl-dTdTdTdTdTdTdTdTdT-3’	Ss10 polyT 5’Fl	5’Fl	IDT

APPENDIX III Anti-RIG-I mAb Generation Phase I ELISA Results

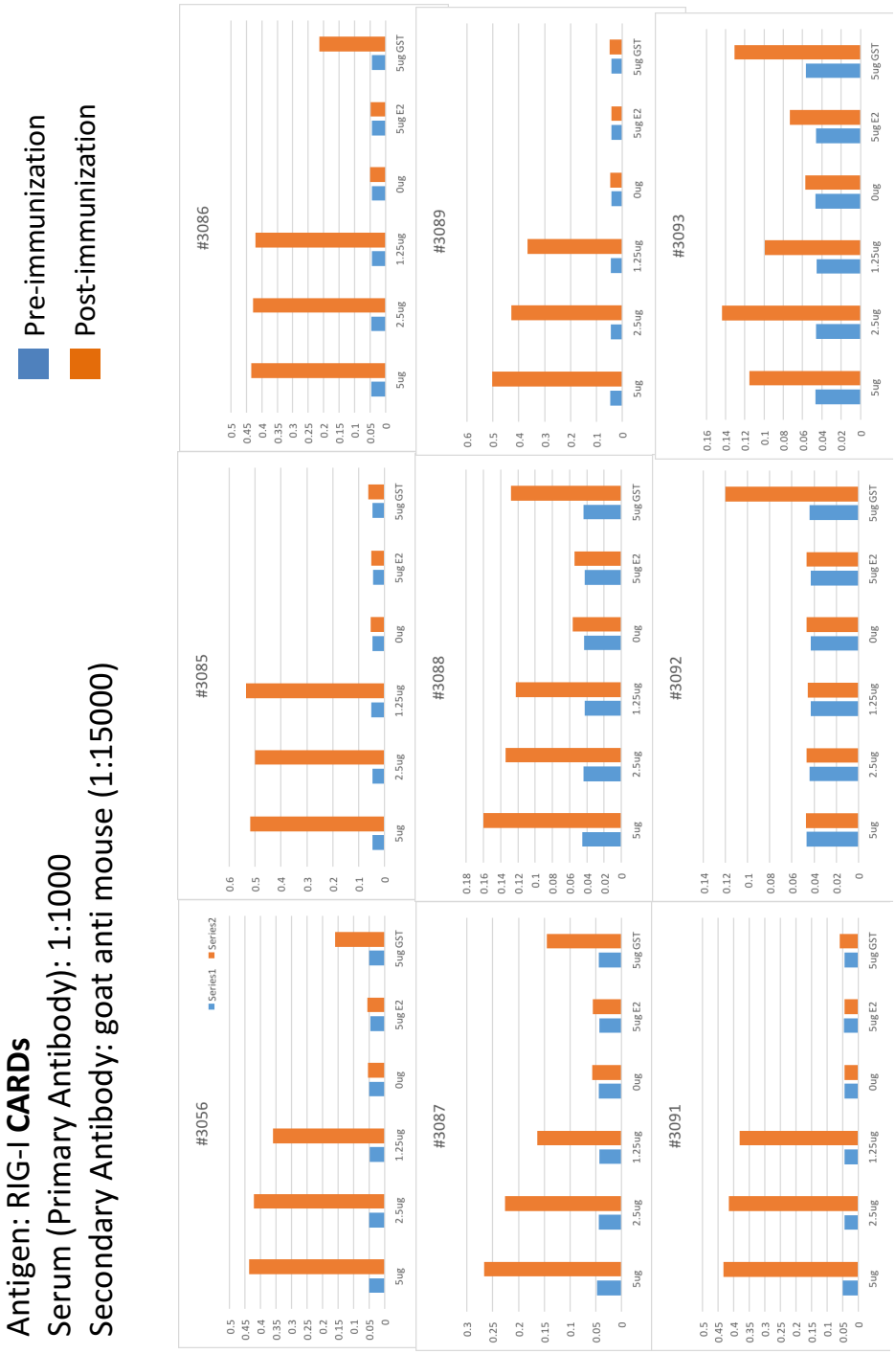

Antigen: **Full-length RIG-I**
Serum (Primary Antibody): 1:1000
Secondary Antibody: goat anti mouse (1:15000)

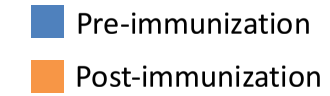

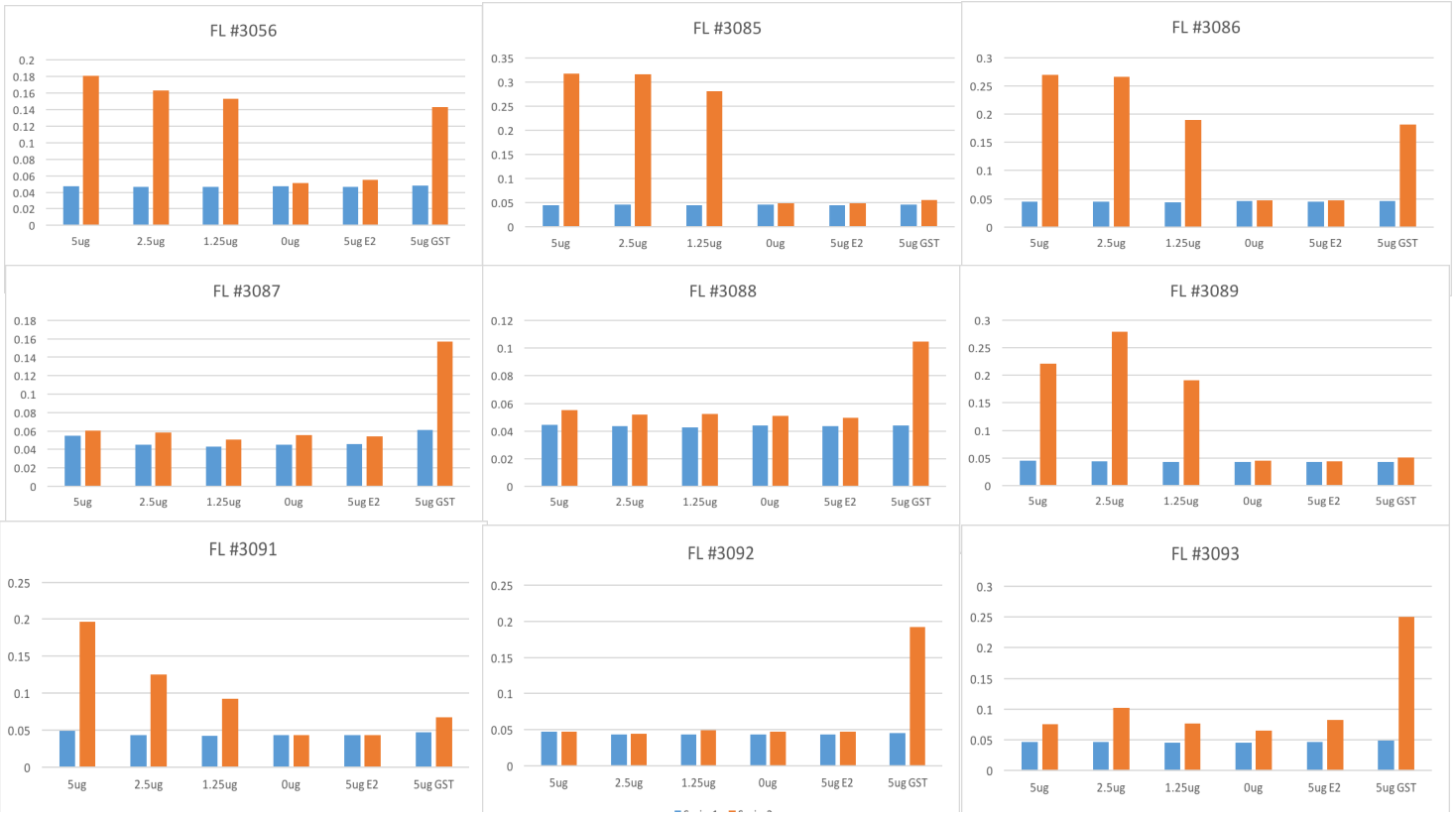

Antigen: Full-length RIG-I +5’ppp HP RNA
Serum (Primary Antibody): 1:1000
Secondary Antibody: goat anti mouse (1:15000)

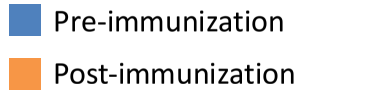

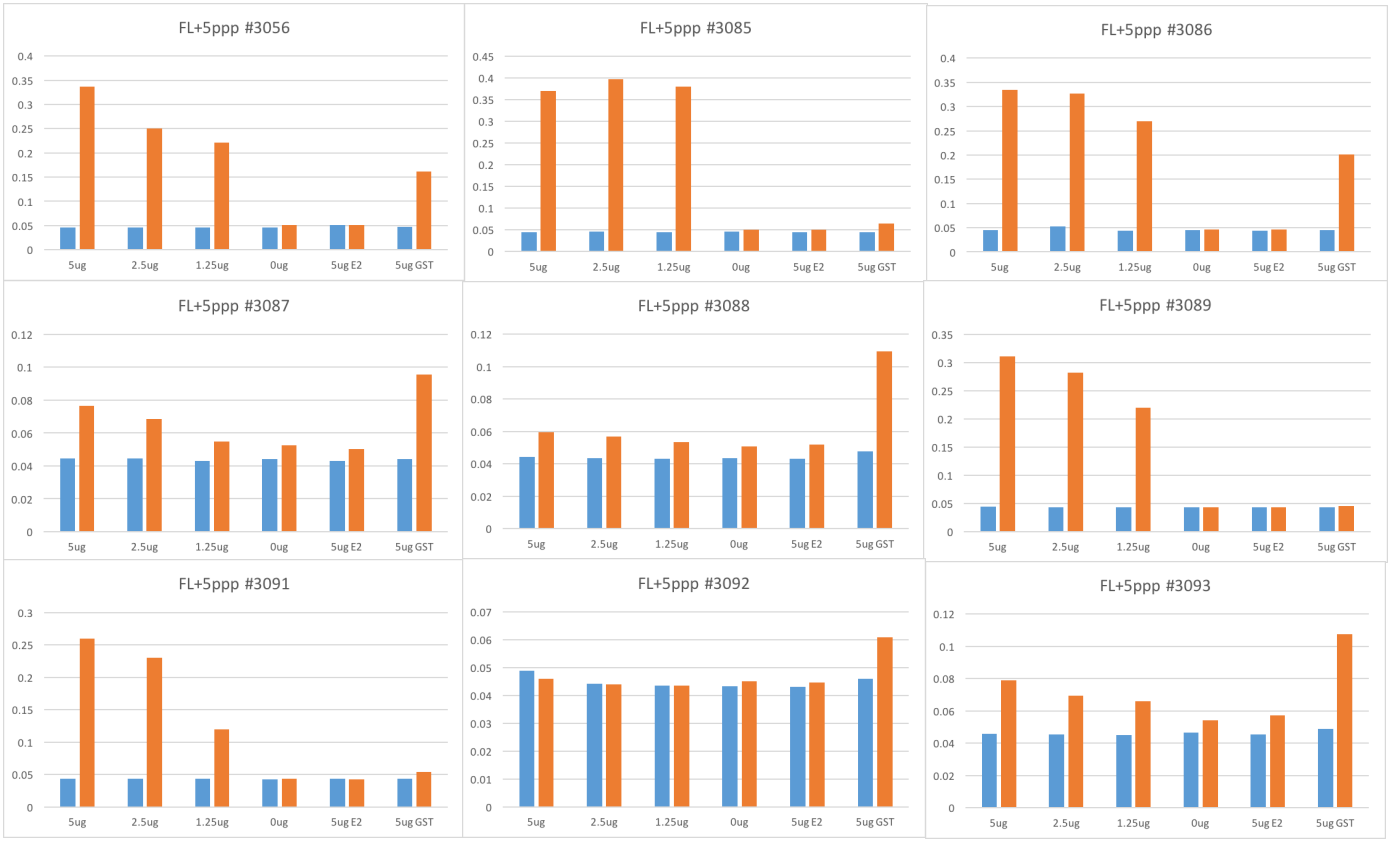

Anti-RIG-I mAb Generation Phase II ELISA Results


24D1
27B5
23F11
25G1
23D12
25F12
CARDs
FL
FL+RNA
5ug
2.5ug
1.25ug
PBS-t
EndoH
E2
*


28H8
28E8
31E8
28B11
29B3
28H12
5ug
2.5ug
1.25ug
PBS-t
EndoH
E2
CARDs
FL
FL+RNA


36D9
39B5
35E12
38H5
31H8
37C12
5ug
2.5ug
1.25ug
PBS-t
EndoH
E2
CARDs
FL
FL+RNA


42A3
45D1
41A8
43D1
40C7
42B12
5ug
2.5ug
1.25ug
PBS-t
EndoH
E2
CARDs
FL
FL+RNA


48C11
50B9
46E5
49C9
45E1
49A11
5ug
2.5ug
1.25ug
PBS-t
EndoH
E2
CARDs
FL
FL+RNA


52F9
55C1
52C8
55A11
51H4
53F12
5ug
2.5ug
1.25ug
PBS-t
EndoH
E2
CARDs
FL
FL+RNA


56C1
55H9
60B5
55E10
58D6
56G3
5ug
2.5ug
1.25ug
PBS-t
EndoH
E2
CARDs
FL
FL+RNA


64C9
63G3
68C12
61G7
68C6
65E3
CARDs
FL
FL+RNA
5ug
2.5ug
1.25ug
PBS-t
EndoH
E2

Anti-RIG-I mAb Generation Phase III ELISA Results

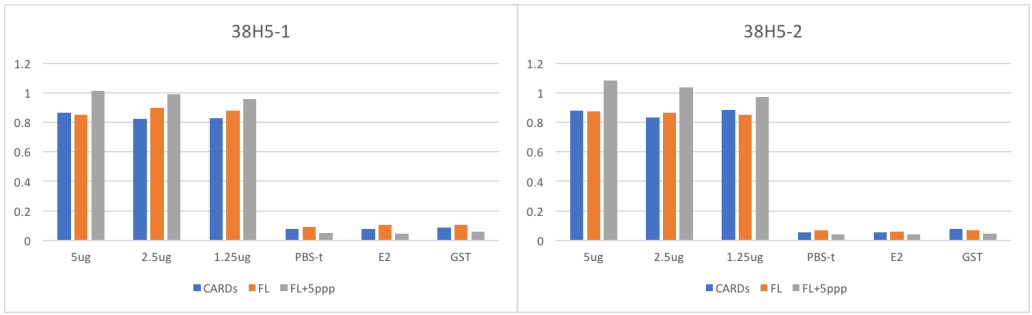

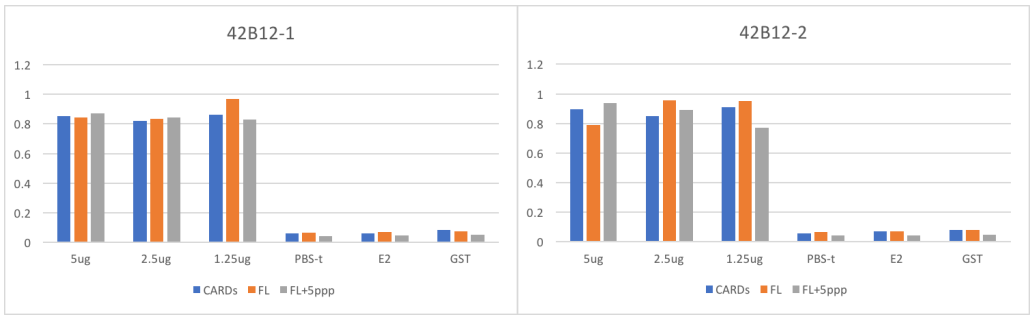

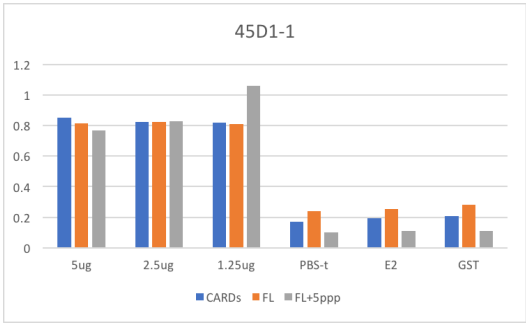

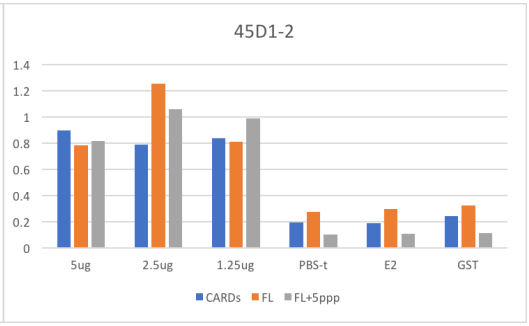

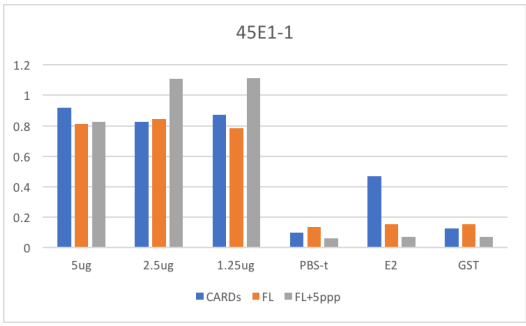

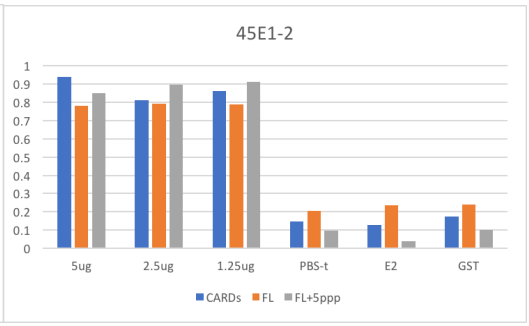

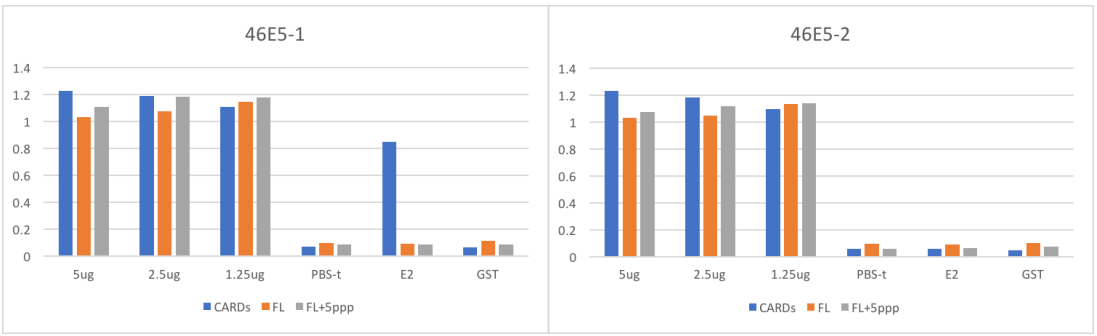
46E5-1
1.4
1.2
1
0.8
0.6
0.4
0.2
0
5ug
2.5ug
1.25ug
PBS-t
E2
GST
CARDs
FL
FL+5ppp

46E5-2
1.4
1.2
1
0.8
0.6
0.4
0.2
0
5ug
2.5ug
1.25ug
PBS-t
E2
GST
CARDs
FL
FL+5ppp

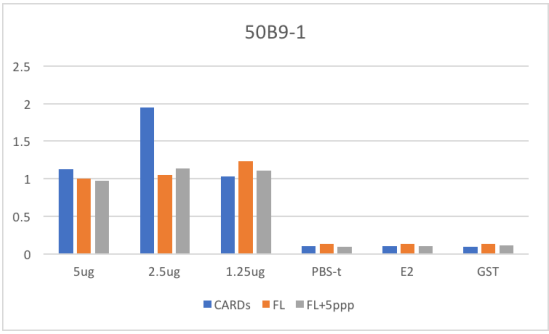
50B9-1
2.5
2
1.5
1
0.5
0
5ug
2.5ug
1.25ug
PBS-t
E2
GST
CARDs
FL
FL+5ppp

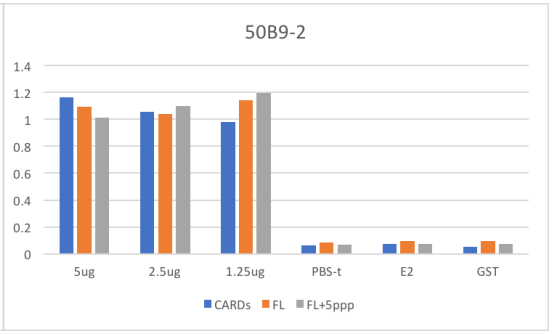
50B9-2
1.4
1.2
1
0.8
0.6
0.4
0.2
0
5ug
2.5ug
1.25ug
PBS-t
E2
GST
CARDs
FL
FL+5ppp

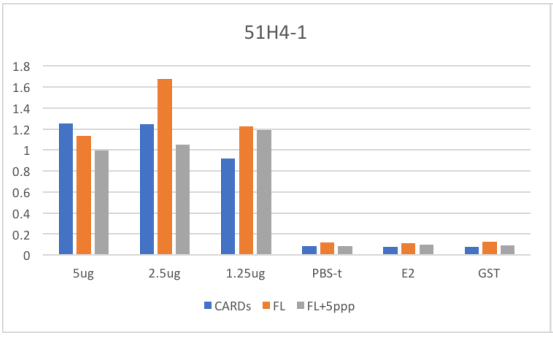
51H4-1
1.8
1.6
1.4
1.2
1
0.8
0.6
0.4
0.2
0
5ug
2.5ug
1.25ug
PBS-t
E2
GST
CARDs
FL
FL+5ppp

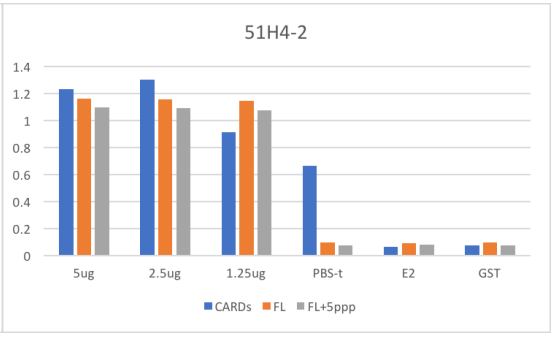
51H4-2
1.4
1.2
1
0.8
0.6
0.4
0.2
0
5ug
2.5ug
1.25ug
PBS-t
E2
GST
CARDs
FL
FL+5ppp

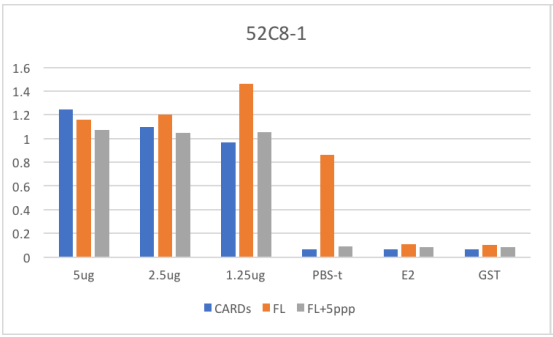
52C8-1
1.6
1.4
1.2
1
0.8
0.6
0.4
0.2
0
5ug
2.5ug
1.25ug
PBS-t
E2
GST
CARDs
FL
FL+5ppp

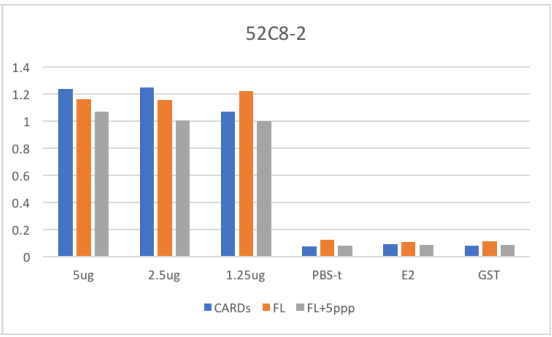
52C8-2
1.4
1.2
1
0.8
0.6
0.4
0.2
0
5ug
2.5ug
1.25ug
PBS-t
E2
GST
CARDs
FL
FL+5ppp

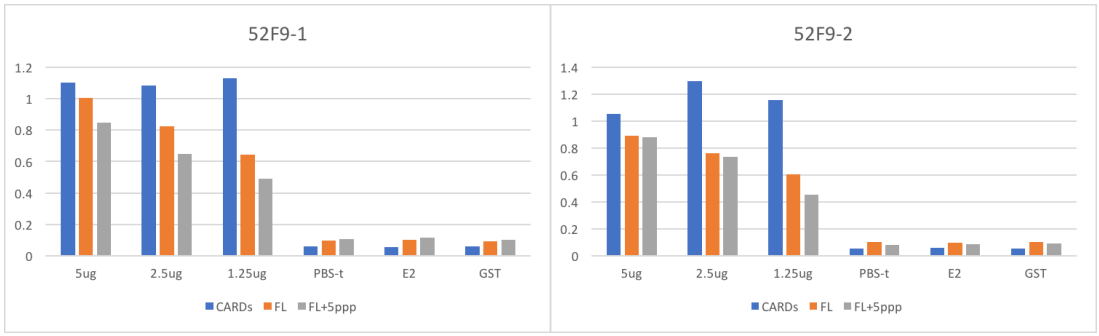
52F9-1
1.2
1
0.8
0.6
0.4
0.2
0
5ug
2.5ug
1.25ug
PBS-t
E2
GST
CARDs
FL
FL+5ppp

52F9-2
1.4
1.2
1
0.8
0.6
0.4
0.2
0
5ug
2.5ug
1.25ug
PBS-t
E2
GST
CARDs
FL
FL+5ppp

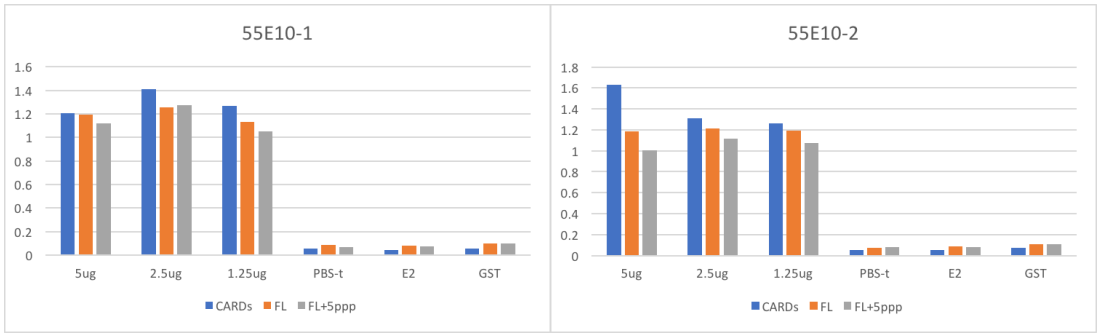
55E10-1
1.6
1.4
1.2
1
0.8
0.6
0.4
0.2
0
5ug
2.5ug
1.25ug
PBS-t
E2
GST
CARDs
FL
FL+5ppp

55E10-2
1.8
1.6
1.4
1.2
1
0.8
0.6
0.4
0.2
0
5ug
2.5ug
1.25ug
PBS-t
E2
GST
CARDs
FL
FL+5ppp

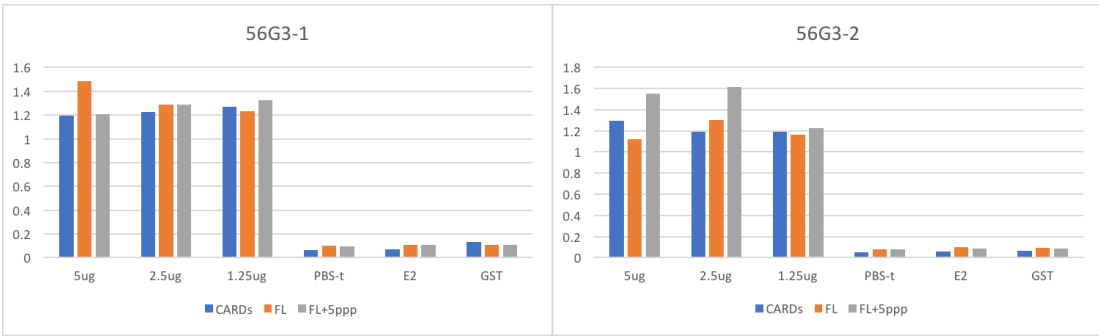
56G3-1
1.6
1.4
1.2
1
0.8
0.6
0.4
0.2
0
5ug
2.5ug
1.25ug
PBS-t
E2
GST
CARDs
FL
FL+5ppp

56G3-2
1.8
1.6
1.4
1.2
1
0.8
0.6
0.4
0.2
0
5ug
2.5ug
1.25ug
PBS-t
E2
GST
CARDs
FL
FL+5ppp

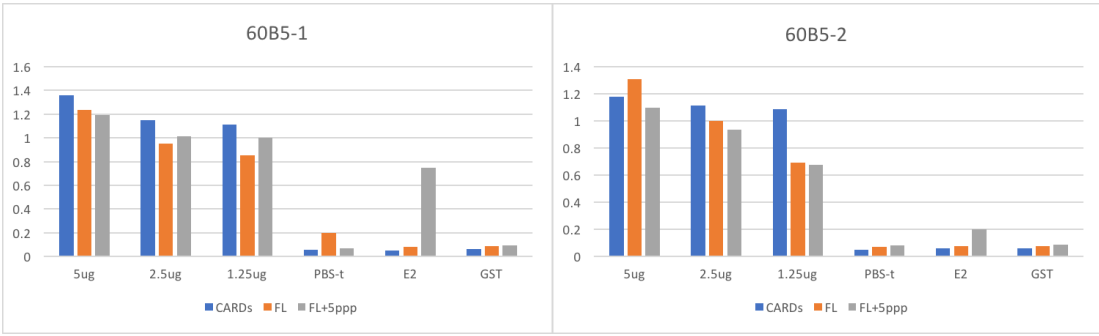
60B5-1
1.6
1.4
1.2
1
0.8
0.6
0.4
0.2
0
5ug
2.5ug
1.25ug
PBS-t
E2
GST
CARDs
FL
FL+5ppp

60B5-2
1.4
1.2
1
0.8
0.6
0.4
0.2
0
5ug
2.5ug
1.25ug
PBS-t
E2
GST
CARDs
FL
FL+5ppp

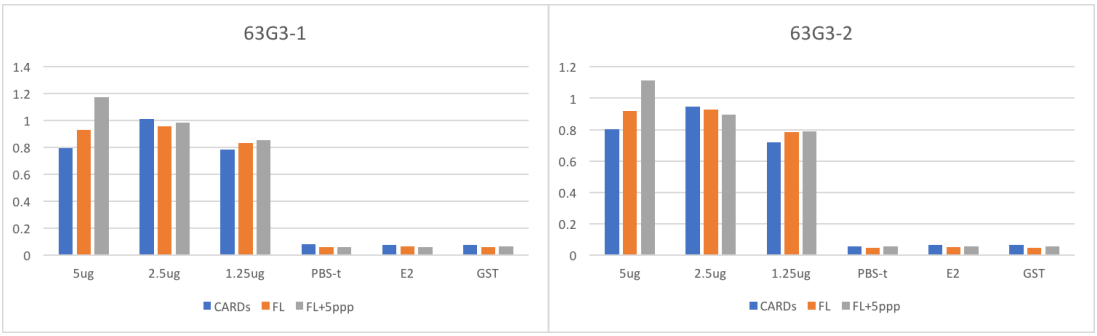
63G3-1
1.4
1.2
1
0.8
0.6
0.4
0.2
0
5ug
2.5ug
1.25ug
PBS-t
E2
GST
CARDs
FL
FL+5ppp

63G3-2
1.2
1
0.8
0.6
0.4
0.2
0
5ug
2.5ug
1.25ug
PBS-t
E2
GST
CARDs
FL
FL+5ppp

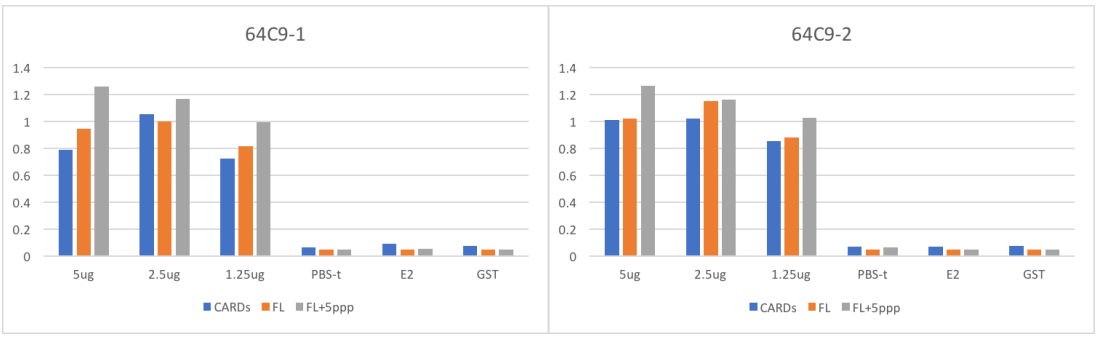
64C9-1
1.4
1.2
1
0.8
0.6
0.4
0.2
0
5ug
2.5ug
1.25ug
PBS-t
E2
GST
CARDs
FL
FL+5ppp

64C9-2
1.4
1.2
1
0.8
0.6
0.4
0.2
0
5ug
2.5ug
1.25ug
PBS-t
E2
GST
CARDs
FL
FL+5ppp

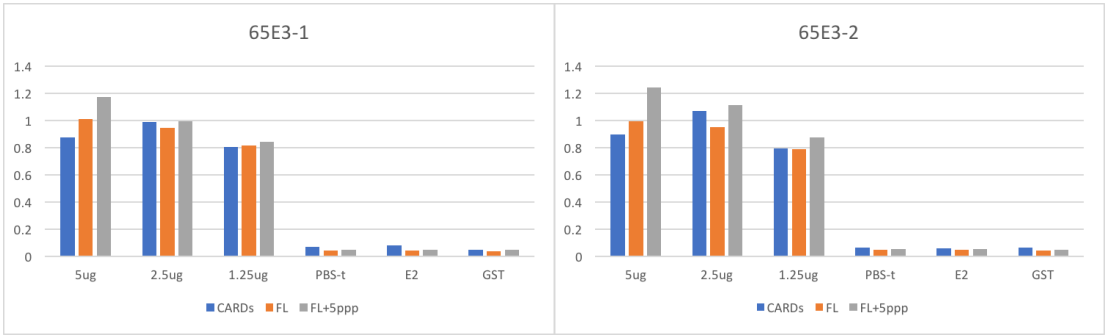
65E3-1
1.4
1.2
1
0.8
0.6
0.4
0.2
0
5ug
2.5ug
1.25ug
PBS-t
E2
GST
CARDs
FL
FL+5ppp

65E3-2
1.4
1.2
1
0.8
0.6
0.4
0.2
0
5ug
2.5ug
1.25ug
PBS-t
E2
GST
CARDs
FL
FL+5ppp

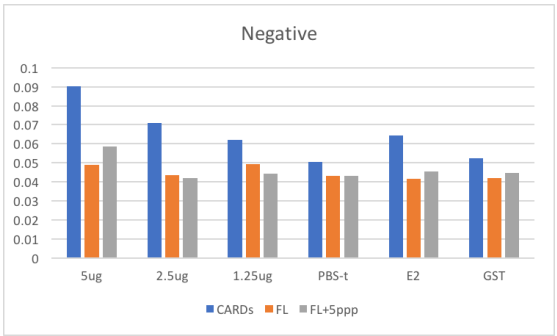
Negative
0.1
0.09
0.08
0.07
0.06
0.05
0.04
0.03
0.02
0.01
0
5ug
2.5ug
1.25ug
PBS-t
E2
GST
CARDs
FL
FL+5ppp

APPENDIX IV Oligo Sequence of

LGP2ATGGAGCTTCGGTCCTACCAATGGGAGGTGATCATGCCTGCCCTGGAGGGCAAGAATATCATCATC
TGGCTGCCCACGGGTGCCGGGAAGACCCGGGCGGCTGCTTATGTGGCCAAGCGGCACCTAGAGACTGT
GGATGGAGCCAAGGTGGTTGTATTGGTCAACAGGGTGCACCTGGTGACCCAGCATGGTGAAGAGTTCA
GGCGCATGCTGGATGGACGCTGGACCGTGACAACCCTGAGTGGGGACATGGGACCACGTGCTGGCTTT
GGCCACCTGGCCCGGTGCCATGACCTGCTCATCTGCACAGCAGAGCTTCTGCAGATGGCACTGACCAGCC
CCGAGGAGGAGGAGCACGTGGAGCTCACTGTCTTCTCCCTGATCGTGGTGGATGAGTGCCACCACACGC
ACAAGGACACCGTCTACAACGTCATCATGAGCCAGTACCTAGAACTTAAACTCCAGAGGGCACAGCCGCT
ACCCCAGGTGCTGGGTCTCACAGCCTCCCCAGGCACTGGCGGGGCCTCCAAACTCGATGGGGCCATCAA
CCACGTCCTGCAGCTCTGTGCCAACTTGGACACGTGGTGCATCATGTCACCCCAGAACTGCTGCCCCCAG
CTGCAGGAGCACAGCCAACAGCCTTGCAAACAGTACAACCTCTGCCACAGGCGCAGCCAGGATCCGTTT
GGGGACTTGCTGAAGAAGCTCATGGACCAAATCCATGACCACCTGGAGATGCCTGAGTTGAGCCGGAAA
TTTGGGACGCAAATGTATGAGCAGCAGGTGGTGAAGCTGAGTGAGGCTGCGGCTTTGGCTGGGCTTCA
GGAGCAACGGGTGTATGCGCTTCACCTGAGGCGCTACAATGACGCGCTGCTCATCCATGACACCGTCCG
CGCCGTGGATGCCTTGGCTGCGCTGCAGGATTTCTATCACAGGGAGCACGTCACTAAAACCCAGATCCTG
TGTGCCGAGCGCCGGCTGCTGGCCCTGTTCGATGACCGCAAGAATGAGCTGGCCCACTTGGCAACTCAT
GGCCCAGAGAATCCAAAACTGGAGATGCTGGAAAAGATCCTGCAAAGGCAGTTCAGTAGCTCTAACAGC
CCTCGGGGTATCATCTTCACCCGCACCCGCCAAAGCGCACACTCCCTCCTGCTCTGGCTCCAGCAGCAACA
GGGCCTGCAGACTGTGGACATCCGGGCCCAGCTACTGATTGGGGCTGGGAACAGCAGCCAGAGCACCC
ACATGACCCAGAGGGACCAGCAAGAAGTGATCCAGAAGTTCCAAGATGGAACCCTGAACCTTCTGGTGG
CCACGAGTGTGGCGGAGGAGGGGCTGGACATCCCACATTGCAATGTGGTGGTGCGTTATGGGCTCTTGA
CCAATGAAATCTCCATGGTCCAGGCCAGGGGCCGTGCCTGGGCCGATCAGAGTGTATACGCGTTTGTAG
CAACTGAAGGTAGCCGGGAGCTGAAGCGGGAGCTGATCAACGAGGCGCTGGAGACGCTAATGGAGCA
GGCAGTGGCTGCTGTGCAGAAAATGGACCAGGCCGAGTACCAGGCCAAGATCCGGGATCTGCAGCAGG
CAGCCTTGACCAAGCGGGCGGCCCAGGCAGCCCAGCGGGAGAACCAGCGGCAGCAGTTCCCAGTGGAG
CACGTGCAGCTACTCTGCATCAACTGCATGGTGGCTGTGGGCCATGGCAGCGACCTGCGGAAGGTGGAG
GGCACCCACCATGTCAATGTGAACCCCAACTTCTCGAACTACTATAATGTCTCCAGGGATCCTGTGGTCAT
CAACAAAGTCTTCAAGGACTGGAAGCCTGGGGGTGTCATCAGCTGCAGGAACTGTGGGGAGGTCTGGG
GTCTGCAGATGATCTACAAGTCAGTGAAGCTGCCAGTGCTCAAAGTCCGCAGCATGCTGCTGGAGACCC
CTCAGGGGCGGATCCAGGCCAAAAAGTGGTCCCGCGTGCCCTTCTCCGTGCCTGACTTTGACTTCCTGCA
GCATTGTGCCGAGAACTTGTCGGACCTCTCCCTGGACTGA

APPENDIX V MALDI-MS Result of LGP2

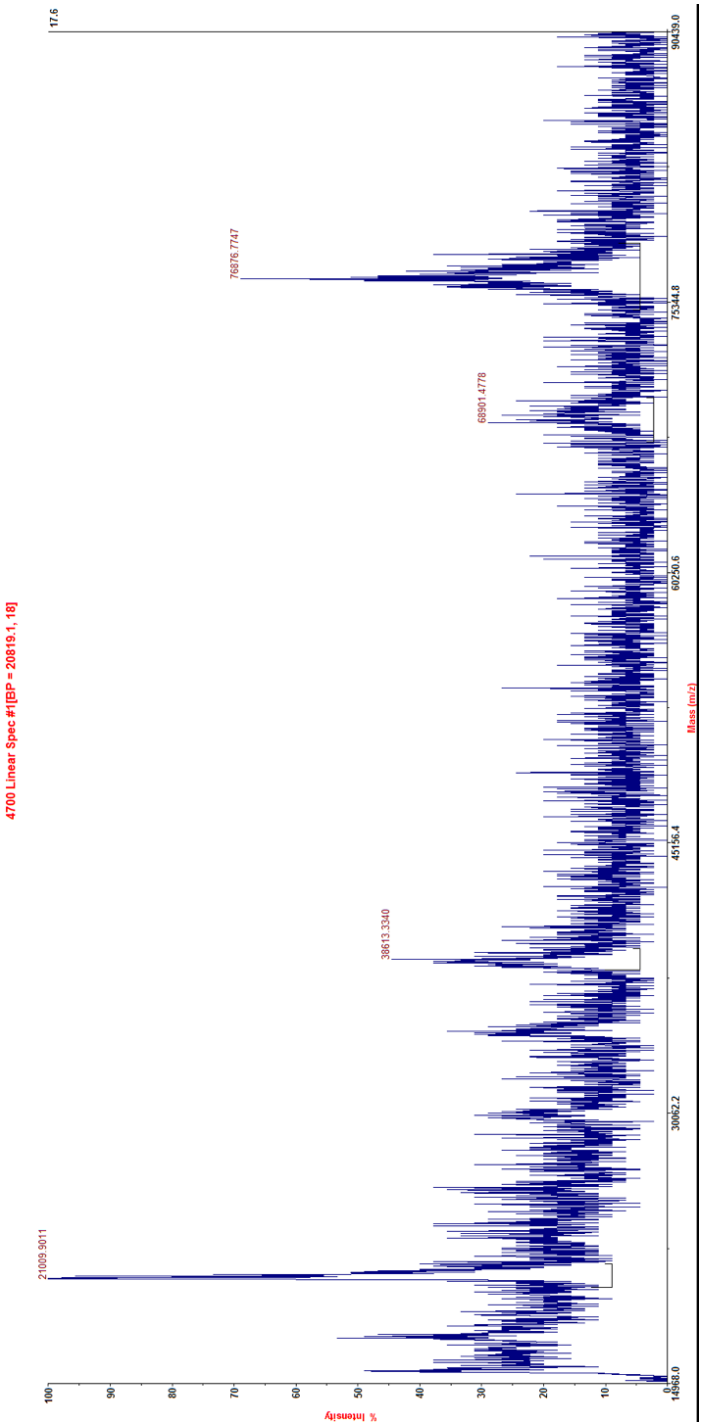

REFERENCES

1. Kumar H, Kawai T, Akira S. Pathogen Recognition by the Innate Immune System. Int Rev Immunol. 2011 Jan;30(1):16–34.
2. Medzhitov R. Recognition of microorganisms and activation of the immune response. Nature. 2007 Oct 18;449(7164):819–26.
3. Yoneyama M, Kikuchi M, Matsumoto K, Imaizumi T, Miyagishi M, Taira K, et al. Shared and Unique Functions of the DExD/H-Box Helicases RIG-I, MDA5, and LGP2 in Antiviral Innate Immunity. J Immunol. 2005 Sep 1;175(5):2851–8.
4. Palm NW, Medzhitov R. Pattern recognition receptors and control of adaptive immunity. Immunol Rev. 2009 Jan;227(1):221–33.
5. McNab F, Mayer-Barber K, Sher A, Wack A, O'Garra A. Type I interferons in infectious disease. Nat Rev Immunol. 2015 Jan 23;15(2):87–103.
6. Deretic V, Saitoh T, Akira S. Autophagy in infection, inflammation and immunity. Nat Rev Immunol. 2013 Oct;13(10):722–37.
7. Lamkanfi M, Dixit VM. Mechanisms and functions of inflammasomes. Cell. 2014 May 22;157(5):1013–22.
8. Katze MG, He Y, Gale MJ. Viruses and interferon: a fight for supremacy. Nat Rev Immunol. 2002 Sep;2(9):675–87.
9. Brubaker SW, Bonham KS, Zanoni I, Kagan JC. Innate Immune Pattern Recognition: A Cell Biological Perspective. Annu Rev Immunol. 2015 Mar 21;33(1):257–90.
10. Andrejeva J, Childs KS, Young DF, Carlos TS, Stock N, Goodbourn S, et al. The V proteins of paramyxoviruses bind the IFN-inducible RNA helicase, mda-5, and inhibit its activation of the IFN-beta promoter. Proc Natl Acad Sci U S A. 2004 Dec 7;101(49):17264–9.
11. Rothenfusser S, Goutagny N, DiPerna G, Gong M, Monks BG, Schoenemeyer A, et al. The RNA helicase Lgp2 inhibits TLR-independent sensing of viral replication by retinoic acid-inducible gene-I. J Immunol Baltim Md 1950. 2005 Oct 15;175(8):5260–8.
12. Kato H, Takeuchi O, Sato S, Yoneyama M, Yamamoto M, Matsui K, et al. Differential roles of MDA5 and RIG-I helicases in the recognition of RNA viruses. Nature. 2006 Apr 9;441(7089):101–5.
13. Gitlin L, Barchet W, Gilfillan S, Cella M, Beutler B, Flavell RA, et al. Essential role of mda-5 in type I IFN responses to polyriboinosinic:polyribocytidylic acid and encephalomyocarditis picornavirus. Proc Natl Acad Sci U S A. 2006 May 30;103(22):8459–64.
14. McCartney SA, Thackray LB, Gitlin L, Gilfillan S, Virgin HW, Colonna M. MDA-5 recognition of a murine norovirus. PLoS Pathog. 2008 Jul 18;4(7):e1000108.
15. Loo Y-M, Gale M. Immune Signaling by RIG-I-like Receptors. Immunity. 2011 May;34(5):680–92.
16. Yoneyama M, Kikuchi M, Natsukawa T, Shinobu N, Imaizumi T, Miyagishi M, et al. The RNA helicase RIG-I has an essential function in double-stranded RNA-induced innate antiviral responses. Nat Immunol. 2004 Jul;5(7):730–7.
17. Hornung V, Ellegast J, Kim S, Brzózka K, Jung A, Kato H, et al. 5'-Triphosphate RNA is the ligand for RIG-I. Science. 2006;314(5801):994–997.
18. Pichlmair A, Schulz O, Tan CP, Naslund TI, Liljestrom P, Weber F, et al. RIG-I-Mediated Antiviral Responses to Single-Stranded RNA Bearing 5'-Phosphates. Science. 2006 Nov 10;314(5801):997–1001.
19. Schlee M, Roth A, Hornung V, Hagmann CA, Wimmenauer V, Barchet W, et al. Recognition of 5' Triphosphate by RIG-I Helicase Requires Short Blunt Double-Stranded RNA as Contained in Panhandle of Negative-Strand Virus. Immunity. 2009 Jul;31(1):25–34.

20. Schmidt A, Schwerd T, Hamm W, Hellmuth JC, Cui S, Wenzel M, et al. 5′-triphosphate RNA requires base-paired structures to activate antiviral signaling via RIG-I. Proc Natl Acad Sci U S A. 2009 Jul 21;106(29):12067–72.
21. Schlee M, Hartmann G. The chase for the RIG-I ligand--recent advances. Mol Ther J Am Soc Gene Ther. 2010 Jul;18(7):1254–62.
22. Saito T, Owen DM, Jiang F, Marcotrigiano J, Gale MJ. Innate immunity induced by composition-dependent RIG-I recognition of hepatitis C virus RNA. Nature. 2008 Jul 24;454(7203):523–7.
23. Uzri D, Gehrke L. Nucleotide sequences and modifications that determine RIG-I/RNA binding and signaling activities. J Virol. 2009 May;83(9):4174–84.
24. Kell A, Stoddard M, Li H, Marcotrigiano J, Shaw GM, Gale MJ. Pathogen-Associated Molecular Pattern Recognition of Hepatitis C Virus Transmitted/Founder Variants by RIG-I Is Dependent on U-Core Length. J Virol. 2015 Nov;89(21):11056–68.
25. Goubau D, Schlee M, Deddouche S, Pruijssers AJ, Zillinger T, Goldeck M, et al. Antiviral immunity via RIG-I-mediated recognition of RNA bearing 5′-diphosphates. Nature. 2014 Aug 10;514(7522):372–5.
26. Malathi K, Saito T, Crochet N, Barton DJ, Gale MJ, Silverman RH. RNase L releases a small RNA from HCV RNA that refolds into a potent PAMP. RNA N Y N. 2010 Nov;16(11):2108–19.
27. Takahasi K, Yoneyama M, Nishihori T, Hirai R, Kumeta H, Narita R, et al. Nonself RNA-sensing mechanism of RIG-I helicase and activation of antiviral immune responses. Mol Cell. 2008 Feb 29;29(4):428–40.
28. Dixit E, Kagan JC. Intracellular Pathogen Detection by RIG-I-Like Receptors. In: Advances in Immunology [Internet]. Elsevier; 2013 [cited 2017 Oct 19]. p. 99–125. Available from: http://linkinghub.elsevier.com/retrieve/pii/B9780124105249000049
29. Kohlway A, Luo D, Rawling DC, Ding SC, Pyle AM. Defining the functional determinants for RNA surveillance by RIG-I. EMBO Rep. 2013 Sep;14(9):772–9.
30. Kato H, Takeuchi O, Mikamo-Satoh E, Hirai R, Kawai T, Matsushita K, et al. Length-dependent recognition of double-stranded ribonucleic acids by retinoic acid-inducible gene-I and melanoma differentiation-associated gene 5. J Exp Med. 2008 Jul 7;205(7):1601–10.
31. Pichlmair A, Schulz O, Tan C-P, Rehwinkel J, Kato H, Takeuchi O, et al. Activation of MDA5 requires higher-order RNA structures generated during virus infection. J Virol. 2009 Oct;83(20):10761–9.
32. Peisley A, Lin C, Wu B, Orme-Johnson M, Liu M, Walz T, et al. Cooperative assembly and dynamic disassembly of MDA5 filaments for viral dsRNA recognition. Proc Natl Acad Sci U S A. 2011 Dec 27;108(52):21010–5.
33. Peisley A, Jo MH, Lin C, Wu B, Orme-Johnson M, Walz T, et al. Kinetic mechanism for viral dsRNA length discrimination by MDA5 filaments. Proc Natl Acad Sci U S A. 2012 Dec 4;109(49):E3340-3349.
34. Berke IC, Modis Y. MDA5 cooperatively forms dimers and ATP-sensitive filaments upon binding double-stranded RNA. EMBO J. 2012 Apr 4;31(7):1714–26.
35. Rodriguez KR, Bruns AM, Horvath CM. MDA5 and LGP2: accomplices and antagonists of antiviral signal transduction. J Virol. 2014 Aug;88(15):8194–200.
36. Zhu Z, Zhang X, Wang G, Zheng H. The laboratory of genetics and physiology 2: emerging insights into the controversial functions of this RIG-I-like receptor. BioMed Res Int. 2014;2014:960190.
37. Bruns AM, Pollpeter D, Hadizadeh N, Myong S, Marko JF, Horvath CM. ATP hydrolysis enhances RNA recognition and antiviral signal transduction by the innate immune sensor, laboratory of genetics and physiology 2 (LGP2). J Biol Chem. 2013 Jan 11;288(2):938–46.

38. Liniger M, Summerfield A, Zimmer G, McCullough KC, Ruggli N. Chicken cells sense influenza A virus infection through MDA5 and CARDIF signaling involving LGP2. J Virol. 2012 Jan;86(2):705–17.
39. Murali A, Li X, Ranjith-Kumar CT, Bhardwaj K, Holzenburg A, Li P, et al. Structure and function of LGP2, a DEX(D/H) helicase that regulates the innate immunity response. J Biol Chem. 2008 Jun 6;283(23):15825–33.
40. Satoh T, Kato H, Kumagai Y, Yoneyama M, Sato S, Matsushita K, et al. LGP2 is a positive regulator of RIG-I- and MDA5-mediated antiviral responses. Proc Natl Acad Sci U S A. 2010 Jan 26;107(4):1512–7.
41. Moresco EMY, Beutler B. LGP2: positive about viral sensing. Proc Natl Acad Sci U S A. 2010 Jan 26;107(4):1261–2.
42. Pollpeter D, Komuro A, Barber GN, Horvath CM. Impaired Cellular Responses to Cytosolic DNA or Infection with Listeria monocytogenes and Vaccinia Virus in the Absence of the Murine LGP2 Protein. Kremer EJ, editor. PLoS ONE. 2011 Apr 14;6(4):e18842.
43. Wan Q, Wang L, Su J, Yang C, Peng L, Chen L. Genetic structure, polymorphism identification of LGP2 gene and their relationship with the resistance/susceptibility to GCRV in grass carp, Ctenopharyngodon idella. Gene. 2013 May 25;521(1):166–75.
44. Bruns AM, Leser GP, Lamb RA, Horvath CM. The innate immune sensor LGP2 activates antiviral signaling by regulating. Mol Cell. 2014 Sep 4;55(5):771–81.
45. Deddouche S, Goubau D, Rehwinkel J, Chakravarty P, Begum S, Maillard PV, et al. Identification of an LGP2-associated MDA5 agonist in picornavirus-infected cells. eLife. 2014 Feb 18;3:e01535.
46. Li X, Ranjith-Kumar CT, Brooks MT, Dharmaiah S, Herr AB, Kao C, et al. The RIG-I-like receptor LGP2 recognizes the termini of double-stranded RNA. J Biol Chem. 2009 May 15;284(20):13881–91.
47. Pippig DA, Hellmuth JC, Cui S, Kirchhofer A, Lammens K, Lammens A, et al. The regulatory domain of the RIG-I family ATPase LGP2 senses double-stranded RNA. Nucleic Acids Res. 2009 Apr;37(6):2014–25.
48. Uchikawa E, Lethier M, Malet H, Brunel J, Gerlier D, Cusack S. Structural Analysis of dsRNA Binding to Anti-viral Pattern Recognition Receptors LGP2 and MDA5. Mol Cell. 2016 May;62(4):586–602.
49. Childs KS, Randall RE, Goodbourn S. LGP2 plays a critical role in sensitizing mda-5 to activation by double-stranded RNA. PloS One. 2013;8(5):e64202.
50. Jiang F, Ramanathan A, Miller MT, Tang G-Q, Gale M, Patel SS, et al. Structural basis of RNA recognition and activation by innate immune receptor RIG-I. Nature. 2011 Sep 25;479(7373):423–7.
51. Luo D, Ding SC, Vela A, Kohlway A, Lindenbach BD, Pyle AM. Structural insights into RNA recognition by RIG-I. Cell. 2011 Oct 14;147(2):409–22.
52. Kowalinski E, Lunardi T, McCarthy AA, Louber J, Brunel J, Grigorov B, et al. Structural basis for the activation of innate immune pattern-recognition receptor. Cell. 2011 Oct 14;147(2):423–35.
53. Wang Y, Ludwig J, Schuberth C, Goldeck M, Schlee M, Li H, et al. Structural and functional insights into 5′-ppp RNA pattern recognition by the innate immune receptor RIG-I. Nat Struct Mol Biol. 2010 Jul;17(7):781–7.
54. Lu C, Xu H, Ranjith-Kumar CT, Brooks MT, Hou TY, Hu F, et al. The structural basis of 5′ triphosphate double-stranded RNA recognition by RIG-I. Struct Lond Engl 1993. 2010 Aug 11;18(8):1032–43.

55. Gack MU, Shin YC, Joo C-H, Urano T, Liang C, Sun L, et al. TRIM25 RING-finger E3 ubiquitin ligase is essential for RIG-I-mediated antiviral activity. Nature. 2007 Apr 19;446(7138):916–20.
56. Oshiumi H, Matsumoto M, Hatakeyama S, Seya T. Riplet/RNF135, a RING finger protein, ubiquitinates RIG-I to promote interferon-beta induction during the early phase of viral infection. J Biol Chem. 2009 Jan 9;284(2):807–17.
57. Zeng W, Sun L, Jiang X, Chen X, Hou F, Adhikari A, et al. Reconstitution of the RIG-I pathway reveals a signaling role of unanchored polyubiquitin chains in innate immunity. Cell. 2010 Apr 16;141(2):315–30.
58. Jiang X, Kinch LN, Brautigam CA, Chen X, Du F, Grishin NV, et al. Ubiquitin-induced oligomerization of the RNA sensors RIG-I and MDA5 activates antiviral innate immune response. Immunity. 2012 Jun 29;36(6):959–73.
59. Maharaj NP, Wies E, Stoll A, Gack MU. Conventional protein kinase C-alpha (PKC-alpha) and PKC-beta negatively regulate. J Virol. 2012 Feb;86(3):1358–71.
60. Wies E, Wang MK, Maharaj NP, Chen K, Zhou S, Finberg RW, et al. Dephosphorylation of the RNA sensors RIG-I and MDA5 by the phosphatase PP1 is essential for innate immune signaling. Immunity. 2013 Mar 21;38(3):437–49.
61. Sun Z, Ren H, Liu Y, Teeling JL, Gu J. Phosphorylation of RIG-I by casein kinase II inhibits its antiviral response. J Virol. 2011 Jan;85(2):1036–47.
62. Willemsen J, Wicht O, Wolanski JC, Baur N, Bastian S, Haas DA, et al. Phosphorylation-Dependent Feedback Inhibition of RIG-I by DAPK1 Identified by Kinome-wide siRNA Screening. Mol Cell. 2017 Feb 2;65(3):403–415.e8.
63. Saito T, Hirai R, Loo Y-M, Owen D, Johnson CL, Sinha SC, et al. Regulation of innate antiviral defenses through a shared repressor domain in. Proc Natl Acad Sci U S A. 2007 Jan 9;104(2):582–7.
64. Cui S, Eisenacher K, Kirchhofer A, Brzozka K, Lammens A, Lammens K, et al. The C-terminal regulatory domain is the RNA 5'-triphosphate sensor of RIG-I. Mol Cell. 2008 Feb 1;29(2):169–79.
65. Weber M, Gawanbacht A, Habjan M, Rang A, Borner C, Schmidt AM, et al. Incoming RNA virus nucleocapsids containing a 5'-triphosphorylated genome activate RIG-I and antiviral signaling. Cell Host Microbe. 2013 Mar 13;13(3):336–46.
66. Louber J, Kowalinski E, Bloyet L-M, Brunel J, Cusack S, Gerlier D. RIG-I self-oligomerization is either dispensable or very transient for signal transduction. PloS One. 2014;9(9):e108770.
67. Patel JR, Jain A, Chou Y, Baum A, Ha T, García-Sastre A. ATPase-driven oligomerization of RIG-I on RNA allows optimal activation of type-I interferon. EMBO Rep. 2013 Jul 12;14(9):780–7.
68. Corby MJ, Stoneman MR, Biener G, Paprocki JD, Kolli R, Raicu V, et al. Quantitative microspectroscopic imaging reveals viral and cellular RNA helicase interactions in live cells. J Biol Chem. 2017 Jul 7;292(27):11165–77.
69. Schmidt A, Rothenfusser S, Hopfner K-P. Sensing of viral nucleic acids by RIG-I: from translocation to translation. Eur J Cell Biol. 2012 Jan;91(1):78–85.
70. Shatkin AJ. Capping of eucaryotic mRNAs. Cell. 1976 Dec;9(4 PT 2):645–53.
71. Filipowicz W, Furuichi Y, Sierra JM, Muthukrishnan S, Shatkin AJ, Ochoa S. A protein binding the methylated 5'-terminal sequence, m7GpppN, of eukaryotic messenger RNA. Proc Natl Acad Sci U S A. 1976 May;73(5):1559–63.
72. Furuichi Y, Shatkin AJ. Viral and cellular mRNA capping: past and prospects. Adv Virus Res. 2000;55:135–84.

73. Marcotrigiano J, Gingras AC, Sonenberg N, Burley SK. Cocrystal structure of the messenger RNA 5' cap-binding protein (eIF4E) bound to. Cell. 1997 Jun 13;89(6):951–61.
74. Decroly E, Ferron F, Lescar J, Canard B. Conventional and unconventional mechanisms for capping viral mRNA. Nat Rev Microbiol. 2011 Dec 5;10(1):51–65.
75. Hyde JL, Diamond MS. Innate immune restriction and antagonism of viral RNA lacking 2-O methylation. Virology. 2015 May;479–480:66–74.
76. Jang M-A, Kim EK, Now H, Nguyen NTH, Kim W-J, Yoo J-Y, et al. Mutations in DDX58, which Encodes RIG-I, Cause Atypical Singleton-Merten Syndrome. Am J Hum Genet. 2015 Feb;96(2):266–74.
77. Lu C, MacDougall M. RIG-I-Like Receptor Signaling in Singleton-Merten Syndrome. Front Genet [Internet]. 2017 Sep 12 [cited 2017 Oct 21];8. Available from: http://journal.frontiersin.org/article/10.3389/fgene.2017.00118/full
78. Lässig C, Matheisl S, Sparrer KM, de Oliveira Mann CC, Moldt M, Patel JR, et al. ATP hydrolysis by the viral RNA sensor RIG-I prevents unintentional recognition of self-RNA. eLife [Internet]. 2015 Nov 26 [cited 2017 Oct 19];4. Available from: https://elifesciences.org/articles/10859
79. Louber J, Brunel J, Uchikawa E, Cusack S, Gerlier D. Kinetic discrimination of self/non-self RNA by the ATPase activity of RIG-I and MDA5. BMC Biol. 2015 Jul 28;13:54.
80. Lässig C, Hopfner K-P. Discrimination of cytosolic self and non-self RNA by RIG-I-like receptors. J Biol Chem. 2017 Jun 2;292(22):9000–9.
81. Rutsch F, MacDougall M, Lu C, Buers I, Mamaeva O, Nitschke Y, et al. A specific IFIH1 gain-of-function mutation causes Singleton-Merten syndrome. Am J Hum Genet. 2015 Feb 5;96(2):275–82.
82. Leslie, A.G.W. & Powell, H.R. Processing diffraction data with MOSFLM. In Evolving Methods for Macromolecular Crystallography. In: Randy J. Read Joel L. Sussman, editor. Evolving Methods for Macromolecular Crystallography. Springer Verlag; p. 41–51. (NATO Science Series II: Mathematics, Physics and Chemistry; vol. 245).
83. Battye TGG, Kontogiannis L, Johnson O, Powell HR, Leslie AGW. *iMOSFLM* : a new graphical interface for diffraction-image processing with *MOSFLM*. Acta Crystallogr D Biol Crystallogr. 2011 Apr 1;67(4):271–81.
84. The CCP4 suite: programs for protein crystallography. Acta Crystallogr D Biol Crystallogr. 1994 Sep 1;50(Pt 5):760–3.
85. Emsley P, Cowtan K. Coot: model-building tools for molecular graphics. Acta Crystallogr D Biol Crystallogr. 2004 Dec;60(Pt 12 Pt 1):2126–32.
86. Terwilliger TC, DiMaio F, Read RJ, Baker D, Bunkóczi G, Adams PD, et al. phenix.mr_rosetta: molecular replacement and model rebuilding with Phenix and Rosetta. J Struct Funct Genomics. 2012 Jun;13(2):81–90.
87. Acerbo AS, Cook MJ, Gillilan RE. Upgrade of MacCHESS facility for X-ray scattering of biological macromolecules in solution. J Synchrotron Radiat. 2015 Jan;22(1):180–6.
88. Skou S, Gillilan RE, Ando N. Synchrotron-based small-angle X-ray scattering of proteins in solution. Nat Protoc. 2014 Jul;9(7):1727–39.
89. Petoukhov MV, Franke D, Shkumatov AV, Tria G, Kikhney AG, Gajda M, et al. New developments in the ATSAS program package for small-angle scattering data analysis. J Appl Crystallogr. 2012 Apr 1;45(Pt 2):342–50.
90. Zinm BH. The Dependence of the Scattering of Light on Angle and Concentration in Linear Polymer Solutions. J Phys Colloid Chem. 1948 Jan 1;52(1):260–7.
91. Tang G-Q, Bandwar RP, Patel SS. Extended Upstream A-T Sequence Increases T7 Promoter Strength. J Biol Chem. 2005 Dec 9;280(49):40707–13.

92. Ramanathan A, Devarkar SC, Jiang F, Miller MT, Khan AG, Marcotrigiano J, et al. The autoinhibitory CARD2-Hel2i Interface of RIG-I governs RNA selection. Nucleic Acids Res. 2016 Jan 29;44(2):896–909.
93. Fairman-Williams ME, Guenther U-P, Jankowsky E. SF1 and SF2 helicases: family matters. Curr Opin Struct Biol. 2010 Jun;20(3):313–24.
94. Daffis S, Szretter KJ, Schriewer J, Li J, Youn S, Errett J, et al. 2'-O methylation of the viral mRNA cap evades host restriction by IFIT family members. Nature. 2010 Nov 18;468(7322):452–6.
95. Szretter KJ, Daniels BP, Cho H, Gainey MD, Yokoyama WM, Gale MJ, et al. 2'-O methylation of the viral mRNA cap by West Nile virus evades ifit1-dependent and -independent mechanisms of host restriction in vivo. PLoS Pathog. 2012;8(5):e1002698.
96. Abbas YM, Pichlmair A, Gorna MW, Superti-Furga G, Nagar B. Structural basis for viral 5'-PPP-RNA recognition by human IFIT proteins. Nature. 2013 Feb 7;494(7435):60–4.
97. Sen GC, Fensterl V. Crystal structure of IFIT2 (ISG54) predicts functional properties of IFITs. Cell Res. 2012 Oct;22(10):1407–9.
98. Sarkar D, Desalle R, Fisher PB. Evolution of MDA-5/RIG-I-dependent innate immunity: independent evolution by domain grafting. Proc Natl Acad Sci U S A. 2008 Nov 4;105(44):17040–5.
99. Schuberth-Wagner C, Ludwig J, Bruder AK, Herzner A-M, Zillinger T, Goldeck M, et al. A Conserved Histidine in the RNA Sensor RIG-I Controls Immune Tolerance to. Immunity. 2015 Jul 21;43(1):41–51.
100. Pollard TD. A guide to simple and informative binding assays. Mol Biol Cell. 2010 Dec;21(23):4061–7.
101. Vitour D, Meurs EF. Regulation of interferon production by RIG-I and LGP2: a lesson in self-control. Sci STKE Signal Transduct Knowl Environ. 2007 May 1;2007(384):pe20.
102. Uchikawa E, Lethier M, Malet H, Brunel J, Gerlier D, Cusack S. Structural Analysis of dsRNA Binding to Anti-viral Pattern Recognition Receptors LGP2 and MDA5. Mol Cell. 2016 May 19;62(4):586–602.
103. Ramanathan A, Devarkar SC, Jiang F, Miller MT, Khan AG, Marcotrigiano J, et al. The autoinhibitory CARD2-Hel2i Interface of RIG-I governs RNA selection. Nucleic Acids Res. 2016 Jan 29;44(2):896–909.
104. Poeck H, Besch R, Maihoefer C, Renn M, Tormo D, Morskaya SS, et al. 5'-Triphosphate-siRNA: turning gene silencing and Rig-I activation against melanoma. Nat Med. 2008 Nov;14(11):1256–63.

ABBREVIATIONS

PAMP: Pathogen-Associated Molecular Pattern

PRR: Pattern Recognition Receptors

IFN: Interferon

ISGs: Interferon Stimulated Genes

TLR: Toll-Like Receptors

CLR: C-type Lectin Receptors

NLR: NOD-Like Receptors

RLR: RIG-I -Like -Receptors

ALR: AIM2-Like Receptors

RIG-I: Retinoic Acid Inducible Gene-I

MDA-5: Melanoma Differentiation Associated protein-5

LGP-2: Laboratory of Genetics and Physiology-2

MAVS: Mitochondria Antiviral Signaling protein

CARD: Caspase Activation and Recruitment Domain

CTD: C-terminal Domain

RD: Repressor Domain

ss: single stranded

ds: double stranded

bp: base pair

HP: Hairpin

ppp/5'ppp : 5' triphosphate

nt: nucleotide

Fl: Fluorescein

ATP: Adenosine triphosphate

SEC: Size Exclusion Chromatography

MALS: Multi-Angle Light Scattering

mAb: monoclonal antibody